

การสังเคราะห์แม่เหล็กนาโนคอมพอสิตสำหรับการนำส่งโปรตีน

นางสาวชลารัตน์ แสงเรืองฤทธิ์



จุฬาลงกรณ์มหาวิทยาลัย

CHULALONGKORN UNIVERSITY

บทคัดย่อและแฟ้มข้อมูลฉบับเต็มของวิทยานิพนธ์ตั้งแต่ปีการศึกษา 2554 ที่ให้บริการในคลังปัญญาจุฬาฯ (CUIR)  
เป็นแฟ้มข้อมูลของนิสิตเจ้าของวิทยานิพนธ์ ที่ส่งผ่านทางบัณฑิตวิทยาลัย

The abstract and full text of theses from the academic year 2011 in Chulalongkorn University Intellectual Repository (CUIR)  
are the thesis authors' files submitted through the University Graduate School.

วิทยานิพนธ์นี้เป็นส่วนหนึ่งของการศึกษาตามหลักสูตรปริญญาวิทยาศาสตรดุษฎีบัณฑิต

สาขาวิชาเคมี ภาควิชาเคมี

คณะวิทยาศาสตร์ จุฬาลงกรณ์มหาวิทยาลัย

ปีการศึกษา 2559

ลิขสิทธิ์ของจุฬาลงกรณ์มหาวิทยาลัย

SYNTHESIS OF MAGNETIC NANOCOMPOSITES FOR PROTEIN DELIVERY

Miss Chalathan Saengruengrit



A Dissertation Submitted in Partial Fulfillment of the Requirements  
for the Degree of Doctor of Philosophy Program in Chemistry

Department of Chemistry

Faculty of Science

Chulalongkorn University

Academic Year 2016

Copyright of Chulalongkorn University



ชลาธาร แสงเรืองฤทธิ์ : การสังเคราะห์แม่เหล็กนาโนคอมพอสิตสำหรับการนำส่งโปรตีน (SYNTHESIS OF MAGNETIC NANOCOMPOSITES FOR PROTEIN DELIVERY) อ.ที่  
 ปรึกษาวิทยานิพนธ์หลัก: ดร.นำพล อินสิน, อ.ที่ปรึกษาวิทยานิพนธ์ร่วม: ผศ. ทญ. ดร.พัชรี  
 ฤทธิ์ประจักษ์, 93 หน้า.

การพัฒนาประสิทธิภาพของวัคซีน และความสามารถในการนำส่งแอนติเจนไปสู่เซลล์  
 แอนติเจนพรีเซนติ่งหรือที่ทำหน้าที่นำเสนอแอนติเจน เป็นหนทางที่จะสามารถเห็นว่าการ  
 ตอบสนองของภูมิคุ้มกัน งานวิจัยนี้แสดงให้เห็นถึงความสำเร็จในการใช้อนุภาคคอมพอสิตระหว่าง  
 ซูเปอร์พาราแมกเนติกของนาโนเหล็กออกไซด์และพอลิเมอร์ (SPION-Polymer) ที่มีความเป็นพิษต่ำ  
 สนามแม่เหล็ก ในการเปรียบเทียบระหว่างพอลิเมอร์สองชนิด ได้แก่ พอลิแลคติกโคไกลโคลิคเอซิด  
 (PLGA) และพอลิอะคริลิกที่ถูกดัดแปร (mPAA) โดยอนุภาค SPION-PLGA แสดงการตอบสนองต่อ  
 สนามแม่เหล็กที่แรงกว่า SPION-mPAA ดังนั้นจึงเลือก SPION-PLGA ในการติดโปรตีนโบวิน  
 เซรัมอะบูมินเพื่อเป็นแบบจำลองแอนติเจน จากนั้นนำอนุภาคที่สังเคราะห์ได้มาทำการตรวจสอบ  
 เอกลักษณ์โดยเครื่องมือต่างๆ ได้แก่ กล้องจุลทรรศน์อิเล็กตรอนแบบส่องผ่าน กล้องจุลทรรศน์  
 อิเล็กตรอนแบบส่องกราด เครื่องไดนามิคไลส์สแกตเตอร์ริง อินฟราเรดสเปกโตรสโคปี และซูเปอร์  
 คอนดักติงควันตัมอินเตอร์เฟอเรนซ์-ไวเบรติงแชนเนลเปิดแมกนีโตมิเตอร์

การทดสอบความเป็นพิษต่อเซลล์ และการเข้าสู่เซลล์ของอนุภาค SPION-PLGA ที่ติด  
 โปรตีน พบว่าอนุภาคขนาด 500 นาโนเมตร มีประสิทธิภาพในการเข้าสู่เซลล์ได้ดี ภายใต้การ  
 เห็นย่นาจากสนามแม่เหล็กภายนอก นอกจากนี้ภายใต้การนำส่งของ SPION-PLGA ทำให้เกิดการ  
 ตอบสนองของระบบภูมิคุ้มกันโดยการหลั่งโมเลกุลบนพื้นผิวของเซลล์ไซโตไคน์และเคโมไคน์  
 MHCII CD80 และ CD86 และการสร้าง IL-12, IFN-g and IL-6 ได้ดีภายใต้การเห็นย่นาของ  
 สนามแม่เหล็กเช่นกัน ผู้วิจัยคาดว่าผลการทดลองนี้จะเป็นจุดเริ่มต้นของงานวิจัยเกี่ยวกับวัคซีนที่  
 เกี่ยวข้องกับอนุภาคคอมพอสิตระหว่าง SPION และพอลิเมอร์ PLGA

ภาควิชา	เคมี	ลายมือชื่อนิสิต .....
สาขาวิชา	เคมี	ลายมือชื่อ อ.ที่ปรึกษาหลัก .....
ปีการศึกษา	2559	ลายมือชื่อ อ.ที่ปรึกษาร่วม .....

# # 5672809223 : MAJOR CHEMISTRY

KEYWORDS: IRON OXIDE SUPERPARAMAGNETIC NANOPARTICLES / PROTEIN ANTIGEN DELIVERY / VACCINE / PRIMARY DENDRITIC CELL / IMMUNE RESPONSE / POLYMER

CHALATHAN SAENGRUENGRIT: SYNTHESIS OF MAGNETIC NANOCOMPOSITES FOR PROTEIN DELIVERY. ADVISOR: NUMPON INSIN, Ph.D., CO-ADVISOR: ASST. PROF. PATCHAREE RITPRAJAK, DDS, Ph.D., 93 pp.

In order to develop effective vaccines, an ability to deliver antigen into antigen presenting cells in such a way that the immune responses are induced, must be conquered. This study demonstrates that such requirement can be achieved through the combination of a magnetic field and the relatively non-toxic composite particles of superparamagnetic iron oxide nanoparticles and polymer (SPION-Polymer). In comparison of two biocompatible polymers, poly(lactic-co-glycolic acid) (PLGA) and modified poly(acrylic acid) (mPAA), SPION-PLGA demonstrated stronger magnetic response than SPION-mPAA. We chose SPION-PLGA to load bovine serum albumin (BSA, a protein antigen model). The particles were characterized using various techniques including transmission electron microscopy (TEM), field emission scanning electron microscopy (FESEM), dynamic light scattering (DLS), infrared spectroscopy (IR) and Superconducting Quantum Interference Device-Vibrating Sample Magnetometer (SQUID-VSM).

The SPION-PLGA loading BSA was tested for cytotoxicity and cellular uptake, before delivered them into bone-marrow derived primary dendritic cells (BM-DCs). Significant enhancement of cellular uptake of the 500 nm BSA-loaded SPION-PLGA particles can be achieved under the use of an external magnetic field. Moreover, this combined SPION-PLGA carrier and an external magnetic field can significantly enhance BM-DC maturation by upregulating MHC II, CD80 and CD86 expression. Immune response induction by this strategy is verified through a significant upregulation of the IL-12, IFN-g and IL-6 production. We anticipate these findings to be a starting point for vaccine researches involving the combined magnetic field and SPION-PLGA composite particles.

Department: Chemistry

Field of Study: Chemistry

Academic Year: 2016

Student's Signature .....

Advisor's Signature .....

Co-Advisor's Signature .....

## ACKNOWLEDGEMENTS

First of all, I would like to appreciate Dr. Numpon Insin and Assistant Professor Dr. Patcharee Ritprajak, who are my thesis adviser and my co-adviser, for not only giving me valuable assistance to successfully accomplish my thesis, but also providing all of gainful information and knowledge for my thesis.

For worthy comments and advices, I would like to thank my thesis committee, Associate Professor Dr. Vudhichai Parasuk, Associate Professor Dr. Nungnuj Muangsin, Dr. Pannee Leeladee and Dr. Suwassa Bamrungsup. This research would have not been completed without all of their kindness. In addition, I am grateful to the Oral Biology Research Center, Faculty of Dentistry, Chulalongkorn University for facility support. Moreover, I would also give thanks to all of member in the research unit. Particularly, Miss Nguyen Ngoc Yen Thu and Mr. Promchat Charoenpat.

Furthermore, I would like to special specially thanks of all members of my Chemistry Research Unit who are always supportive. Especially, Miss Wishulada Injumpa, Mr. Korakot Niyomsat, Mr. Phranot Ajkidkarn and Miss Padtaraporn Chunhom.

In addition, I am thankful to Semiconductor Physics, Institute of Physics, Technische Universität Chemnitz, and also specially thank to research members Prof. Dr. Georgeta Salvan and Mr. Apoova Sharma for kindly supportive for the experiment in Germany.

Moreover, this work and me are supported by Ratchadaphiseksomphot Endowment Fund (RES560530153-HR) and Science Achievement Scholarship of Thailand (SAST), Chulalongkorn Graduate School, and the 90th Anniversary of Chulalongkorn University Fund.

Finally, I would like to give greatly thank for my family who supports all of everything in my life and my thesis.

## CONTENTS

	Page
THAI ABSTRACT .....	iv
ENGLISH ABSTRACT .....	v
ACKNOWLEDGEMENTS .....	vi
CONTENTS .....	vii
LIST OF TABLES .....	xi
LISTS OF FIGURES .....	xii
LIST OF ABBREVIATIONS .....	1
CHAPTER I INTRODUCTION .....	1
1.1 Statement of the problem .....	1
1.2 Objectives of this thesis.....	2
1.3 Scope of this thesis .....	2
CHAPTER II THEORIES AND LITERATURE REVIEWS .....	4
2.1 Magnetic Nanoparticles and Nanocomposites with Polymers .....	4
2.1.1 Magnetic nanoparticles .....	4
2.1.1.1 Principle of nanoparticles .....	4
2.1.2.2 Magnetic nanoparticles.....	4
2.1.2 Magnetic nanocomposites with polymers.....	6
2.1.3 Principle of synthesis.....	8
2.1.3.1 Magnetic nanoparticle synthesis .....	8
2.1.3.1.1 Co-precipitation method.....	8
2.3.1.1.2 Thermal decomposition method.....	9
2.1.3.2 Preparation of magnetic nanocomposites with polymer.....	11

	Page
2.2 Principle of Immune System and Vaccine Delivery .....	13
2.2.1 Principle of immune system and immune response.....	13
2.2.2 Principle of vaccine delivery.....	16
2.2.3 Principle of cytotoxicity testing (MTT assay).....	18
2.2.4 Principle of measurement of immune response .....	19
2.2.3.2 Flow cytometry analysis (FACs).....	19
2.2.3.3 Sandwich enzyme-linked immunosorbent assay (Sandwich ELISA).....	20
2.3 Literature Reviews.....	21
2.3.1 Superparamagnetic iron oxide nanoparticles (SPIONs) in drug delivery.....	21
2.3.2 Polymer-based micro/nanoparticles design for vaccine delivery .....	24
CHAPTER III EXPERIMENTS.....	31
3.1 Synthesis of Superparamagnetic Iron Oxide Nanoparticles (SPIONs).....	34
3.1.1 Synthesis of SPIONs using a thermal decomposition method .....	34
3.1.2 Synthesis of SPIONs using a co-precipitation method .....	35
3.2 Preparation of BSA/SPIONs-Polymer.....	35
3.2.1 SPION-coated with modified poly(acrylic acid) (SPIONs-mPAA) .....	35
3.2.2 SPIONs-coated with Poly(D,L-lactide-co-glycolide) (SPIONs-PLGA) .....	37
3.3 Particles Characterization .....	38
3.4 SPION and BSA Protein Loading Content .....	39
3.5 Cytotoxicity Testing .....	39
3.6 Cellular Uptake.....	40
3.7 Induction of Dendritic Cell Maturation and Cytokine Production .....	41



	Page
CHAPTER IV RESULTS AND DISCUSSION .....	43
4.1 Characterization of SPIONs .....	43
4.1.1 Characterization of synthesized SPIONs morphology and size with TEM and FESEM .....	43
4.1.2 Characterization of synthesized SPIONs crystal structures with X-ray diffraction .....	44
4.1.2 Magnetic properties characterization of synthesized SPIONs with superconducting quantum interference device-vibrating sample magnetometer (SQUID-VSM) .....	45
4.2 Characterization of BSA/SPIONs-Polymer .....	49
4.2.1 Characterization of SPIONs-coated with modified poly(acrylic acid) (SPION-mPAA) .....	49
4.2.1.1 Characterization of functional group of mPAA and BSA/SPION- mPAA with Fourier transform infrared spectrometer (FTIR) ....	49
4.2.1.2 Characterization of SPION-mPAA morphology and sizes with TEM and FESEM .....	50
4.2.2 SPIONs-coated with Poly(D,L-lactide-co-gylcolide) (SPION-PLGA) .....	54
4.2.2.1 Characterization of SPION-PLGA and BSA/SPION-PLGA morphology, size and charge with TEM, FESEM and Zetasizer analysis .....	54
4.2.2.2 Characterization of functional groups of PLGA and BSA/SPION- PLGA using Furier transform infrared spectrometer (FTIR) .....	57
4.2.2.3 Detection of Iron and BSA protein content in the SPION-PLGA and BSA/SPION-PLGA with inductively-coupled plasma optical emission spectrometer (ICP-OES) and UV-Visible Spectroscopy .....	58

	Page
4.2.2.4 Investigation of PLGA particles stability.....	59
4.3 Cytotoxicity Testing and Cellular Uptake and Protein Delivery.....	61
4.3.1 Cytotoxicity testing.....	61
4.3.2 Cellular uptake of particles and protein delivery.....	63
4.4 Induction of Dendritic Cell Maturation and Cytokine Production .....	68
4.4.1 Induction of dendritic cell Maturation with flow cytometry analysis (FACS).....	68
4.4.2 Cytokine Production performing with ELISA assay .....	71
CHAPTER V CONCLUSION.....	75
REFERENCES .....	77
VITA.....	93

## LIST OF TABLES

Table	Page
2.1 Examples of SPION surface modification with polymers using various chemical and physical interactions.....	13
3.1 List of instruments.....	31
3.2 List of chemical.....	32
3.3 List of biological reagents.....	33
4.1 Characteristics of particles hydrodynamic sizes, polydispersity indices (PDI), and zeta potentials using a Zetasizer.....	55
4.2 Investigation of SPION loading and protein loading contents of all prepared particles. ....	59
A1 Inhibitory dose concentration (IC50) of SPIONs, PLGA particles and nanocomposites (mg/mL) on Raw264.7 cells at various time incubations. ....	90

## LISTS OF FIGURES

Figure	Page
2.1 The summary of different magnetic properties from intrinsic properties and properties arising when the size decreasing to nanomaterial. The spin arrangement in (a) ferromagnet (FM) and (b) antiferromagnet (AFM), (c) a magnetization curve of ferromagnetic bulk materials or permanent magnets, (d) the magnetic moments and magnetization curve of a superparamagnet (SPM), (e) an interaction at the interface layers of a ferromagnetic and an antiferromagnetic produces the exchange bias effect and (f) a magnetization curve of antiferromagnetic materials. (D=diameter, D <sub>c</sub> =critical diameter) ..... 5	5
2.2 Iron oxide structures: (a) the hematite, (b) magnetite and (c) maghemite (the black ball is Fe <sup>2+</sup> , the green ball is Fe <sup>3+</sup> and the red ball is O <sup>2-</sup> ). ..... 6	6
2.3 Biocompatible polymer structures illustration: poly(lactic-co-glycolic acid), poly(ethylene glycol), chitosan, polyacrylic acid and dextran. .... 8	8
2.4 Scheme for reaction mechanism of magnetic iron oxide (magnetite) nanoparticles in aqueous mixture of iron (III) and iron (II) chloride under basic condition. .... 9	9
2.5 Schematic of thermal decomposition method at 350 °C various time affecting nucleation and growth of the monodisperse nanoparticles. .... 10	10
2.6 Illustration of the immune cells divide into two major types: innate and adaptive immunities with the straddle at the interface. .... 14	14
2.7 The illustration of how pathogen or vaccine particles induce innate and adaptive immune responses. (a) Vaccines are taken via intramuscular, intradermal or other ways, and then they confront the local immune cells such as DCs. (b) The antigens induce DC maturation and migration from muscle to lymphoid organs through blood or lymphatic systems. (c) DCs present an antigen to CD8 and CD4 T cell via MHC I and class II, respectively. In addition DCs express co-stimulatory molecules to activate T cells. After activation, CD8 T cell differentiate to CTLs	

and CD4 T cell differentiate to Th cells. CTLs directly killing the target cells infected by pathogens while T helper (Th) cells support B cells to generate antibody, and help other cells. ....	15
<b>2.8</b> Schematic diagram of immunological mechanism of micro- or nanoparticles adjuvant carrying antigen .....	17
<b>2.9</b> Schematic diagram of immunological mechanism of endosome escape enhancement using the particle carriers (Gel MP) in vaccine delivery system .....	18
<b>2.10</b> Reaction of MTT (yellow)) with mitochondrial reductase to yield the Formazan product (purple). ....	19
<b>2.11</b> Schematic diagram of a flow cytometer illustrates the cells staining and apparatus in a flow cytometer (1) Forward-scatter detector, (2) side-scatter detector, (3) fluorescence detector, (4) filters and mirrors, and (5) charged deflection plates. (FSC = forward scattering and SSC = side scattering).....	20
<b>2.12</b> Schematic representation of sandwich ELISA process. ....	21
<b>2.13</b> Schematic representation of folate conjugated PLGA encapsulating sorafenib and SPIONs for cancer cells treatment with various formulations (SRF = sorafenib drug, MNP = magnetic nanoparticles and FA = folic acid). ....	22
<b>2.14</b> Schematic Illustration of MNP/T7-PLGA particles and tumor-targeting delivery via the T7-mediated and magnetic-guided (upper figure). The nanoparticle distribution in mice imaging after injection via tail vein at 4 hours (MAG = magnet) (lower figure).....	23
<b>2.15</b> Confocal microscope images of macrophages (J774A.1) after 24 h incubation with 300 µg/mL of 430 nm (A), 1.9 µm (B) and 4.8 µm (C) chitosan particles (upper figures). Cytokine production (A-D) and surface marker (E-F) of J774A.1 after activation with particle of different sizes (lower figures). ....	26
<b>2.16</b> Zetasizer analysis of surface charge on PLA modified with chitosan (CS), chitosan chloride (CSC) and polyethylenimine (PEI) (upper figure). MFI graph and fluorescent microscope images of distribution of particles and the antigen (Ag)	

delivery to macrophage cells, B-G, showing Ag and particles-based carriers as listed in graph A (lower figures). (MFI = mean fluorescence intensity from flow cytometry analysis, Green and Red signals represent particles and cell membrane, respectively).....	28
<b>2.17</b> Contact angles of various polymeric particles for evaluation of hydrophobicities and SEM images of particles for observation of their shapes and sizes. ....	29
<b>3.1</b> Schematic illustration of reaction for modified poly acrylic acid (mPAA) preparation. ....	36
<b>3.2</b> Schematic illustration of preparation of SPIONs coated with mPAA containing BSA (BSA/SPION-mPAA). ....	36
<b>3.3</b> Schematic of preparation of (A) PLGA encapsulating SPIONs (SPIONs-PLGA) and (B) PLGA encapsulating SPIONs and BSA (BSA/SPIONs-PLGA).....	37
<b>4.1</b> Transmission electron microscopy (TEM) images of SPIONs synthesized from (A) thermal decomposition and (B) co-preparation methods.....	44
<b>4.2</b> The XRD patterns of the synthesized superparamagnetic iron oxide nanoparticles (SPIONs) compared with the standard pattern files JCPDS 19-0629 (magnetite) and JCPDS 39-1346 (maghemite).....	45
<b>4.3</b> SQUID-VSM measured M(H) hysteresis loop for quartz substrate, glue and sample holder (background) for in-plane applied magnetic field at 20 K and 300 K. ....	46
<b>4.4</b> (A) M(T) hysteresis curve of SPION at 500 Oe for temperature between 15 K to 350 K and (B) SQUID-VSM measured normalized M(H) hysteresis loop for SPION in-plane applied a magnetic field at 15 K and 350 K. ....	48
<b>4.5</b> Fourier transform infrared spectroscopy (FT-IR) of (A) poly(acrylic acid) (PAA) (B) modified poly(acrylic acid) (mPAA) (C) superparamagnetic iron oxide nanoparticles (SPION)-mPAA and (D) BSA protein-coated SPION-mPAA (BSA/SPION-mPAA) .....	50
<b>4.6</b> (A) Transmission electron microscopy (TEM) image and (B) Field Emission Scanning Electron Microscopy (FESEM) image of obtained SPION-mPAA particles.....	51

<b>4.7</b> Scheme illustrate the preparation of SPION coated with mPAA (blue) from the SPION coated with oleic acid. ....	51
<b>4.8</b> SEM-EDX of SPION-mPAA (A) SEM image and EDX mapping of various elements: (B) Fe, (C) O and (D) C, and (F) EDX spectra showing all elements in SPION-mPAA particles. ....	52
<b>4.9</b> SEM-EDX of BSA/SPION-mPAA (A) SEM image and EDX mapping of various elements (B) Fe, (C) O and (D) C, and (F) EDX spectra showing all elements in BSA/SPION-mPAA particles. ....	53
<b>4.10</b> FESEM images showing the morphologies of particles (A) PLGA-L and (B) PLGA-S. ....	55
<b>4.11</b> TEM images of SPION encapsulated in PLGA (A) SPION-PLGA-L, (B) SPION-PLGA-S, and SPION with BSA encapsulated in PLGA (C) BSA/SPION-PLGA-L and (D) BSA/SPION-PLGA-S. ....	56
<b>4.12</b> Proposed structures of SPIONs encapsulated in PLGA (A) SPION-PLGA (oil/water emulsion) and (B) BSA/SPION-PLGA (water/oil/water double emulsion). ....	57
<b>4.13</b> FTIR spectra of (A) SPIONs, (B) Poly(D,L-lactide-co-glycolide) PLGA, (C) SPION-PLGA and (D) BSA-loaded SPION-PLGA (BSA/SPION-PLGA) particles. ....	57
<b>4.14</b> FESEM images of PLGA-L particles (A-C) and PLGA-S (D-F) after being incubated in a 24 well-plate at 37 °C with 5% CO <sub>2</sub> in PBS buffer pH 7.4 for 1 (A, D), 2 (B, E), and 7 (C, F) days. ....	60
<b>4.15</b> Cytotoxicity of the SPION, PLGA and SPION-PLGA with and without BSA protein in macrophages cell line (Raw 264.7). Cell viability from the MTT assay after incubating the cells with the tested particles at 37 °C with 5% CO <sub>2</sub> for 24 h, 48 h and 72 h. Data are shown as mean $\pm$ SD, derived from 3 repeats. ....	63
<b>4.16</b> Cellular uptake of particles. Fluorescent microscopic images of particles uptake into Raw 264.7 cells under various light wavelength (A) normal white light, (B) blue fluorescence from nucleus of Raw 264.7 cells stained with DAPI dye, (C) red	

- fluorescence from particles encapsulating TAMRA dye and (D) overlay of nucleuses (blue) and particles (red). ..... 64
- 4.17** Cellular uptake of particles. Fluorescent microscopic images of RAW264.7 cells after 1 h (Row 1) and 3 h (Row 2) incubation at 37 °C with 5% CO<sub>2</sub>, under no magnetic field and under 2,600 Gauss magnetic field, with BSA-unloaded SPION-PLGA particles: TAMRA-labeled SPION-PLGA-L, TAMRA-labeled SPION-PLGA-S. Scale bars in all figures indicate 40 µm. .... 65
- 4.18** Cellular uptake of TAMRA- labeled BSA particles. Fluorescent microscopic images of RAW264.7 cells after 3 h- incubation at 37 °C with 5% CO<sub>2</sub>, under no magnetic field and under 2,600 Gauss magnetic field, BSA-loaded SPION-free particles (Row 1), TAMRA-labeled BSA/PLGA-L, TAMRA-labeled BSA/PLGA-S, TAMRA-labeled BSA-loaded SPION-PLGA particles (Row 2), TAMRA-labeled BSA/SPION-PLGA-L, TAMRA-labeled BSA/SPION-PLGA-S in absence/presence of magnetic field. Scale bars in all figures indicate 40 µm. .... 66
- 4.19** Cellular uptake of particles. Confocal laser scanning microscopic (CLSM) images of RAW264.7 cells (nuclease cells: blue) with TAMRA-labeled SPION-PLGA-L (TAMRA: red) after 3 h incubation at 37 °C with 5% CO<sub>2</sub>, under 2,600 Gauss magnetic field. .... 67
- 4.20** Induction of DC maturation. BM-DCs were incubated with each of the PLGA and SPION-PLGA particles (100 µg/mL) at 37 °C under 5% CO<sub>2</sub> in the presence of 2,600 Gauss magnetic field for 3 h, then the magnetic field was removed and incubation was carried out for another 48 h. BM-DC maturation markers were determined by flow cytometric analysis. The DC marker, CD11c was gated and the mean fluorescence intensity (MFI) of CD80, CD86 and MHC class II were evaluated. \*indicates the statistical significant difference between the samples, as determined by one way ANOVA Tukey HSD (n=3) at p < 0.05. .... 69
- 4.21** Induction of DC maturation. BM-DCs were incubated with each of the SPION-PLGA-S particles (100 µg/mL) at 37 °C under 5% CO<sub>2</sub> incubation for another 48 h, under absence of magnetic field. BM-DC maturation markers were determined by



- flow cytometric analysis. The DC marker, CD11c was gated and the mean fluorescence intensity (MFI) of CD80, CD86 and MHC class II were evaluated. .... 70
- 4.22** Induction of DC maturation. BM-DCs were incubated with each of the BSA/PLGA and BSA/SPION-PLGA particles (100 µg/mL) at 37 °C under 5% CO<sub>2</sub> in the presence of 2,600 Gauss magnetic field for 3 h, then the magnetic field was removed and incubation was carried out for another 48 h. BM-DC maturation markers were determined by flow cytometric analysis. The DC marker, CD11c was gated and the mean fluorescence intensity (MFI) of CD80, CD86 and MHC class II were evaluated. \* indicates the statistical significant difference between the samples, as determined by one way ANOVA Tukey HSD (n=3) at p < 0.05... 71
- 4.23** Stimulation of cytokine production. BM-DCs were incubated with each of the tested PLGA and SPION-PLGA particles (100 µg/mL) at 37 °C under 5% CO<sub>2</sub> in the presence of 2,600 Gauss magnetic field for 3 h. Then the magnetic field was removed and incubation was carried out for another 48 h. Cytokine analysis was evaluated through ELISA. \* indicates the statistical significant difference between the samples, as determined by one way ANOVA Tukey HSD (n=3) at p < 0.05... 73
- 4.24** Stimulation of cytokine production. BM-DCs were incubated with each of the BSA-loaded particles (100 µg/mL) at 37 °C under 5% CO<sub>2</sub> in the presence of 2,600 Gauss magnetic field for 3 h, then the magnetic field was removed and incubation was carried out for another 48 h. Cytokine analysis was evaluated through ELISA. \* indicates the statistical significant difference between the samples, as determined by one way ANOVA Tukey HSD (n=3) at p < 0.05. .... 74
- A1** SPIONs and SPIONs-polymer particles including (A) SPIONs, (B) SPION-mPAA, (C) SPION-PLGA-L and (D) SPION-PLGA-S without and with a magnet for 1 h. .... 86
- A2** TGA curves for measuring weight loss of PLGA (Blue), SPION-PLGA (Green), and BSA/SPION-PLGA particles (Red) ..... 86
- A3** Examples of Zeta sizer analysis of (A) particles size curve and polydispersity indices (PDI), and (B) zeta potential curve ..... 87

- A4** Particle contamination testing, particles and DI water spreading onto brain heart infusion (BHI) agar after 2 day incubation at 37 °C with 5% CO<sub>2</sub>. (BHI agar is recommended as a universal medium for testing aerobic bacteria and primary recovery of fungi contaminations)..... 88
- A5** Cytotoxicity study after cellular uptake of particles onto Raw264.7 in 96-well plate and 12-well plate..... 88
- A6** ELISA tasting of supernatant dendritic cells in 96-well plate (A) after adding TMB substrate and (B) after stop reaction using H<sub>2</sub>SO<sub>4</sub>..... 89
- A7** Cytotoxicity of the SPION, PLGA and SPION-PLGA with and without BSA protein in dendritic cell line (Jaw II). Cell viability from the MTT assay after incubating the cells with the tested particles at 37 °C with 5% CO<sub>2</sub> for 24 h. Data are shown as mean  $\pm$  SD, derived from 3 repeats..... 89
- A8** Examples of flow cytometry analysis data from control (dendritic cells were unstimulated) and particles (activated with particles): forward scattering (FSC) against side scattering (SSC), and cell population of surface maturation marker CD11c, CD80, CD86 and MHC II..... 91
- A9** Examples of flow cytometry analysis data from control (dendritic cells were unstimulated) and particles (activated with particles): forward scattering (FSC) against side scattering (SSC), and cell surface expression of CD11c, (C) CD80, (D) CD86 and (F) MHC II. Filled histograms represent isotype matched control antibody staining. Numbers indicate MFI of stained cells. .... 92

## LIST OF ABBREVIATIONS

SPION	=	Superparamagnetic iron oxide nanoparticles
PLGA	=	Poly(lactic-co-glycolic acid)
BSA	=	Bovine serum albumin
L	=	Large size
S	=	Small size
mPAA	=	Modified poly(acrylic acid)
BM-DCs	=	Bone marrow derived dendritic cells
Raw264.7	=	Macrophage cell line
TAMRA	=	5-Carboxy-tetramethylrhodamineN-succinimidyl ester dye
CD80	=	Cluster of differentiation 80
CD86	=	Cluster of Differentiation 86
MHC II	=	Major histocompatibility complex class II
IL-12	=	Interleukin 12
IL-6	=	Interleukin 6
IFN- $\gamma$	=	Interferon gamma
TNF- $\alpha$	=	Tumor necrosis factor alpha

# CHAPTER I

## INTRODUCTION

### 1.1 Statement of the problem

Vaccination is one of the most successful prevention of many diseases which cause by bacterial, virus or other pathogen infection.[1] Recently, nanoparticles-based antigen delivery increasingly plays a role in vaccine development due to many advantages such as their ability to carry, transport and protect antigen from enzymatic degradation.[1, 2] Moreover, they can act as immune-stimulant adjuvants to provoke immune responses.[3] In the vaccination process, after vaccine are added into the human body through intradermal or intramuscular injection, the vaccine components are taken up into antigen presenting cells (APCs) such as dendritic cells (DCs) and macrophages, and then APCs express the specific protein antigen and migrate to activate T lymphocytes for generating body immunization.[4] Therefore, APCs play a key role to generate the immune in the body so it is important to design the particles for targeting to APCs.[5]

Currently, polymeric nanoparticles are widely used to deliver the antigen because there are long chain molecules and multifunctional chemical groups easy to design for binding with antigen and stimulating the APCs. However, the polymer-based particles often lack of sufficient efficiency uptake into the APCs.[4, 6] Therefore, in this work we focus on investigation of superparamagnetic iron oxide nanoparticles (SPIONs) collaborating with polymeric particles for increasing antigen transfection into the APCs. The SPIONs have been of significant attention in drug delivery systems because of their superparamagnetic character. SPIONs are dispersed well in solutions in absence of a magnetic field and can be directed to specific targets under the induction of an external magnetic field.[7] Moreover, there are reports indicating that the SPIONs exhibited the immunogenicity in activation of APCs in and induction T cells response. [8, 9]

We hypothesized that the superparamagnetic character and immune induction ability of SPIONs are possible for antigen delivery. As mentioned, we proposed the novel protein antigen delivery system by using the SPIONs and biocompatible polymers: poly(lactic-co-glycolic acid) (PLGA) and modified Poly(acrylic acid) (mPAA). They were investigated for their cellular delivery potential and immunogenicity in macrophage cell line and bone-marrow derived DC (BM-DC), respectively. PLGA and mPAA was selected because of their high biocompatibility, and ability combine with SPIONs for protein transportation and immune modulation.[10, 11] We foresee that the delivery system under an external magnetic field will be a future platform for the needle-free immunization.

## **1.2 Objectives of this thesis**

1.2.1 To synthesize SPION composite with Polymer: PLGA and mPAA (SPION-Polymer) for protein delivery.

1.2.2 To use the obtained SPION-Polymer of different sizes for protein delivery and activation of the antigen presenting cells (APCs) under an induction of external magnetic field.

## **1.3 Scope of this thesis**

Firstly, the SPIONs were synthesized via two different methods: co-precipitation and thermal decomposition methods. Then, we selection the suitable shape, size, and dispersion of SPION for preparing nanocomposites of SPIONs and polymers PLGA and mPAA encapsulating BSA protein. For verification of the structures and their magnetic properties, the SPIONs were characterized by X-ray powder diffraction (XRD) and superconducting quantum interference device- Vibrating sample magnetometer (SQUID-VSM). Then, the morphology and charge polymers and nanocomposites particles were determined by transmission electron microscope (TEM), field emission scanning electron microscopy (FESEM) and zetasizer analysis. Fourier transmission infrared spectroscopy (FTIR) and thermogravimetry analysis (TGA) were performed to confirm the polymer coating. The concentration of SPION and BSA protein in the nanocomposites were investigated by inductively coupled plasma optical emission

spectrometer (ICP-OES) and UV- visible spectroscopy, respectively. Furthermore, cytotoxicity of particles was analyzed using MTT assay. Fluorescence microscope was used to investigate the uptake of nanocomposites into macrophage cells. Finally, the promotion of bone marrow-derived dendritic cells (BM-DCs) maturation were tested in dendritic cells.



## CHAPTER II

### THEORIES AND LITERATURE REVIEWS

#### 2.1 Magnetic Nanoparticles and Nanocomposites with Polymers

##### 2.1.1 Magnetic nanoparticles

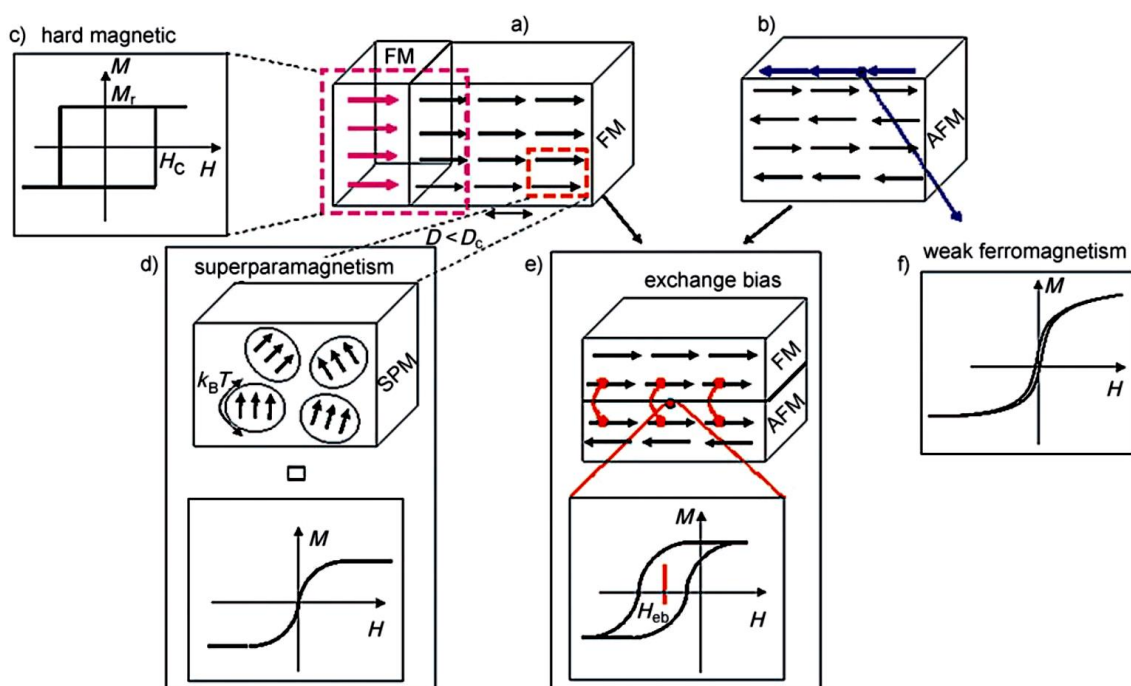
###### 2.1.1.1 Principle of nanoparticles

Nanoparticles or nanomaterials are often defined as particles in the size range of 1 to 100 nm, where the particle size of materials is reduced to nanoscale size or particles composed of few atoms. The properties of nanomaterials change from bulk materials, but are still different from a single atom. It can be mentioned that nanoparticles show behavior as intermediate between bulk material and atomic or molecular structures. The nanoparticle properties change from bulk because the nanoparticle maintain a much greater surface area per unit volume ratio, which has a strong influence on the overall properties of particles. Surface atoms are chemically more active compared with core atoms due to the lack of their neighboring atoms.[12] The novel chemical and physical properties of nanoparticles often change from bulk particles such as optical property, conductivity, catalytic activity, magnetic property, and band gap energy. Therefore, nanoparticles can be used in many applications such as metal nanoparticles have been interested as high performance heterogeneous catalysis where the catalytic reaction occurs at the surface. They can also be useful in bioapplications especially in drug delivery system because nanoparticles can disperse well in solution and their surface can be functionalized for tagging drugs.[13, 14]

###### 2.1.2.2 Magnetic nanoparticles

The dominant magnetic nanoparticle properties that are different from bulk materials depending on size and surface effects. The summary of magnetic characters occurring in different types of magnetism are shown in Figure 2.1. Illustration of bulk magnetic material showing ferromagnetic (FM) phase or permanent magnet (Figure 2.1a). High remanence magnetization ( $M_r$ ) and high coercivity ( $H_c$ ) is shown as hysteresis curve (Figure 2.1c). For antiferromagnetic material (Figure 2.1b), electrons spins

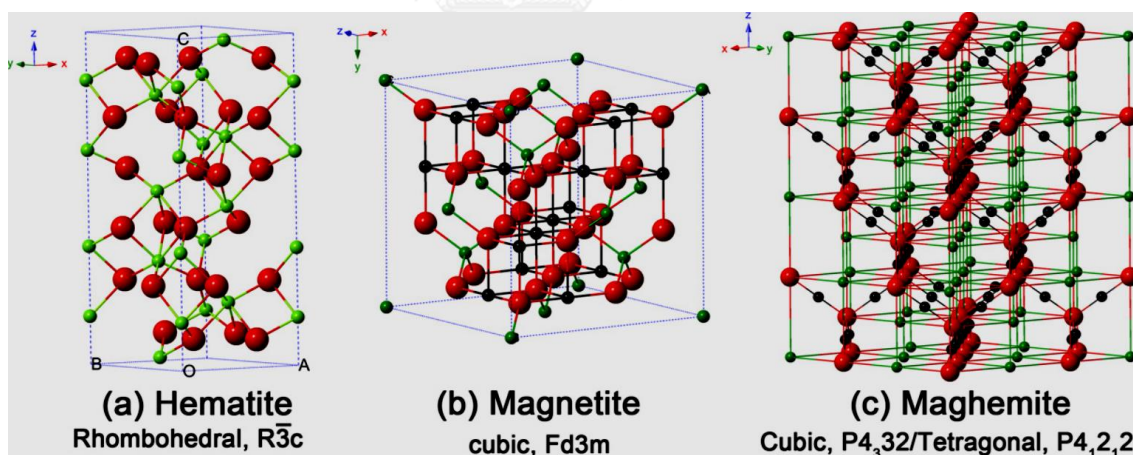
alignment in opposite directions with neighboring spins (different sub-lattices) causes weak magnetic response as shown in the curve in Figure 2.1f. Figure 2.1d illustrates that when bulk FM material size reduce to nanoscale (single domain), it demonstrates the superparamagnetic phenomenon, where the magnetic moments fluctuate depending on thermal energy. The superparamagnetic character shows no remanence nor coercivity, and no hysteresis loop as shown in the magnetization curve similarly to paramagnetic materials. Nevertheless, the magnetic response or magnetic susceptibility is similar to ferromagnetic or ferromagnetic in that the strong magnetization can be observed from intensity of magnetizations. [15, 16]



**Figure 2.1** The summary of different magnetic properties from intrinsic properties and properties arising when the size decreasing to nanomaterial. The spin arrangement in (a) ferromagnet (FM) and (b) antiferromagnet (AFM), (c) a magnetization curve of ferromagnetic bulk materials or permanent magnets, (d) the magnetic moments and magnetization curve of a superparamagnet (SPM), (e) an interaction at the interface layers of a ferromagnetic and an antiferromagnetic produces the exchange bias effect and (f) a magnetization curve of antiferromagnetic materials. ( $D$ =diameter,  $D_c$ =critical diameter) [16]



The iron oxide nanoparticle is one type of magnetic nanoparticles. It was generally called superparamagnetic iron oxide nanoparticle (SPION). There are three major crystalline structures of iron oxide including magnetite ( $\text{Fe}_3\text{O}_4$ ), maghemite ( $\gamma\text{-Fe}_2\text{O}_3$ ) and hematite ( $\alpha\text{-Fe}_2\text{O}_3$ ) structures as shown in Figure 2.2. Hematite is the most stable iron oxide under ambient condition, but the magnetic property is antiferromagnetic or weakly responsive under a magnetic field. Only magnetite and maghemite structures possess ferrimagnetic property, so they show stronger magnetic response. The structure of magnetite is a spinel with a formula of  $\text{AB}_2\text{O}_4$ , and the ferrimagnetic structures occur from alternating of Fe(II) and Fe(III) in lattices. Maghemite is oxidized product of magnetite that has the same lattice structure but all iron atoms are Fe(III). [17] When the bulk iron oxide (ferro- or ferrimagnetic) reduce in size to nanoscale, superparamagnetic phenomenon that we mentioned will arise. The iron-based nanoparticle or SPION become superparamagnetic at diameter of lower than 25 nm. [18]



**Figure 2.2** Iron oxide structures: (a) the hematite, (b) magnetite and (c) maghemite (the black ball is  $\text{Fe}^{2+}$ , the green ball is  $\text{Fe}^{3+}$  and the red ball is  $\text{O}^{2-}$ ). [17]

### 2.1.2 Magnetic nanocomposites with polymers

The nanocomposite is one type of composite materials with a combination of at least one nanoparticle combine with different nanoscale components or other bulk

matrices such as liposome, porous silica and polymer to improve the nanoparticle properties such as electrical, thermal, optical, electrochemical, catalytic properties, addition of functional groups and lower toxicity.[19]

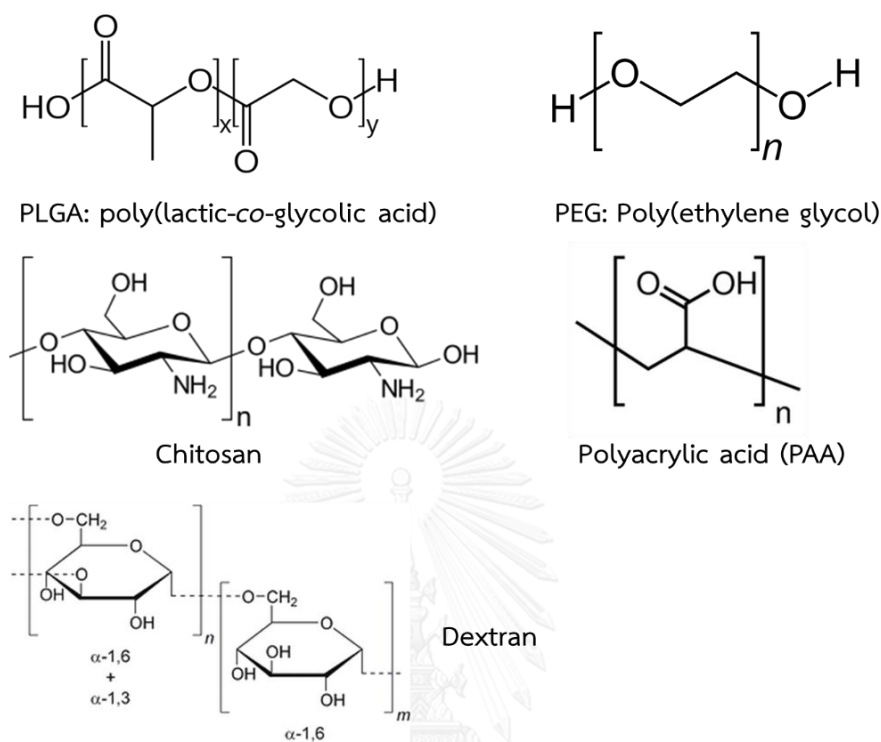
The magnetic nanoparticles or superparamagnetic iron oxide nanoparticle (SPIONs) are often coated or encapsulated using polymers to avoid agglomeration and modify their properties. In principle, the coating will generate electrostatic repulsion or steric repulsion around the SPION, so the SPIONs will disperse well as a stable colloid in solvent. SPIONs can be coated with polymers via chemically interaction such as covalent linkage, direct conjugation, click chemistry or physically adsorption (electrostatic, hydrophilic, hydrophobic interactions). [16, 20]

In biological applications, the SPIONs are often modified with functional groups on their surface for tagging drug, protein or gene and improving other activities. They will bind with suitable polymers containing functional groups such as phosphates (polyphosphoric acid), carboxylic acids (poly(lactic acid), poly (glycolic acid), poly( $\epsilon$ -caprolactone)), and sulfates (Poly(vinyl sulfate)).

Moreover, SPIONs can be coated with biocompatible polymers such as poly(lactic-co-glycolic acid), poly(ethylene glycol), dextran, polyacrylic acid and chitosan to reduce toxicity. [1, 20] The structure of these polymers are illustrated in Figure 2.3. For example:

- Poly(lactic-co-glycolic acid) or PLGA is negatively charged polyester, co-polymer of glycolic acid and lactic acid, which are biocompatible and biodegradable polymers.
- Poly(ethylene glycol) or PEG is a linear synthetic hydrophilic polyether and homopolymer of ethylene oxide.
- Dextran is a branched polysaccharide consisting of glucose subunits, and it is hydrophilic polymer.
- Polyacrylic acid is a synthetic homopolymers of acrylic acid, which is a weakly negatively charged polymer.

- Chitosan is a cationic and hydrophilic polymer that is biocompatible and bioabsorbable polymer.



**Figure 2.3** Biocompatible polymer structures illustration: poly(lactic-co-glycolic acid), poly(ethylene glycol), chitosan, polyacrylic acid and dextran.

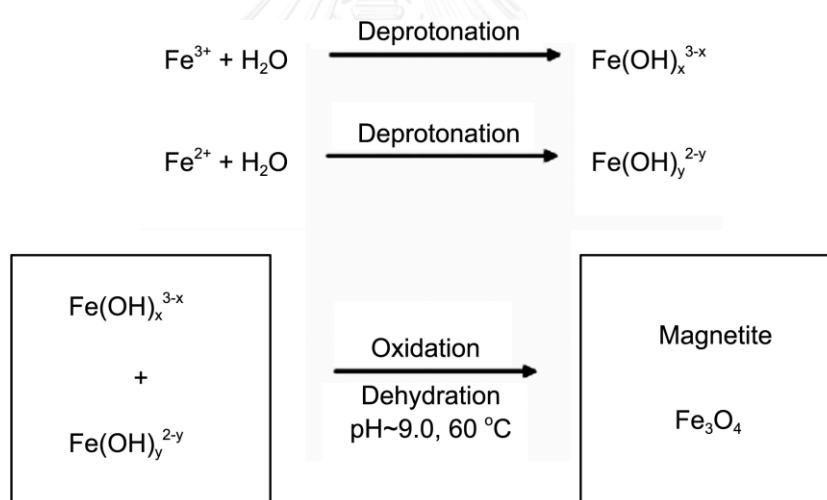
### 2.1.3 Principle of synthesis

#### 2.1.3.1 Magnetic nanoparticle synthesis

##### 2.1.3.1.1 Co-precipitation method

This method is an easy way to synthesize magnetic nanoparticles in aqueous medium, especially iron oxides nanoparticles (magnetite;  $\text{Fe}_3\text{O}_4$  or maghemite;  $\gamma\text{-Fe}_2\text{O}_3$ ) from aqueous  $\text{Fe}^{2+}$  or  $\text{Fe}^{3+}$  salt under basic condition at reaction temperature between 20 and 90 °C. The magnetic nanoparticle morphology and composition usually depend on the kind of precursor salts such as chloride, sulfate and nitrate salts. Moreover, the ratio of  $\text{Fe}^{2+}/\text{Fe}^{3+}$  ions, pH value, reaction temperature, and ionic strength of the solvent can affect the particle morphology. For example, of magnetic iron oxide nanoparticles was synthesized using co-precipitation method as shown in

Figure 2.4. [21] Generally, this method does not require stabilizing or reducing agents in the synthesis, but there are a few researches reported that the polymer stabilizer such as polyvinylalcohol (PVA) was used for controlling the nanoparticles sizes. From the experiment of co-precipitation synthesis, the saturation magnetization of magnetic nanoparticles are found in the range of 30–50 emu/g (for magnetite nanoparticles).[22] These values are lower compared to the bulk magnetite material of 90 emu/g. However, magnetite ( $\text{Fe}_3\text{O}_4$ ), nanoparticles from this method are not very stable under ambient conditions as they are easily oxidized to maghemite ( $\gamma\text{-Fe}_2\text{O}_3$ ) or dissolved in acidic condition. Maghemite exhibits similar ferrimagnet character, but oxidation problem is less than magnetite. Moreover, the maghemite particles remain chemically stable under alkaline and acidic conditions. Although this method is easy to use, it is difficult to control the particle size, and the resulted particles tend to be polydispersed.[16, 21]

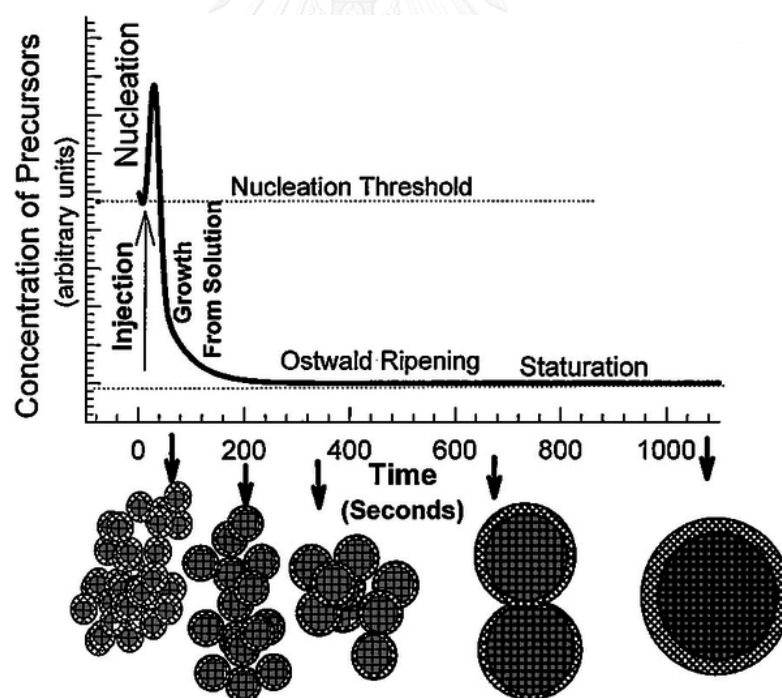


**Figure 2.4** Scheme for reaction mechanism of magnetic iron oxide (magnetite) nanoparticles in aqueous mixture of iron (III) and iron (II) chloride under basic condition. [21]

#### 2.3.1.1.2 Thermal decomposition method

Thermal decomposition method concept is a synthesis of high quality nanomaterials or semiconductor from oxides in non-aqueous media at high temperature. The synthesis of high quality magnetic nanoparticles from this method

has been developed for control size, shape and monodispersity of magnetic nanocrystals using thermal decomposition of organometallic precursors containing stabilizing surfactants in high boiling point organic solvents.[23] Normally, the precursors are metal organometallic compounds including metal oleate, metal acetylacetonates, metal cupferronates, (Metal = Fe, Mn, Co, Ni, Cr). [24, 25] The surfactants that are often used include fatty acids, hexadecylamine and oleic acid. In theory, the organometallic precursor, the surfactant, and solvent ratios are important parameters for the control of the size and morphology of magnetic nanoparticles. Moreover, reaction temperature and reaction time may also be essential in control of their morphology as exhibited in Figure 2.5. From the schematic illustration of the magnetic nanoparticles synthesized at high temperature in absence of surfactants, increase of particles size and agglomeration depend on reaction time.[26]



*Figure 2.5 Schematic of thermal decomposition method at 350 °C various time affecting nucleation and growth of the monodisperse nanoparticles.[26]*

### 2.1.3.2 Preparation of magnetic nanocomposites with polymer

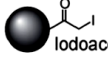

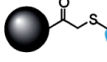
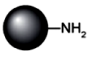
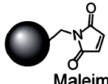

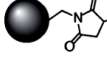
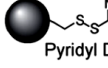

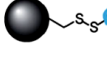
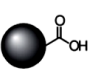
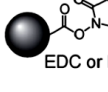
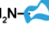
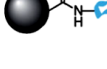
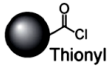
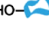
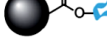


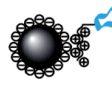
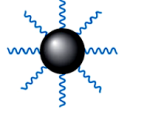

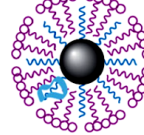
The magnetic nanoparticles or SPIONs have been modified with polymers and drug/gene by chemical or physical interactions using many methods such as conjugation via active ligands, electrostatic interaction, hydrophobic/hydrophilic interaction and emulsion/double emulsion method as shown in Table 2.1. [27, 28] The modification include:

- Direct nanoparticle conjugation. The reactive ligands are directly bonded on SPION surface with strong interaction. This method is not widely used to prepare the SPION-Polymer composite. It is often used for active ligands containing small molecules such as folic acid, peptides and antibodies.[20]
- Electrostatic interaction. This process is commonly used in the SPIONs loading plasmid DNA onto their surface. In general, the SPIONs are coated with cationic or anionic polymers on their surface, and these ion can interact with opposite ion from DNA or protein. Therefore, this method is suitable for carrying plasmid DNA, proteins or molecules with charge.
- Hydrophobic/hydrophilic interactions. This method is very useful for adsorbing neutral hydrophobic/hydrophilic drugs. The SPIONs are created with hydrophobic layers onto their surface that can adsorb hydrophobic polymers or drugs, and the drugs easily release in cell when the polymer coating degrades. In this method, the particles are sensitive to ambient conditions and difficult to control over molecular orientation of bound ligands. Therefore, this interaction is appropriate for drug loading and releasing at target cells.
- Emulsion. This process involves emulsion which is a mixture of two liquid phases such as water and oil phases that can emulsified with polymer containing both polar and non-polar functional groups. For controlling the stability of colloid emulsion, oil in water (o/w) phase can be performed using mechanical homogenizer or sonicator in presence of surfactants or emulsifiers and the non-polar molecule in oil will be encapsulated in the polar part of the surfactant. The double emulsion is similar to emulsion method, but there are

three phases of liquid such as water in oil in water (w/o/w). This process benefits for encapsulating drugs or other molecules that can be control released in various conditions.



**Table 2.1** Examples of SPION surface modification with polymers using various chemical and physical interactions. [20]

Linker chemistry conjugation					
Starting nanoparticle	Linker chemistry	Reactive ligand	Conjugate	Typical ligands	Notes
	 Iodoacetyl	+ HS- 			Stable linkage
 Amine	 Maleimide	+ HS- 		Activated small molecules, peptides, proteins, antibodies or aptamers	Stable linkage, sulfhydryl selective
	 Pyridyl Disulfide	+ HS- 			Sulfhydryl selective, cleavable under reducing condition
 Carboxyl	 EDC or DCC/NHS	+ H <sub>2</sub> N- 		Amine-containing molecules	Stable linkage
	 Thionyl Chloride	+ HO- 		Hydroxyl-containing small molecules	Reacts under anhydrous condition, cleavable under alkaline conditions
Physical interaction attachment					
Starting nanoparticle	Ligand	Functionalized nanoparticle	Typical ligands	Notes	
 Charged surface	+ 	 Electrostatic Interaction	Modified peptides, proteins or antibodies, DNAs or RNAs	Sensitive to the environment	
 Hydrophobic surface	+ 	 Hydrophobic Interaction	Hydrophobic molecules	Sensitive to the environment	

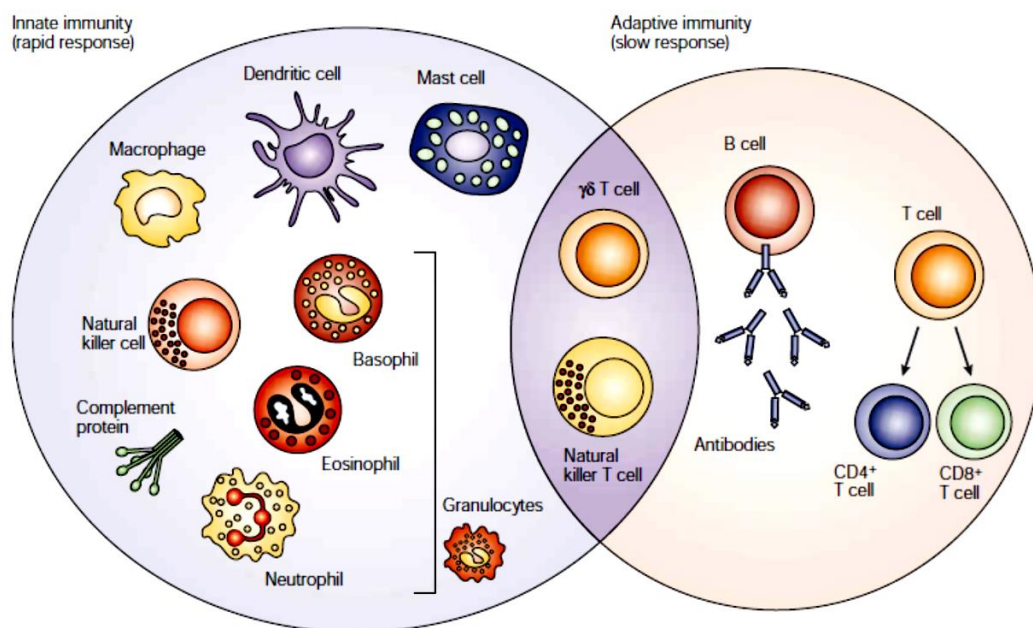
## 2.2 Principle of Immune System and Vaccine Delivery

### 2.2.1 Principle of immune system and immune response

The immune system is a defense system (against diseases) of human or animal body that consists of several biological structures and involving many processes in organisms. There are two types of immunities divided by the difference in specificity, which are innate and the adaptive immunities. Figure 2.6 shows two types of immune cells: the innate cells (dendritic, granulocytes, mast cells, natural killer cells and macrophage cells) and adaptive cells (T cell and B cell lymphocytes). Moreover, natural killer T cells and  $\gamma\delta$ T cells are at the interface of innate and adaptive systems. Innate immunity is the first line defense that provide immediate host defense, but it



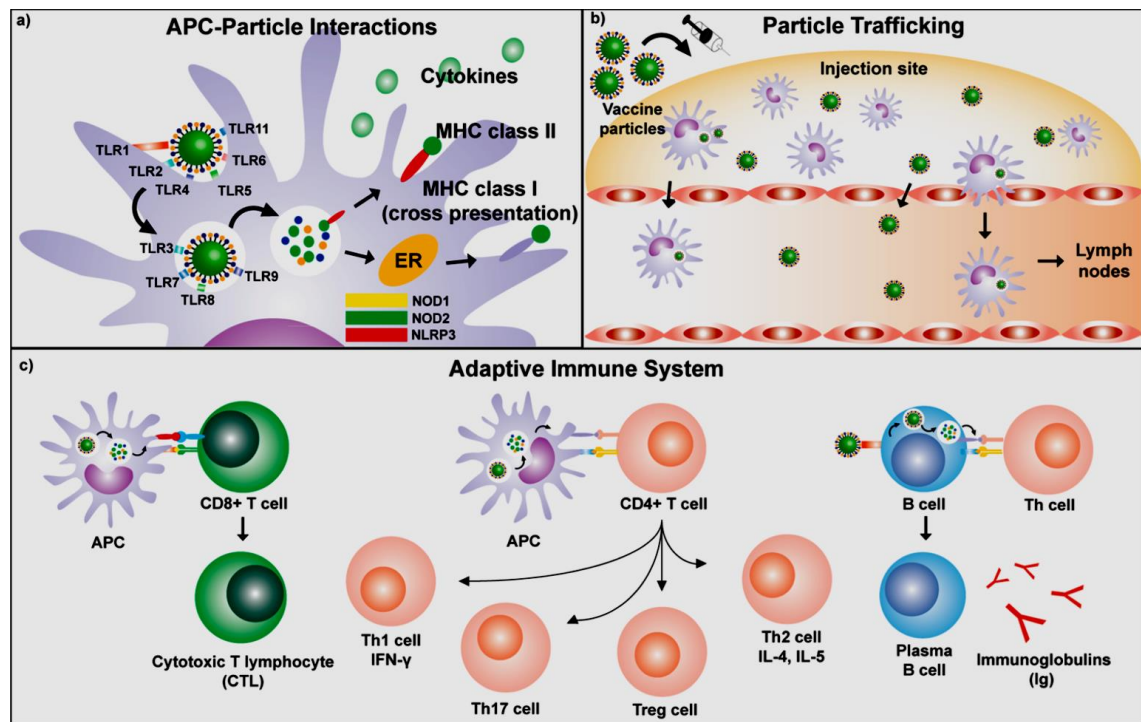
lacks of specificity and has risk to damage normal tissues. This immune is greatly seen in many species even the simplest. Adaptive immunity or specific immunity is found in higher animals such as human. This immune consists of antibody-specific reactions against the antigen from pathogens. The adaptive response is very specific, and it can create immunological memory, but it takes much time (several days or weeks) to develop more robust and rapid responses.[29, 30]



**Figure 2.6** Illustration of the immune cells divide into two major types: innate and adaptive immunities with the straddle at the interface.[30]

In immune system, innate and adaptive immunities are in collaboration, leading to high potential to fight against the pathogens. Innate immunity is the first line defense. In addition, this system comprises an antigen presenting cell (APC), including dendritic cells (DCs), macrophages and B cells, which bridge between innate and adaptive immunity. Figure 2.7 demonstrates the activation of adaptive immunity by DCs, the most potent APCs. After DCs are activated by pathogens or vaccine via intramuscular, intradermal, oral, or mucosal routes (Figure 2.7a), they undergo maturation and migrate to lymphoid organs via lymphatic systems (Figure 2.7b). Subsequently, DCs present antigen via major histocompatibility complex (MHC) to activate T cells. Moreover, DCs secrete cytokines to control and direct T cell

differentiation. Cytotoxic T lymphocytes (CTLs, effector CD8 T cells) are important to fight against intracellular pathogens, virus and cancer, while T helper (Th) cells (effector CD4 T cells) secrete cytokine to support antibody production from B cells and exert other immune and non-immune cell functions.



**Figure 2.7** The illustration of how pathogen or vaccine particles induce innate and adaptive immune responses. **(a)** Vaccines are taken via intramuscular, intradermal or other ways, and then they confront the local immune cells such as DCs. **(b)** The antigens induce DC maturation and migration from muscle to lymphoid organs through blood or lymphatic systems. **(c)** DCs present an antigen to CD8 and CD4 T cell via MHC I and class II, respectively. In addition DCs express co-stimulatory molecules to activate T cells. After activation, CD8 T cell differentiate to CTLs and CD4 T cell differentiate to Th cells. CTLs directly killing the target cells infected by pathogens while T helper (Th) cells support B cells to generate antibody, and help other cells. [31]

### 2.2.2 Principle of vaccine delivery

Vaccination is the most proficient way to prevent or reduce risk of infection caused by bacteria, viruses, or other pathogens. There are several types of prophylaxis vaccines of infectious diseases such as measles, rubella, tetanus, pertussis and yellow fever, leading to the decrease in global death. The conventional vaccine made from attenuated or inactive pathogens, which is successfully protect against infectious disease. However, there is a safety concern of the conventional vaccine since those attenuated or inactive pathogens may become active inside human body. In addition, this the vaccine contains some dangerous part of pathogen so it can cause immune-adverse effects. Therefore the development of subunit vaccine, adjuvant and vaccine delivery system is essential strategy for future vaccine.

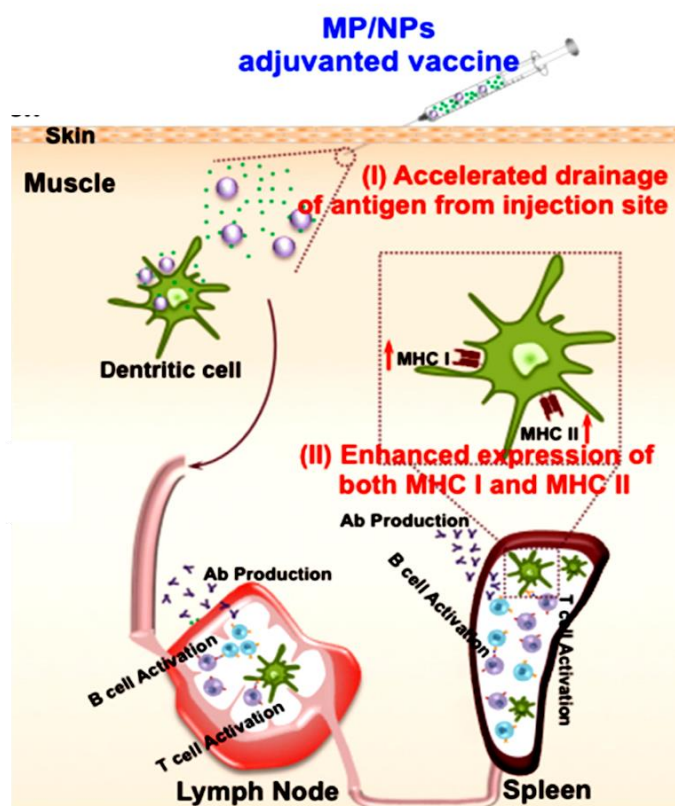
Recently, micro- or nanoparticle-based adjuvant (commonly polymer-based) is more advantageous than traditional vaccine due to its safety, and its properties of pathogen mimicking in size and structure, leading to the preferential interaction with APCs. Moreover, the particle can protect an antigen from rapid enzymatic degradation and denaturation. Thus, the particle-based adjuvant is turning into a promising tool for the potential antigen carrier to target on APCs.[1]

The particle-based vaccine delivery injected via intramuscular or intradermal route provides a longer time for antigen uptake and enhance APC activation as shown in Figure 2.8.[1, 32] In some strategies, the particle is designed to help an antigen escape from a lysosome. By this process, the strong CTL response is generated (Figure 2.9). The positive charge of particles is preferred for endosomal escape because it can lead to osmotic swelling and physical rupture of lysosome. However, the high-positive charge polymer is of concern due to their cytotoxicity.

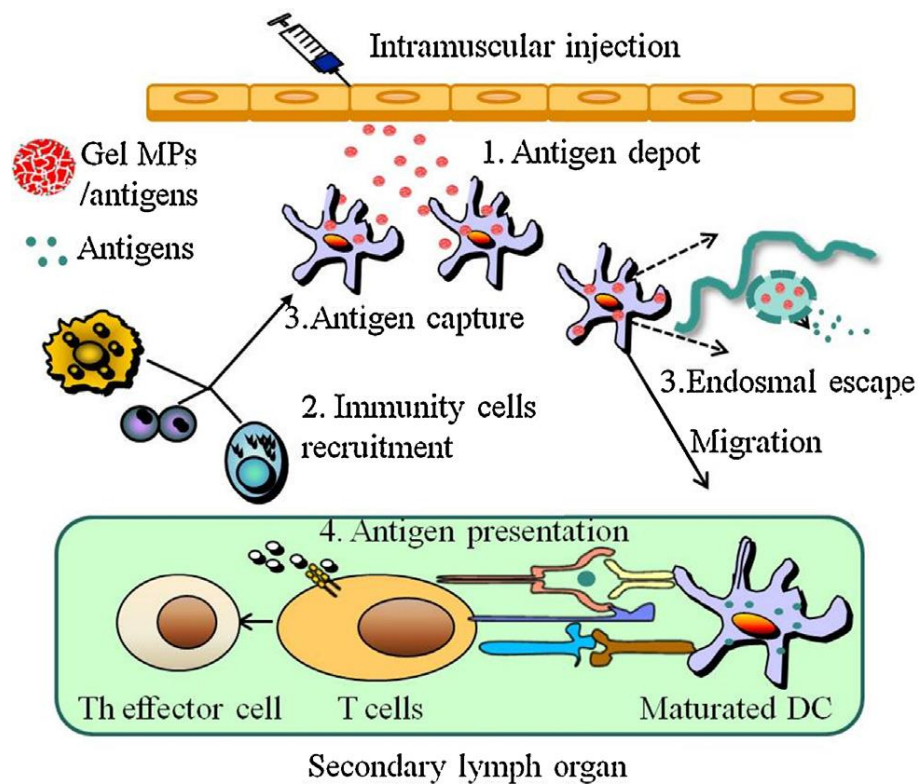
In the vaccine delivery experiment, there are two major types of the cell divided from sources of cells. The two types of cells are cell line and primary cell. Cell lines are continually passaged cells over a long time period and they are a pure population (same homogenous genotypic and phenotypic characteristics), so they can give reproducible results. The cell lines have acquired the ability to proliferate indefinitely,

occasionally through modifications. These cells are easy to use and cost cheaper than primary cells, but they are less biologically relevant as they have lost some characteristics of the original tissue because they were isolated from the tissues for a long time. The common immune cell lines are such as macrophage cell line (Raw 264.7 and J774A.1 cells) and dendritic cell lines (Jaw II cells). [33]

For the primary cells, they are isolated directly from animal or human tissue and the cells cannot be passaged and kept for a long period of time. They are carefully cultured in well-controlled environment supported with medium containing essential nutrients and growth factors, so it is high cost to support their proliferation. However, they have more advantages compared to cell lines such as they have true characteristics of the tissue, so they can represent the cells in various organs. The immune primary cells are usually from bone marrow cells such as bone marrow dendritic cells (BM-DCs) and macrophage cells (BM-MCs). [34]



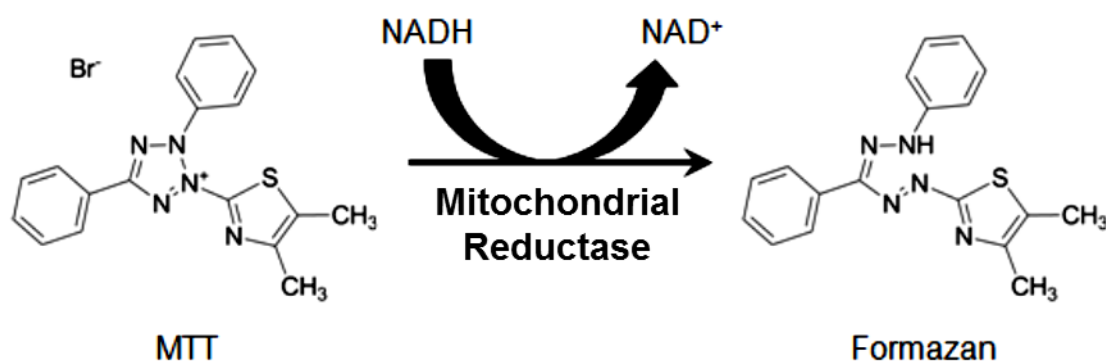
*Figure 2.8 Schematic diagram of immunological mechanism of micro- or nanoparticles adjuvant carrying antigen [1]*



**Figure 2.9** Schematic diagram of immunological mechanism of endosome escape enhancement using the particle carriers (Gel MP) in vaccine delivery system [1]

### 2.2.3 Principle of cytotoxicity testing (MTT assay)

The MTT assay or 3-(4,5-dimethylthiazol-2-yl)-2,5-diphenyltetrazolium bromide reduction assay is a colorimetric detection for analysis of cell viability assessing from cell metabolic activity. In the viable cells, mitochondrial reductase or NADPH oxidoreductase enzymes are present, and this enzyme can reduce the MTT (yellow) to formazan (purple) as exhibited in Figure 2.10. The color change is determined using the absorbance at the wavelength of 570 nm (formazan color), which is related to number of survival cells. This technique is easy, but there is a limit on detection accuracy as it depends on the cellular metabolic activity. The cells may not die, but they have low metabolic activity and give positive results.



**Figure 2.10** Reaction of MTT (yellow) with mitochondrial reductase to yield the Formazan product (purple).[35]

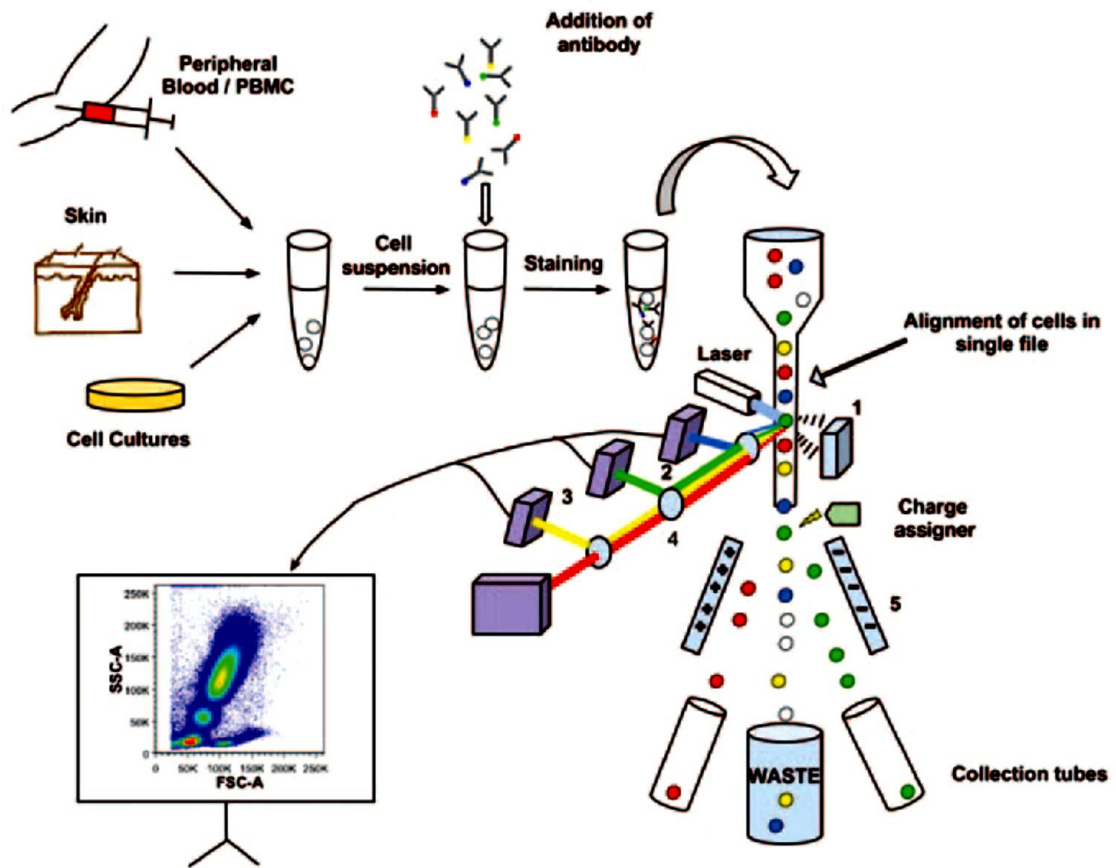
#### 2.2.4 Principle of measurement of immune response

The immune response is usually detected from the surface maturation marker expression and cytokine production from antigen presenting cells using flow cytometry and ELISA, respectively. The detail of these processes are discussed below.

##### 2.2.3.2 Flow cytometry analysis (FACs)

Flow cytometry analysis is a technique widely used to measure the maturation marker on the cell surface because it can detect the population of cells. The flow cytometry is a laser-based detection that measures single flowing of cells through a detector system as shown in Figure 2.11. In the first step, the cells are stained using fluorescent-labeled antibodies specific with cell surface marker of interest. Then, the cells are introduced into the flow cytometer toward a laser. The fluorescent dyes to bind with antibody (fluorophores) are selected based on the specific wavelength of the laser. If cells possess the marker on the surface, the bound antibody–fluorophore will absorb the laser energy in form of light and release energy at specific wavelength when the cells pass through the laser. The emitted light is detected by a fluorescent detector (Figure 2.11 No.2-3). Furthermore, the size and complexity of cells are measured using the light forward and side scattering (FSC and SSC) simultaneously.[36]



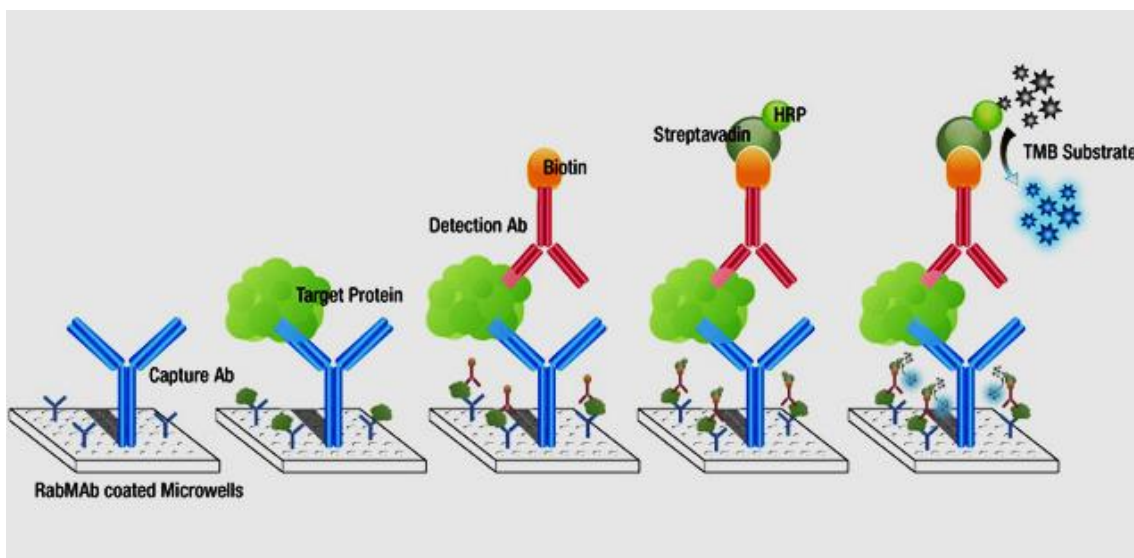


*Figure 2.11 Schematic diagram of a flow cytometer illustrates the cells staining and apparatus in a flow cytometer (1) Forward-scatter detector, (2) side-scatter detector, (3) fluorescence detector, (4) filters and mirrors, and (5) charged deflection plates. (FSC = forward scattering and SSC = side scattering) [36]*

### 2.2.3.3 Sandwich enzyme-linked immunosorbent assay (Sandwich ELISA)

The enzyme-linked immunosorbent assay or ELISA is a detection of a color change of substances when the antibody binds to its specific antigen such as cytokines or other proteins. The schematic process is demonstrated in Figure 2.12. For Sandwich ELISA technique, at first, the capture antibody is immobilized on the micro-plate surface. Then, the samples containing the cytokine (or target protein) are added. Subsequently, the enzyme HRP-tagged detection antibody is added to bind to the cytokine. Finally, TMB (3,3',5,5'-Tetramethylbenzidine) substrate is added to react with

the HRP enzyme, and this reaction generate the blue color product. If the cell samples can secrete the specific cytokine, we can detect amount of the cytokine by measuring the absorbance of the blue color product. [37]



*Figure 2.12 Schematic representation of sandwich ELISA process. [37]*

## 2.3 Literature Reviews

### 2.3.1 Superparamagnetic iron oxide nanoparticles (SPIONs) in drug delivery

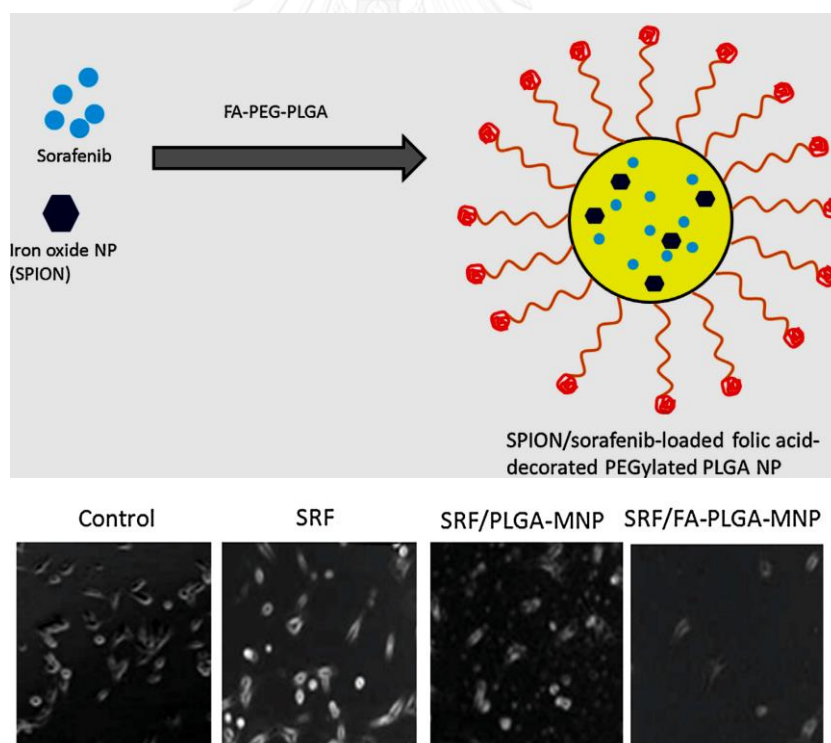
The superparamagnetic iron oxide nanoparticles (SPIONs) are widely used in biomedical applications especially drug and gene delivery systems because of their superparamagnetic character as mentioned above. However, SPIONs lack of functional groups for loading of drugs. Therefore, many researches studied about the SPIONs collaborated with polymers for tagging the drug and gene and reducing SPIONs toxicity for used in delivery system.

In previous researches of SPIONs composited with polymer were used in drug and gene delivery to treatment cancer cells *in vitro* such as Yu and co-workers (2015). They prepared a composite of SPIONs with anticancer drug (sorafenib) encapsulated in PLGA (poly(lactide-co-glycolide)) for liver cancer therapeutics. The results showed that particles enhanced drug uptake and effectively inhibited the cancer cells colony



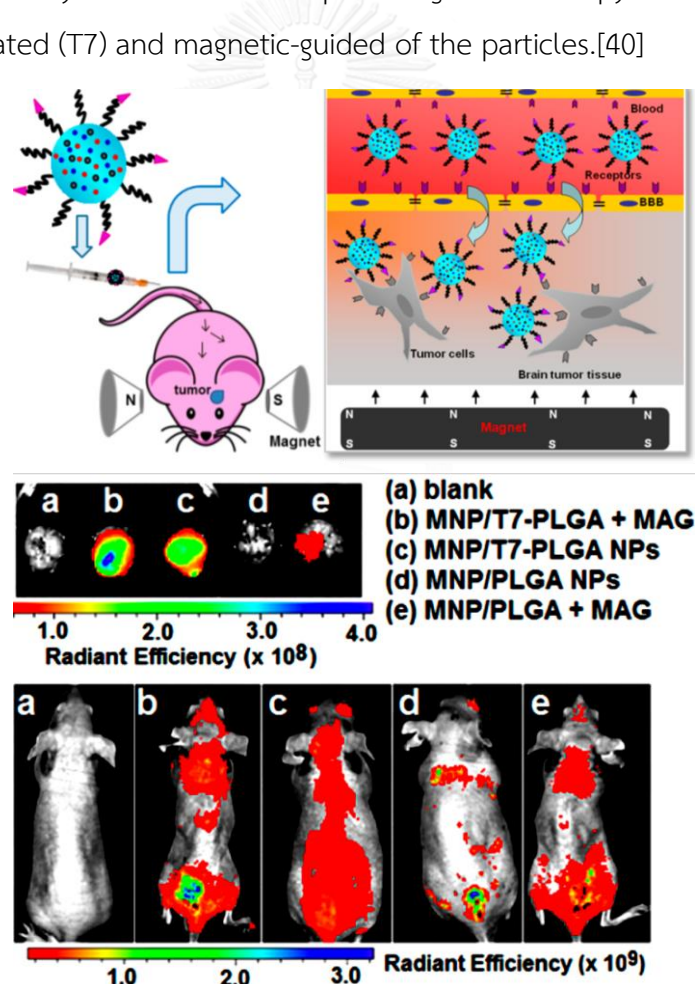
comparing to the cells with only sorafenib drug as shown in Figure 2.13. Tingting and co-workers (2016) synthesized SPIONs coated with silica and polyethylenimine (PEI) for doxorubicin (DOX) drug and gene delivery to the tumor cells *in vitro*. The synthesized nanocomposites with the sizes of 200 nm could deliver the drug and gene to treat the tumor cells and inhibit the tumor cell proliferations under an induction of a magnetic field. Moreover, this nanocomposite without the drug/gene was not toxic to the normal cells (HUVECs cell). [38]

Moreover, from the work by Beibei and co-workers (2016), magnetic nanoparticles (SPIONs) and the drug model were encapsulated in thermo-sensitive PNIPAM polymer (poly(N-isopropylacrylamide)) and silica for cancer thermo-chemotherapy. The investigation found that SPION/PNIPAM/silica particles could potentially deliver the drug model to the cancer cells under an external magnetic field with the control of drug release at 45 °C.[39]



**Figure 2.13** Schematic representation of folate conjugated PLGA encapsulating sorafenib and SPIONs for cancer cells treatment with various formulations (SRF = sorafenib drug, MNP = magnetic nanoparticles and FA = folic acid).

There are investigation on the drug delivery system *in vivo* study using SPIONs-polymer composites such as a research by Yanna and co-workers (2016). The prepared magnetic nanoparticle (MNP) encapsulated in PLGA were coated with transferrin receptor-binding peptide T7 for co-delivery of paclitaxel and curcumin drug for brain tumor therapy *in vivo* (Figure 2.14). The results showed that in presence of an external magnetic field, the SPIONs-PLGA can enhance delivery of paclitaxel and curcumin drug to tumor cells and inhibit the brain tumor cells proliferation (*in vitro*). Moreover, this system can enhance delivery to targeting mice brain as shown in Figure 2.14(b) (MNP/T7-PLGA + MAG; blue signal showed the most intensity of particles into the brain tumor cells). The system exhibited improved glioma therapy efficacy because of receptor-mediated (T7) and magnetic-guided of the particles.[40]



**Figure 2.14** Schematic Illustration of MNP/T7-PLGA particles and tumor-targeting delivery via the T7-mediated and magnetic-guided (*upper figure*). The nanoparticle

*distribution in mice imaging after injection via tail vein at 4 hours (MAG = magnet) (lower figure).[40]*

Besides the cancer cells treatment, the SPIONs collaborated with polymer were used in other deliver systems such as SPIONs-PLGA containing amoxicillin drug to treat disease sites at the gastrointestinal tract under a magnetic induction and control release (PLGA can degrade at low pH of gastrointestinal tract). [21] In addition, polyacrylic acid-coated SPIONs were used in anti-mycobacteria delivery drug for tuberculosis (TB) therapy. The results showed that this system could enhance the inhibition of bacterial growth, and non-toxic to normal cells.

### 2.3.2 Polymer-based micro/nanoparticles design for vaccine delivery

The polymer-based particles are widely used in vaccine delivery system due to the ability to tune the functional group, morphology and other advantages mentioned before. Therefore, there are many previous studies showing the design of the size, shape, charge and hydrophobicity of the polymer for better uptake and stimulating the APCs.

Particle size plays a crucial role in antigen loading, particles uptake into the cells and may affect immune responses. Kanchan and Panda (2007) studied the effect of the size of antigen-loaded polylactide (PLA) particles on macrophage cell line (J774A.1) interaction and the immune response. The PLA microparticles (20  $\mu\text{m}$ ) showed the most antigen loading but their size is similar to the size of J774A.1, thus they could not penetrate into the J774A.1. PLA microparticles (2–8  $\mu\text{m}$ ) could load more antigen and continuously release antigen resulting in higher J774A.1 response than nanoparticle size. However, PLA nanoparticles (400 nm) are efficiently phagocytosed by APCs (J774A.1) and promote cell mediated immune response but with lower response because of less antigen loading.[41]

Manolova and co-worker (2008) observed efficiency of polystyrene particles tagged with fluorescence dye with the size of 20, 500 and 1000 nm to dendritic cells uptake and kinetics of transfer to the lymph node. The results showed that particle size of 20 nm is the fastest uptake into dendritic cells and had already arrived in

popliteal lymph node after 2 h injection because they are very small, and their sizes are similar to virus, which is known to be well transfect into immune cells. In contrast, the particles sizes of 500 and 1000 nm remained at the injection site. [42]

Moreover, Yue and co-workers (2010) investigated the effect of chitosan particles with the size ranging between 430 nm and 4.3  $\mu\text{m}$  for murine macrophage cells (J774A.1) uptake and activation (Figure 2.15). The particle size of 430 nm showed high internalization to J774A.1 cells, and this size can activate the cells to express maturation marker such as cluster of differentiation CD80 and CD86, and secret the cytokine IL-10, IL-12, TNF- $\alpha$  and IFN- $\gamma$  more the particles of the larger sizes (1.9 and 4.8  $\mu\text{m}$ ).[43]



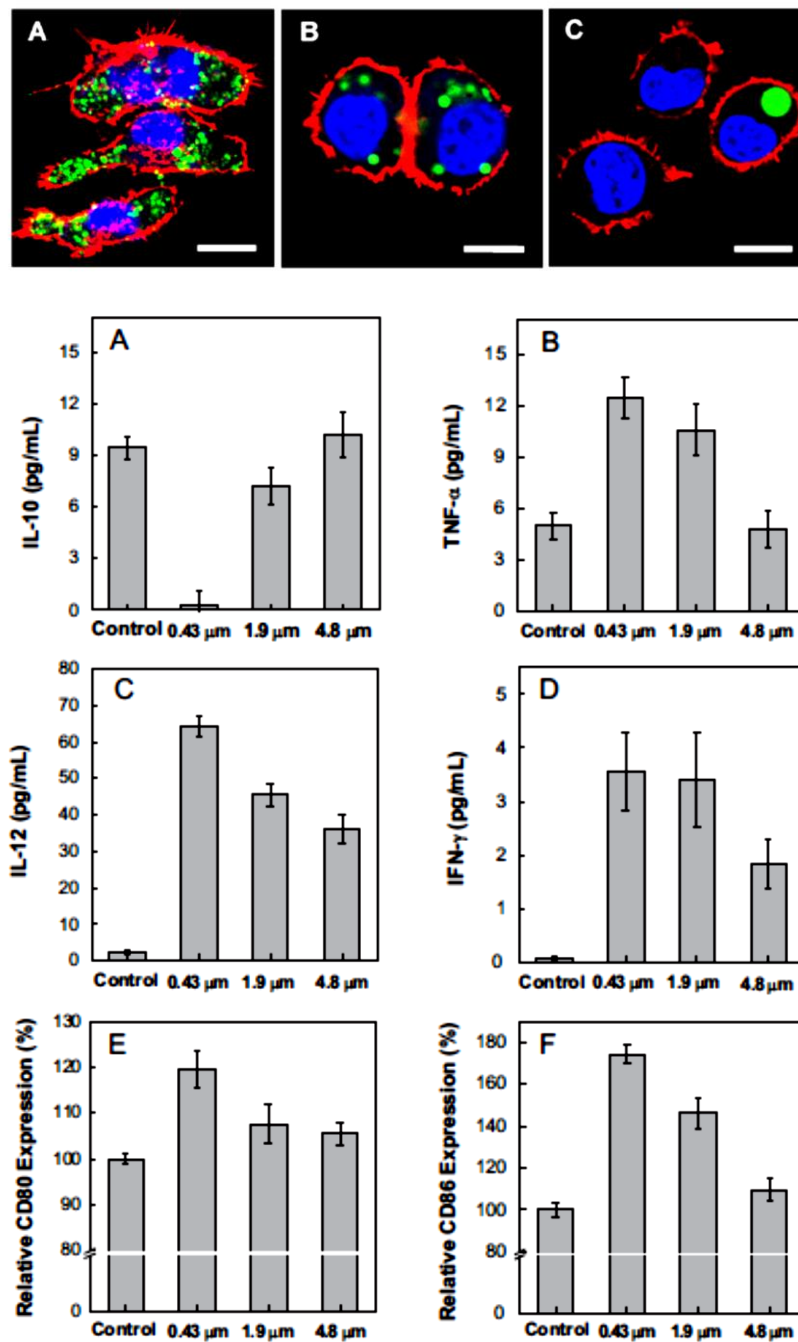


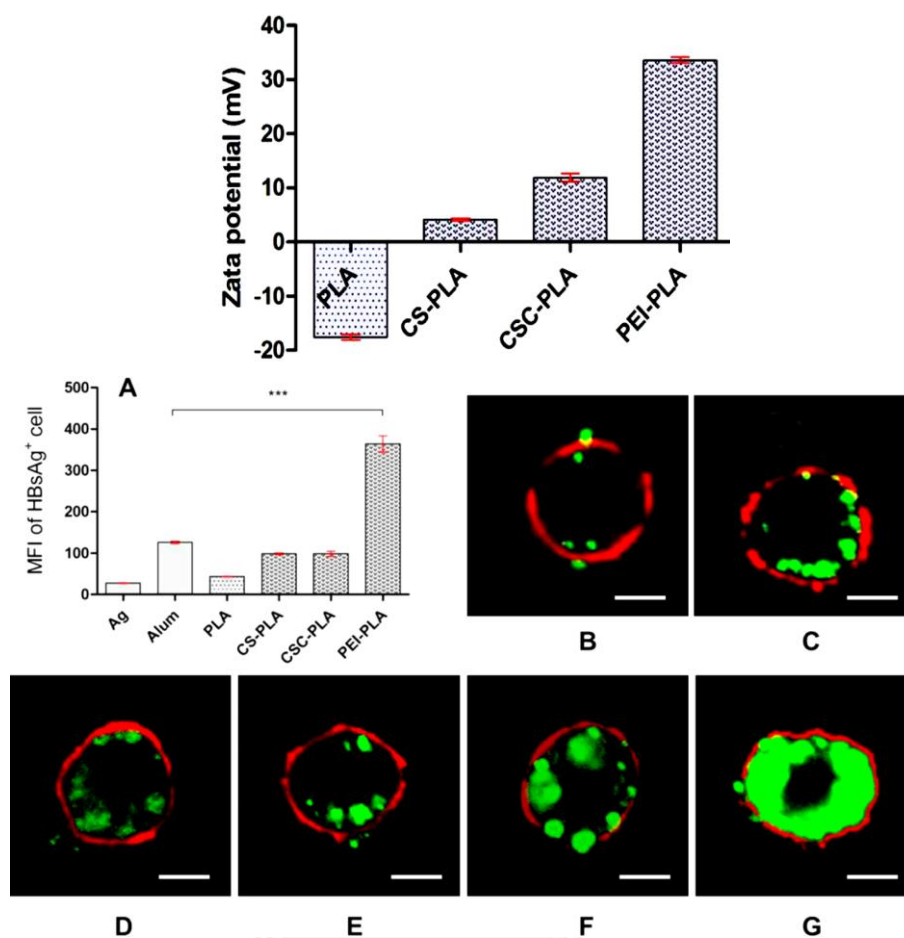
Fig. 6. Cytokine profile of macrophages after stimulation with different sized particles.

Figure 2.15 Confocal microscope images of macrophages (J774A.1) after 24 h incubation with 300 µg/mL of 430 nm (A), 1.9 µm (B) and 4.8 µm (C) chitosan particles (upper figures). Cytokine production (A-D) and surface marker (E-F) of J774A.1 after activation with particle of different sizes (lower figures).

Particle surface charge is one of important features that affects the distribution, the APCs uptake, immune response and cytotoxicity. Yue and co-worker (2011) investigated effect of the chitosan-based nanoparticles (size 200 nm) surface charge on the cells line (epithelial, endothelial and blood cells) uptake and intracellular trafficking. From the results, positive charge could increase the cellular uptake more than neutral and negative charge because cell membrane is negatively charged, and positively charged particles could escape from lysosome after cellular uptake.[44]

Chen and co-worker (2014) prepared PLA particles (size 800 nm) of various surface charges (-17 to +33 mV of zeta potential) for investigation of vaccine delivery systems effect on the mice and detection immune response of the macrophage cells. This study revealed that cationic surface of modified PLA could be effective for antigen loading and enhancement in antigen uptake by APCs, leading to the promotion of the cytokines production better than PLA with other charges (Figure 2.16). However, the surface molecule expression (MHC I, MHC II and CD86) did not show significantly difference between the most positively charged PEI-PLA (+33 mV) and moderate positively charged CSC-PLA (+16 mV).[45]

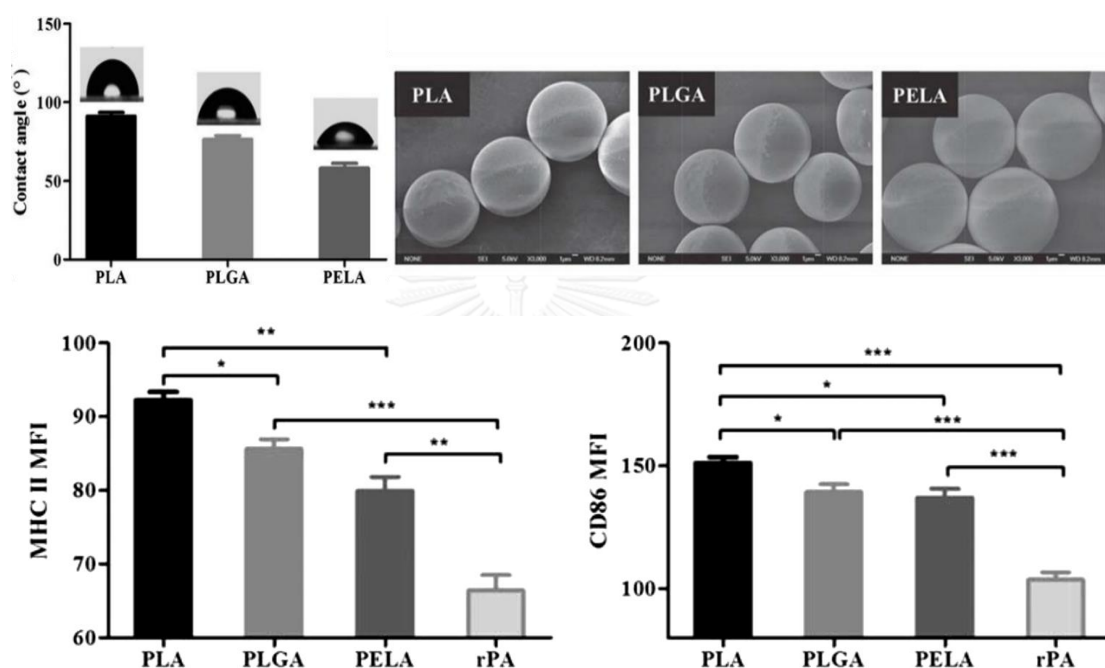




**Figure 2.16** Zetasizer analysis of surface charge on PLA modified with chitosan (CS), chitosan chloride (CSC) and polyethylenimine (PEI) (**upper figure**). MFI graph and fluorescent microscope images of distribution of particles and the antigen (Ag) delivery to macrophage cells, **B-G**, showing Ag and particles-based carriers as listed in graph **A** (**lower figures**). (MFI = mean fluorescence intensity from flow cytometry analysis, Green and Red signals represent particles and cell membrane, respectively)

Surface hydrophobicity also plays an essential role in the interaction between particles and APCs. Liu and co-worker (2013) observed the various hydrophobicity of polymer microparticles (1  $\mu\text{m}$  in diameter) including poly(D,L-lactic acid) (PLA), poly(D,L-lactic-co-glycolic acid) (PLGA) and poly(monomethoxypolyethylene glycol-co-D,L-lactide) (PELA) in dendritic cell internalization and immune response. The contact angles (Figure 2.17) showed that PLA exhibits highest contact angle (90°) or the

strongest hydrophobicity. The increased surface hydrophobicity (PLA microparticles) greatly promoted more antigen into dendritic cells as observed from MHC II and CD86 expression on the cells. Owing to the cell membranes forming lipid bilayer, they exhibit a hydrophobicity between the layers. Therefore, strong hydrophobic and high-molecular weight polymers particles tend to show more efficient and rapid cellular uptake. [46]



**Figure 2.17** Contact angles of various polymeric particles for evaluation of hydrophobicities and SEM images of particles for observation of their shapes and sizes.

Finally, particle shape is an integral property that is believed to be associated with their uptake efficacy. Nevertheless, the shape effect are difficult to study because non-spherical shape are difficult to synthesize upon limited material choices and restricted techniques. Therefore, there are few reports studied the effect of shapes on the cellular uptake but no report involved the effect on immune response. Barua and co-worker (2013) investigated the interaction of the polystyrene of nanospherical, nanorod and nanodisk shapes to three types of breast cancer cell lines and the effect of shapes on cellular uptake. The results showed that nanorods and nanospheres were



quickly internalized to cells depending on the breast cancer cell types.[47] Moreover, another investigation found that the cellular uptake behavior of nanospheres and nanorods in the interplay with different kinds of cells (including endothelia cells and macrophages).[1]

To summarize, the small particles with the size less than 500 nm showed enhancement in cellular uptake. Moreover, the particles of very small size of around 10 to 20 nm could drain lymph nodes and activated the immune cells very well, but they were reported to cause potential cytotoxicity. For the particle surface charges, the positively charged particles demonstrated effectiveness in tagging the antigen (electrostatic interaction) and enhancing cellular uptake and immune response due to the negative charge on cell membrane could well interact with positively charged particles. Nevertheless, the very highly positively charged particles such as PEI polymer exhibited higher toxicity than the slightly positively charged and the negatively charged particles. Moreover, the high hydrophobicity polymer-based particles and nanorod or spherical shape displayed rapid APC uptake because of the reasons that we mentioned before. [1, 48]

From literature reviews of polymer-based particles on immune response, it is a tendency that highly particle uptake is related to high immune response. Moreover, previous reports showed that SPIONs can enhance drug uptake into cells. PLGA is one of the interesting polymers that is widely used to modify SPIONs because it is a biocompatible polymer, and it can gradually release drug at the targeting organs. However, the report of SPIONs encapsulated into PLGA for vaccine delivery systems were not found. Therefore, I am interested in SPIONs incorporated with PLGA or other biocompatible polymers for enhancing cellular uptake and APC activation. Furthermore, spherical particles with size 500 nm and below were reported to be the suitable range for vaccine delivery and chosen in this study.

## CHAPTER III

### EXPERIMENTS

The experimental section is divided into three parts. The first part is the synthesis of superparamagnetic iron oxide nanoparticles (SPIONs), the second part is the preparation SPIONs composited with the biocompatible polymers, and the last part is the investigation of SPIONs-polymer particles in delivery of the protein (BSA/SPIONs-Polymer) for activation the immune cells *in vitro*.

The instruments, chemicals, and biological reagents which are used for the syntheses of SPIONs, SPIONs-polymer and their immunological response were listed below.

**Table 3.1** List of instruments

The Instrument	Model
X-ray Powder Diffraction Spectrometer (XRD)	DMAX2200/Ultima <sup>+</sup> (Rigaku)
Transmission Electron Microscope (TEM)	Tecnai F20 (Philips Electron Optics)
Fourier Transform Infrared Spectrometer (FTIR)	Impact 410 (Nicolet)
Inductively Coupled Plasma Optical Emission Spectrometer (ICP-OES)	Perkin Elmer Optima 2100
Field-Emission Scanning Electron Microscope (FESEM)	JSM7610F (JEOL)
Centrifuge	Centaur 2 (Sanyo)
Magnetic Stirrer	MS 101 (Gem)
Handheld Homogenizer	D-160 Handheld Homogenizer (D Lab Instruments Limited)
Thermogravimetric Analysis (TGA)	Pyris 1 TGA (Perkin Elmer)
Vibrating-Sample Magnetometer (VSM)	LakeShore Model 7404
Particle Size Distribution Analyzer (ZSP)	Zetasizer ZSP
UV-Visible Spectrophotometer	HP 8453

Microplate Reader	Biochrom Anthos Zenyth 200 Microplate Reader
Fluorescence Microscope	BX50 (Olympus)
Flow Cytometric Analysis (FACS)	FACS Calibur <sup>TM</sup> (BD Bioscience)
pH meter	Eutech
Superconducting Quantum Interference Device-Vibrating Sample Magnetometer (SQUID-VSM)	Quantum Design MPMS

**Table 3.2** List of chemical

Chemical	Suppliers
Iron (III) chloride (FeCl <sub>3</sub> )	Aldrich
Iron (II) chloride (FeCl <sub>2</sub> )	Aldrich
Oleic acid (C <sub>16</sub> H <sub>34</sub> O <sub>2</sub> )	Merck
Sodium hydroxide (NaOH)	Merck (pellet for analysis)
Ammonium hydroxide 25% (NH <sub>4</sub> OH)	ACI Labscan
Ethanol (C <sub>2</sub> H <sub>5</sub> OH)	Merck
n-Hexane (C <sub>6</sub> H <sub>14</sub> )	Carlo erba
1-Octadecene (C <sub>18</sub> H <sub>36</sub> )	Aldrich (technical grade)
Ammonium hydroxide (NH <sub>4</sub> OH)	Merck (AR grade 25%)
2-Propanol (C <sub>3</sub> H <sub>7</sub> OH)	Univar (AR grade)
Dichloromethane (CH <sub>2</sub> Cl <sub>2</sub> )	Lab scan (AR grade)
Resomer® RG 504 H, Poly(D,L-lactide-co- glycolide) (PLGA) MW. = 38,000-54,000 g/mol	Aldrich
Poly(acrylic acid) MW. = 9,000-10,000 g/mol	Sigma
Poly(vinyl alcohol) (PVA) MW. ≈ 1,800 g/mol	Aldrich
Poly-L-lysine hydrobromide	Sigma
5-Carboxy-tetramethylrhodamineN-succinimidyl ester (TAMRA)	Sigma
Bovine serum albumin (BSA)	VWR international

Chloroform	ACL Labscan
n-Octylamine	Sigma
Dimethylformamide (DMF)	ACL Labscan
1-Ethyl-3-(3-dimethylaminopropyl) carbodiimide hydrochloride (EDC)	Chem-Impex
Sodium hydroxide pellet (NaOH)	Univar
Hydrochloric acid (HCl)	ACL Labscan
Paraformaldehyde	Sigma
Disodium hydrogen phosphate (Na <sub>2</sub> HPO <sub>4</sub> )	Univar
Potassium dihydrogen orthophosphate (KH <sub>2</sub> PO <sub>4</sub> )	Univar
Sodium Chloride (NaCl)	Univar
Potassium Chloride (KCl)	Univar
4',6-Diamidine-2'-phenylindole dihydrochloride (DAPI)	Sigma
5-TAMRA, SE (5-Carboxytetramethylrhodamine, Succinimidyl Ester (TAMRA)	Sigma

**Table 3.3** List of biological reagents

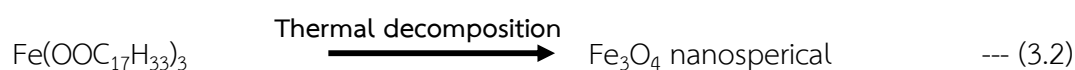
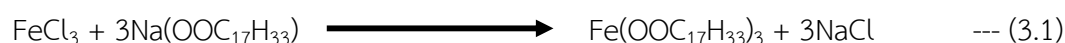
Biological reagents	Suppliers
Dulbecco's modified Eagle's medium (DMEM)	Gibco™ Life Technologies
Roswell Park Memorial Institute medium (RPMI 1640)	Gibco™ Life Technologies
Sodium pyruvate	Gibco™ Life Technologies
Glutamax	Gibco™ Life Technologies
Fetal bovine serum (FBS)	Gibco™ Life Technologies
Penicillin-streptomycin	Gibco™ Life Technologies
ELISA kits	Biolegend
Purified anti-mouse CD16/32 monoclonal antibody (mAb)	Biolegend
PerCP/Cy5.5-labeled anti-mouse I-A/I-E mAb	Biolegend

FITC- labeled anti-mouse CD80 mAb	Biolegend
APC- labeled anti-mouse CD11c mAb	Biolegend
PE- labeled anti-mouse CD86 mAb	eBioscience
TWEEN® 20 for molecular biology	VWR Amresco
(3-(4,5-Dimethylthiazol-2-yl)-2,5-diphenyltetrazolium bromide) (MTT)	Invitrogen
Dimethyl Sulfoxide (DMSO)	VWR Amresco

### 3.1 Synthesis of Superparamagnetic Iron Oxide Nanoparticles (SPIONs)

#### 3.1.1 Synthesis of SPIONs using a thermal decomposition method

The SPIONs were synthesized using a thermal decomposition method as has been previously report[25] according to reaction equations 3.1 and 3.2.

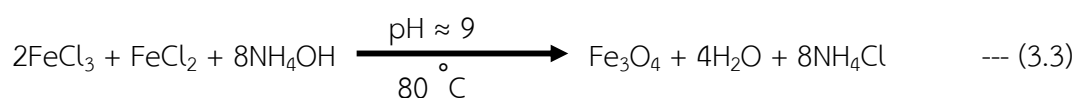


Firstly,  $\text{Fe}(\text{oleate})_3$  was prepared as a precursor starting 8 mmol of iron (III) chloride was dissolved in 10 mL of de-ionized (DI) water. Then, sodium hydroxide solution was prepared by dissolving 24 mmol of sodium hydroxide in 10 mL of DI water. 24 mmol of oleic acid was added in a round bottom flask, and sodium hydroxide solution was added to mix with oleic acid. Subsequently, iron (III) chloride solution and mixture of DI water:ethanol:hexane 12:16:28 by volume (mL) were added into the solution in the round bottom flask. Then, the mixture was stirred and refluxed at 70 °C for 4 hours (Equation 3.1). Next step,  $\text{Fe}(\text{oleate})_3$  was dispersed in hexane layer, so the  $\text{Fe}(\text{oleate})_3$  in mixture was washed using DI water for three times to remove and hexane layer was collected. The  $\text{Fe}(\text{oleate})_3$  in hexane was evaporated using rotary evaporation. Finally, synthesis of SPIONs by thermal decomposition method, The mixture of oleic acid: $\text{Fe}(\text{oleate})_3$ :1-octadecence as 1:6:38 (by mol) was gradually heated to 320 °C with rate of 3.3 °C per minute and holed at this temperature for 30 minutes under  $\text{N}_2$  atmosphere. Then the temperature was reduced to 160 °C under air

atmosphere (Equation 3.2). Finally, SPIONs were washed several times with ethanol with hexane ratio of 10:1.

### 3.1.2 Synthesis of SPIONs using a co-precipitation method

For synthesis using chemical co-precipitation method, it was prepared according to previous research (Equation 3.3).[21]



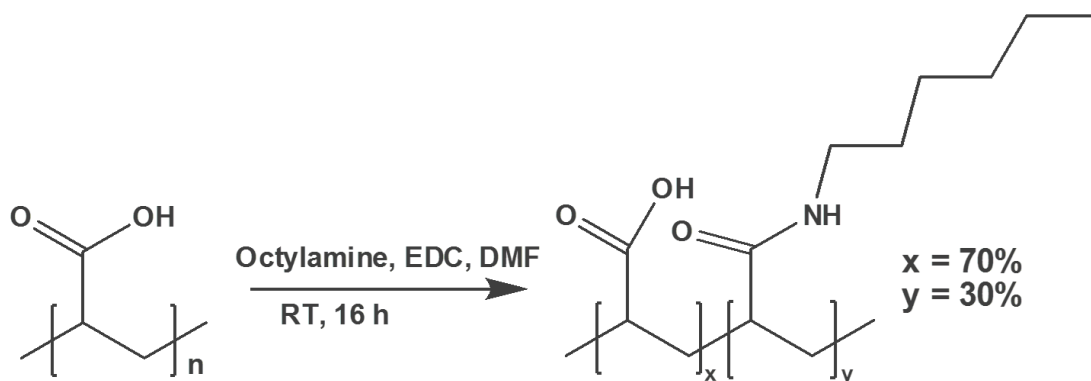
Firstly, 0.32 g of  $\text{FeCl}_2 \cdot 4\text{H}_2\text{O}$  was mixed with 0.75 g of  $\text{FeCl}_3 \cdot 6\text{H}_2\text{O}$  in 32 mL DI water and continuously stirred under nitrogen atmosphere at 80 °C for 1 hour. 4.5 mL of 25%  $\text{NH}_3$  aqueous solution was rapidly added into the solution and stirred for 1 hour until precipitation appeared. Finally, after the reaction mixture was cooled to room temperature, and the precipitated particles were washed several times with hot water and separated by a magnet.

## 3.2 Preparation of BSA/SPIONs-Polymer

### 3.2.1 SPION-coated with modified poly(acrylic acid) (SPIONs-mPAA)

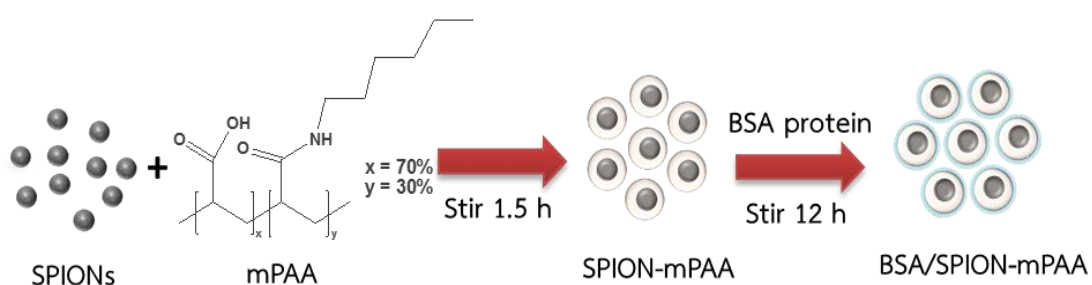
The modified poly(acrylic acid) or mPAA was prepared by functionalization coupling a fraction of carboxylic acid groups of poly(acrylic acid) (MW. 1800 g/mol) with n-octylamine (around 30%) following Figure 3.1.[49] Firstly, poly(acrylic acid) (1.73 g, 0.96 mmol) was mixed with 1-ethyl-3-(3-dimethylaminopropyl) carbodiimide hydrochloride (EDC) (2.30 g) and dimethylformamide (DMF) (15 mL) was added into the mixture under vacuum. Then, 1.6 mL n-octylamine (0.96 mmol) was gradually dropped and continuously stirred under nitrogen atmosphere for 16 hours. DMF was separated from mPAA using a rotary evaporation at 80 °C. Subsequently, the obtained mPAA was precipitated and washed using DI water, ethyl acetate. Then, pH of solution was adjusted to 9 using  $\text{NH}_4\text{OH}$ , and the aqueous layer was collected to precipitate

using hydrochloric acid at pH 3. Finally, the pH of mPAA was adjusted to pH 7, and the polymer was freeze dried to remove water to yield white powder product.



**Figure 3.1** Schematic illustration of reaction for modified poly acrylic acid (mPAA) preparation.

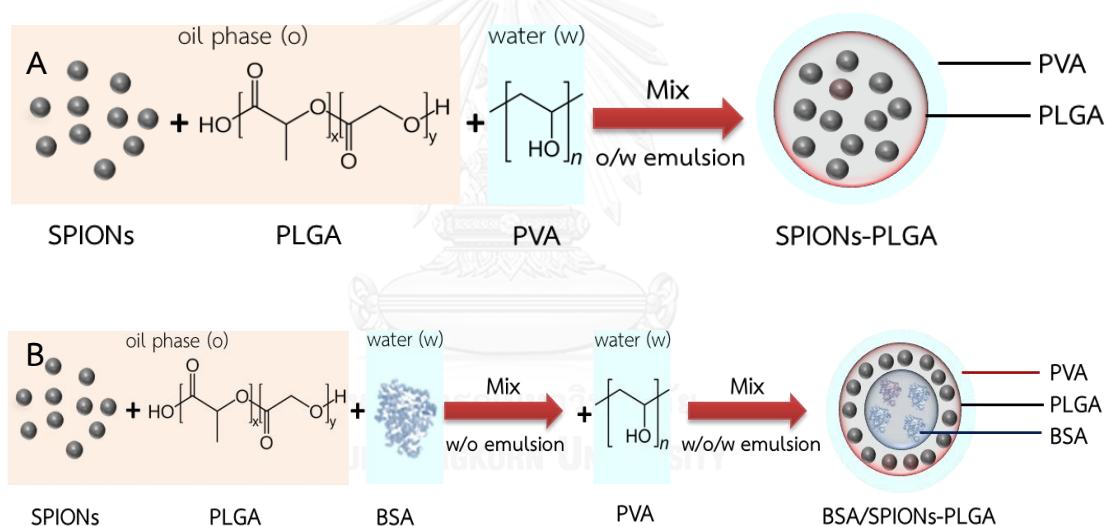
The SPIONs modified with mPAA containing BSA protein (BSA/SPION-mPAA) was prepared according to Figure 3.2. The polymer mPAA (20 mg) was dissolved in 5 mL chloroform and adjusted to pH 8 using 10  $\mu\text{L}$  of 25%  $\text{NH}_3$  aqueous solution. Then, the solution was stirred, and 20 mg MNP in 1 mL chloroform was gradually dropped into the solution. The solution was continuously stirred for 1.5 h. Subsequently, the clearly brown solution was evaporated, and PBS buffer pH 7.4 was gradually dropped under magnetic stirring. Moreover, the SPION-mPAA coated with 10 mg BSA protein was prepared. BSA in PBS buffer was added into the SPION-mPAA solution and stirred for 12 h.



**Figure 3.2** Schematic illustration of preparation of SPIONs coated with mPAA containing BSA (BSA/SPION-mPAA).

### 3.2.2 SPIONs-coated with Poly(D,L-lactide-co-glycolide) (SPIONs-PLGA)

The SPIONs was encapsulated in Poly(D,L-lactide-co-glycolide) (SPIONs-PLGA) using emulsion and SPIONs-PLGA containing BSA protein (BSA/SPIONs-PLGA) using double emulsion method according to Figure 3.3. In this process, SPIONs with oleic acid stabilized on their surface in hexane were dried under vacuum. 25 mg dried SPIONs and 100 mg PLGA were dissolved in 10 mL dichloromethane as the oil phase, while 25 mg BSA protein was dissolved in 0.5 mL DI water as the water phase. The two phases were then mixed together using a handheld homogenizer (22,000 rpm). After 1 min, 120 mg PVA in 30 mL DI water were added into the oily mixture, and the mixture was continuously homogenized for 2 min at room temperature. Finally, dichloromethane was removed by magnetically stirring for 2 h at room temperature.[21]



**Figure 3.3** Schematic of preparation of (A) PLGA encapsulating SPIONs (SPIONs-PLGA) and (B) PLGA encapsulating SPIONs and BSA (BSA/SPIONs-PLGA)

BSA was tagged with TAMRA for cellular uptake experiment using a molar ratio of BSA (MW. 60 kDa) to TAMRA (547 g/mol) of 5: 1. 25 mg BSA in 5 mL DI water was mixed with 200  $\mu$ g TAMRA in 40  $\mu$ L DMSO for 20 minutes. Then, the TAMRA-BSA was washed with DI water using centrifuge dialysis for separating the TAMRA-BSA from the excess TAMRA. BSA/ SPION-PLGA and SPION-PLGA-tagged TAMRA were prepared using double emulsion method as for BSA/SPION-PLGA where TAMRA and BSA-labeled TAMRA are in the water phase.



### 3.3 Particles Characterization

The crystalline phase of the prepared materials was elucidated using X-ray powder diffraction spectrometer (XRD) analysis (DMAX2200/Ultima-plus instrument, Rigaku, Japan) with Cu K radiation ( $1.5418 \text{ \AA}$  source (40kV, 30mA). The samples were placed on a glass holder at scans  $25^\circ\text{C}$  in steps of  $0.03^\circ$  over 2-theta ranging from  $20^\circ$  to  $80^\circ$ .

Morphology and composition of the prepared materials were elucidated using a transmission electron microscope (TEM) (Tecnai F20, Philips Electron Optics, Holland), a field-emission scanning electron microscope (FESEM) (JSM7610F, JEOL, Japan) and scanning electron microscope-energy-dispersive x-ray spectroscopy (SEM-EDX). The solution of samples in hexane or water were dropped on a carbon-coated copper grid for TEM and a glass stuck onto a stub holder for FESEM. Then, samples were dried at room temperature. Moreover, a particle size distribution analyzer (ZSP; Zetasizer, Malvern Instruments Ltd, UK) was performed to determined particles size and charge. The samples were dispersed in 0.01X PBS buffer pH 7 before they were filled in Zetasizer cell holder.

Fourier transform infrared spectra for confirmation of polymer-modified SPIONs were recorded on Nicolet 6700 FT-IR spectrometer. The powder of SPIONs, polymers and their composites were mixed with KBr (ratio 1:1000). The mixed powder was compressed using a hydraulic compressor into film samples.

For the magnetic properties determination of the samples magnetization and blocking temperature were measured using a Superconducting Quantum Interference Device-Vibrating Sample Magnetometer (SQUID-VSM) (Quantum Design). The sample was prepared using drop coating SPION  $10 \mu\text{L}$  on a semi-cylindrical quartz sample holder. The (GE) 7031 varnish was used to glue the sample to the sample holder under standard curing time of 30 min at room temperature. The investigated samples were attached to a quartz sample holder by dilute glue. The temperature dependent magnetization, M-T curve, was measured at a stepwise increase of temperature from 15 K to 350 K in an applied magnetic field of  $H_{\text{app}} = 500 \text{ Oe}$ , whereas magnetic

hysteresis loops, M-H curves, were collected at 15 K and 350 K. The calculation of magnetic response in unit emu/g were analyzed the SPIONs (Fe) weight using ICP-OES.

The PLGA particles stability in DMEM media were observed as the changing in particle sizes and morphology after periodical observation of the aqueous suspension of the particles (1 mg/mL in water) by FESEM after to duration of the 1 to 7 days storage at 37°C under 5% CO<sub>2</sub> similar to cells culturing condition.

### **3.4 SPION and BSA Protein Loading Content**

Amount of BSA loading in the obtained BSA/PLGA and BSA/SPION-PLGA particles was elucidated by extracting the BSA from the particles and quantifying the extracted BSA by UV spectroscopy. To extract out the loaded BSA, the freeze dried BSA/SPION-PLGA particles were dissolved in dichloromethane (to dissolve PLGA), and the mixture was centrifuged at 6000 rcf for 5 min to collect the of protein precipitates. The pellet was reconstituted in PBS buffer, pH 7.4, and the concentration of BSA in the obtained solution was quantified using a UV-Visible Spectrometry (HP 8453; Germany) at 279 nm with the aid of calibration of BSA standards prepared in the same PBS buffer.[50]

Loading of SPIONs in the SPION-PLGA particles and BSA/SPION-PLGA particles was investigated through the iron content of the particles. The sample particles were immersed in 37% hydrochloric acid for 3 h, and water was added to dilute the mixture to 5% HCl. Then, the mixture was filtrated with 0.2 micrometer nylon syringe filter (VertiClean™). The iron content was determined using an Inductively-Coupled Plasma Optical Emission Spectrometer (ICP-OES; Perkin Elmer Optima 2100).

### **3.5 Cytotoxicity Testing**

The macrophage cells line (RAW 264.7) were used to measure the cytotoxicity of the obtained particles using MTT cell viability assay.[51] The cells were cultured in DMEM media with supplementary reagents 10% FBS, 100 U/mL penicillin and 100 µg/mL streptomycin, 4mM L-glutamax, and 1 mM sodium pyruvate. The cells were cultured in the petri dish and incubated in a humidified incubator with 5% CO<sub>2</sub> at 37

°C. Then, the cells were transferred to a 96 well-plate at the concentration of 5,000 to 30,000 cells/well in 200  $\mu$ L DMEM media and cultured for 24 h to allow the cells to adhere on the plate. Subsequently, the SPIONs and their composites were incubated with the cells for the cytotoxicity testing using particles solution 20  $\mu$ L with concentration range of 10 to 1000  $\mu$ g/mL for 24 to 48 h. Afterward, 150  $\mu$ L media were carefully removed, and 150  $\mu$ L fresh media were replaced of the same volume before the addition of 20  $\mu$ L of 12 mM MTT (Invitrogen, CA, USA). The cells were kept in the dark within a humidified incubator for 1 h. Finally, the particles were removed using 100  $\mu$ L PBS buffer replacement for 2 times, and 150  $\mu$ L DMSO were added to dissolve the purple formazan crystal. Absorbance of the samples (cells incubated with particles) and blank (particles in media) at 570 nm was then analyzed using a Microplate Reader (Biochrom Anthos Zenyth 200 Microplate Reader, MA, USA).

### 3.6 Cellular Uptake

The cellular uptake was measured using RAW 264.7 cells and TAMRA dye (5-carboxytetramethylrhodamine succinimidyl ester) represented the particle uptake into the cells. The RAW 264.7 cells were cultured and incubated with the particles: TAMRA-labeled SPION-PLGA and TAMRA-labeled BSA in particles and indicated through a fluorescence microscope.

First of all the cover slips were coated with poly-L-lysine overnight. Then the coated cover slips were washed with PBS buffer and placed in 12-well plates. RAW 264.7 cells in the concentration of  $2.5 \times 10^5$  cells/mL were seeded in 1 mL DMEM media on the coated cover slips in the incubator (37 °C in 5% CO<sub>2</sub>) for 24 h. Then, 100  $\mu$ L of 100  $\mu$ g/mL obtained particles were added into the cells and incubated for 1 h and 3 h. Then, cells were washed for 3 times with PBS buffer, and fixed using 4% paraformaldehyde for 30 min at 4 °C. Subsequently, nucleuses of cells were stained by 30 nM DAPI dye solution (Invitrogen, CA, USA) for 5 min. After staining, the cells were washed with PBS buffer several times to remove the DAPI dye. The cells on cover slip were moved to demonstrate the cellular uptake using fluorescence microscopic

analysis (BX50 Olympus, Japan) with the  $\lambda_{\text{ex/emit}}$  of 330/385 nm and 520/550 nm for DAPI and TAMRA, respectively.

### 3.7 Induction of Dendritic Cell Maturation and Cytokine Production

The induction of dendritic cell maturation and cytokine production were performed using murine bone marrow-derived dendritic cells (BM-DCs) of mice. Female 6-week-old BALB/c mice were obtained from National Laboratory Animal Center, Mahidol University and housed in Animal Center of Chulalongkorn University. All animal procedures were reviewed and approved by Chulalongkorn University Animal Care and Use Committee (protocol number 1573007).

The BM-DCs were generated as previous described.[52, 53] Firstly, the bone marrow cells were prepared and seeded at the concentration of  $1 \times 10^6$  cells in 24-wells plates. The bone marrow cells were cultured in 1 mL of RPMI supplemented with 10% FBS, 100 U/mL penicillin and 100  $\mu\text{g/mL}$  streptomycin, 0.2 mM L-glutamax, in the presence of 10 ng/mL recombinant murine GM-CSF (Peprotech, NJ, USA) and 10 ng/mL recombinant murine IL-4 (Peprotech, NJ, USA) in a humidified incubator for 7 days for the induction of the bone marrow cells to dendritic cells. On Day 7, the BM-DCs were incubated with particles (100  $\mu\text{L}$  of the particle suspension in water) without and with an external magnetic field of approximately 2,600 Gauss (generated from a cylindrical rare-earth magnet placing 4 mm below the plates) for 3 h. After the magnetic field was removed, the cells were continuously incubated for various times. Then the BM-DCs were collected using a cell scraper, and the supernatants were subjected to cytokine secretion analysis. The ability of particles for BM-DCs stimulation is dependent on cells maturation. The BM-DCs maturation were evaluated by first blocking the cellular Fc receptor with anti-mouse CD16/32 mAbs, and staining with fluorescence dye-labeled antibodies against murine CD11c, CD80, CD86 and MHC II. Unstimulated cells (cells that were not incubated with particles) were used as a negative control. All stained and unstained cells were then subjected to a flow cytometric analysis (FACSCalibur<sup>TM</sup>; BD Bioscience, NJ, USA), and analyzed by BD CellQuest<sup>TM</sup> software (BD Bioscience, NJ, USA).

The amount of interleukin-6 (IL-6), interleukin-12 (IL-12), interferon-gamma (IFN- $\gamma$ ), and tumor necrosis factor-alpha (TNF- $\alpha$ ) cytokines in the collected supernatants of cells were determined by sandwich ELISA assay following the Biolegend's protocol.[54] First step, the cytokine-specific capture antibodies was added into 96-wells plate and kept in dark at 4 °C for 16 h. Then the plate was washed several times using washing buffer (PBS buffer containing 0.05% of TWEEN® 20). Subsequently, the supernatant samples were added into the 96-wells plate and incubated for 2 h. After washing, the cytokine-specific detection antibodies with streptavidin-horseradish peroxidase system were added in the plate. 3,3',5,5'-Tetramethylbenzidine (TMB) was used as a substrate. The absorbance was measured at 450 nm using a microplate reader (Biochrom Anthos Zenyth 200 Microplate Reader, MA, USA).



## CHAPTER IV

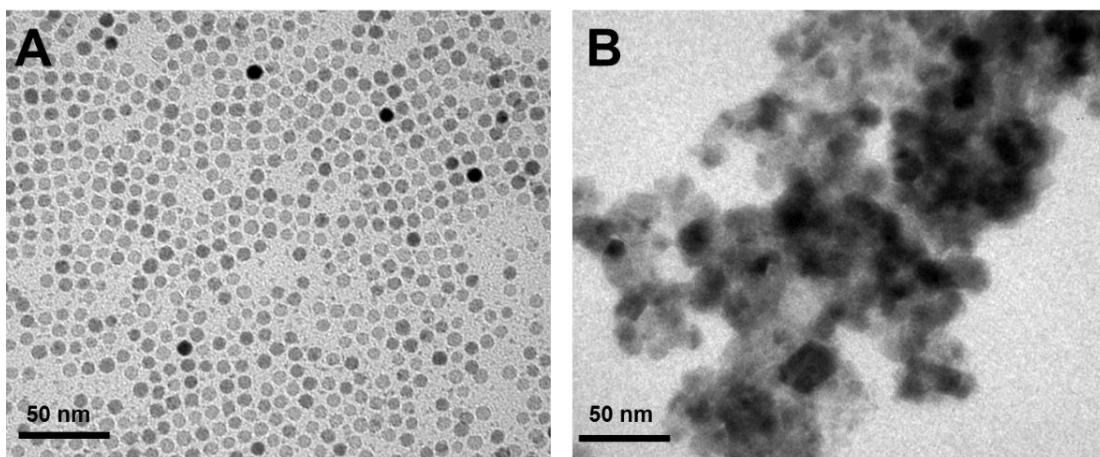
### RESULTS AND DISCUSSION

This chapter describes the results from experiments and discussion of the results. Firstly, the obtained superparamagnetic iron oxide nanoparticles (SPIONs), SPION-Polymers and BSA protein coated or encapsulated SPION-Polymers (BSA/SPION-Polymer) were characterized to identify their compositions, morphology and charge. The SPION and BSA protein content in the composites were determined. For the second part, the particles were tested for their cytotoxicity and protein delivery to cells. For the final part, the particles were investigated for their potential to activate bone marrow-derived dendritic cells.

#### 4.1 Characterization of SPIONs

##### 4.1.1 Characterization of synthesized SPIONs morphology and size with TEM and FESEM

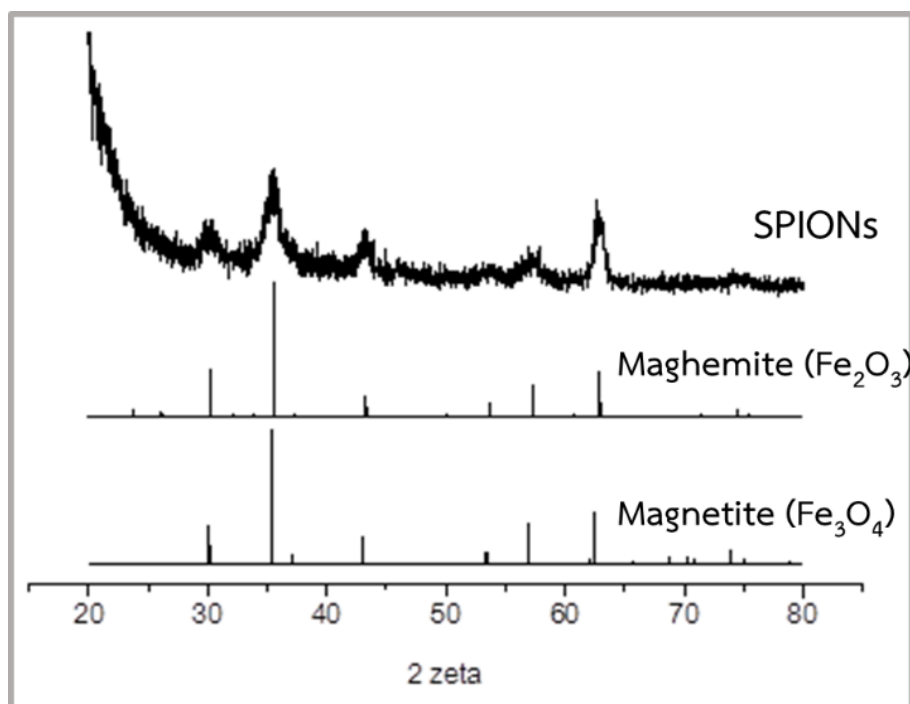
The SPIONs were synthesized with an aim to compare thermal decomposition and co-preparation methods. The TEM images showed the obtained nanoparticles using two different methods (Figure 4.1), the thermal decomposition possessed monodispersed spherical shapes of iron oxide with an average diameter of  $9.81 \pm 0.57$  nm (Figure 4.1A). The thermal decomposition accomplished SPIONs with high crystallinity, relatively monodisperse and well-controlled size distribution because the surfactants and the high temperature successfully control their growth direction.[55] However, the preparation is more complicated than co-precipitation. For the co-preparation method, the aggregations of nanoparticles are observed and their shapes and sizes are difficultly estimated (Figure 4.1B). Therefore, the SPIONs synthesizing from thermal decomposition methods were chosen to prepare the SPION-Polymer nanocomposites for protein delivery because of their narrow size distribution and good dispersion with stronger magnetic response.



**Figure 4.1** Transmission electron microscopy (TEM) images of SPIONs synthesized from (A) thermal decomposition and (B) co-preparation methods.

#### 4.1.2 Characterization of synthesized SPIONs crystal structures with X-ray diffraction

To analyze crystallize structure of selected iron oxide nanoparticles, we analyzed the obtained particles with the X-ray diffraction (XRD). It was found that the XRD pattern matches with the standard pattern files of both JCPDS 19-0629 (Magnetite,  $\text{Fe}_3\text{O}_4$ ) and JCPDS 39-1346 (Maghemite,  $\text{Fe}_2\text{O}_3$ ). Although the XRD could not specify the structure of nanoparticles, both magnetite and maghemite are ferromagnetic and they show strong magnetically responses of the nanoparticles as desired. However, for clear identification of the structure of SPIONs, we expected the black powder of SPIONs synthesized as the same process as previous studies could be mainly of magnetite structure.[25]



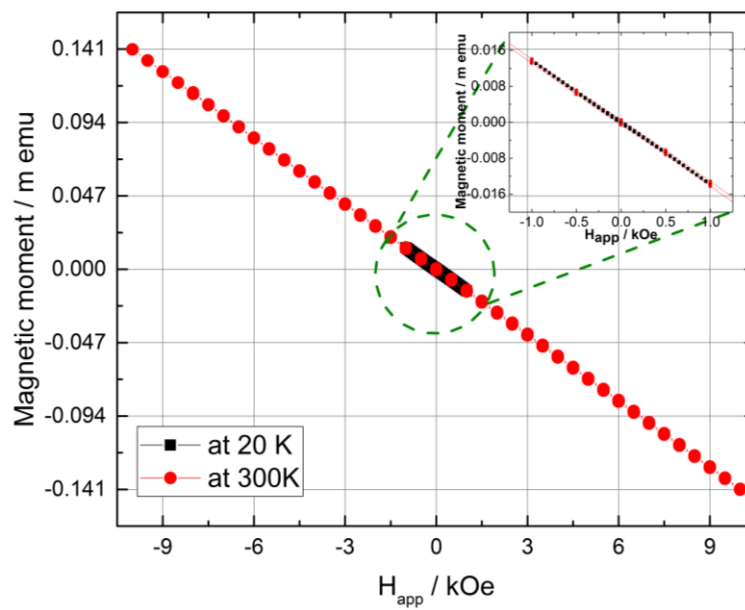
**Figure 4.2** The XRD patterns of the synthesized superparamagnetic iron oxide nanoparticles (SPIONs) compared with the standard pattern files JCPDS 19-0629 (magnetite) and JCPDS 39-1346 (maghemite).

#### 4.1.2 Magnetic properties characterization of synthesized SPIONs with superconducting quantum interference device-vibrating sample magnetometer (SQUID-VSM)

In order to determine the magnetic response of particles, firstly synthesized iron oxide nanoparticles were checked the IR response with cylinder shape magnet. From the observation, they can be induced using an external magnetic suddenly (Appendix: Figure A1 A). Then, the synthesized nanoparticles was measured the blocking temperature. Zero field cooled (ZFC) and field cooled (FC) experiments were performed using SQUID-VSM measurement setup. The magnetic background signal from the sample holder and the quartz substrate were measured as the same condition with SPION samples (Figure 4.3). The sample holder itself contributes negligibly small in measurement. Therefore,  $M(H)$  loop measured is the combined responses of the quartz substrate and the glue. As can be observed in the graph, magnetic background due to the substrate and (GE) 7031 varnish glue is the diamagnetic type. It was observed in this measurement that the glue is not



quantitatively measured, and we could not control the amount of glue dispensed to adhere sample, so such measurement cannot be used for magnetic background correction.

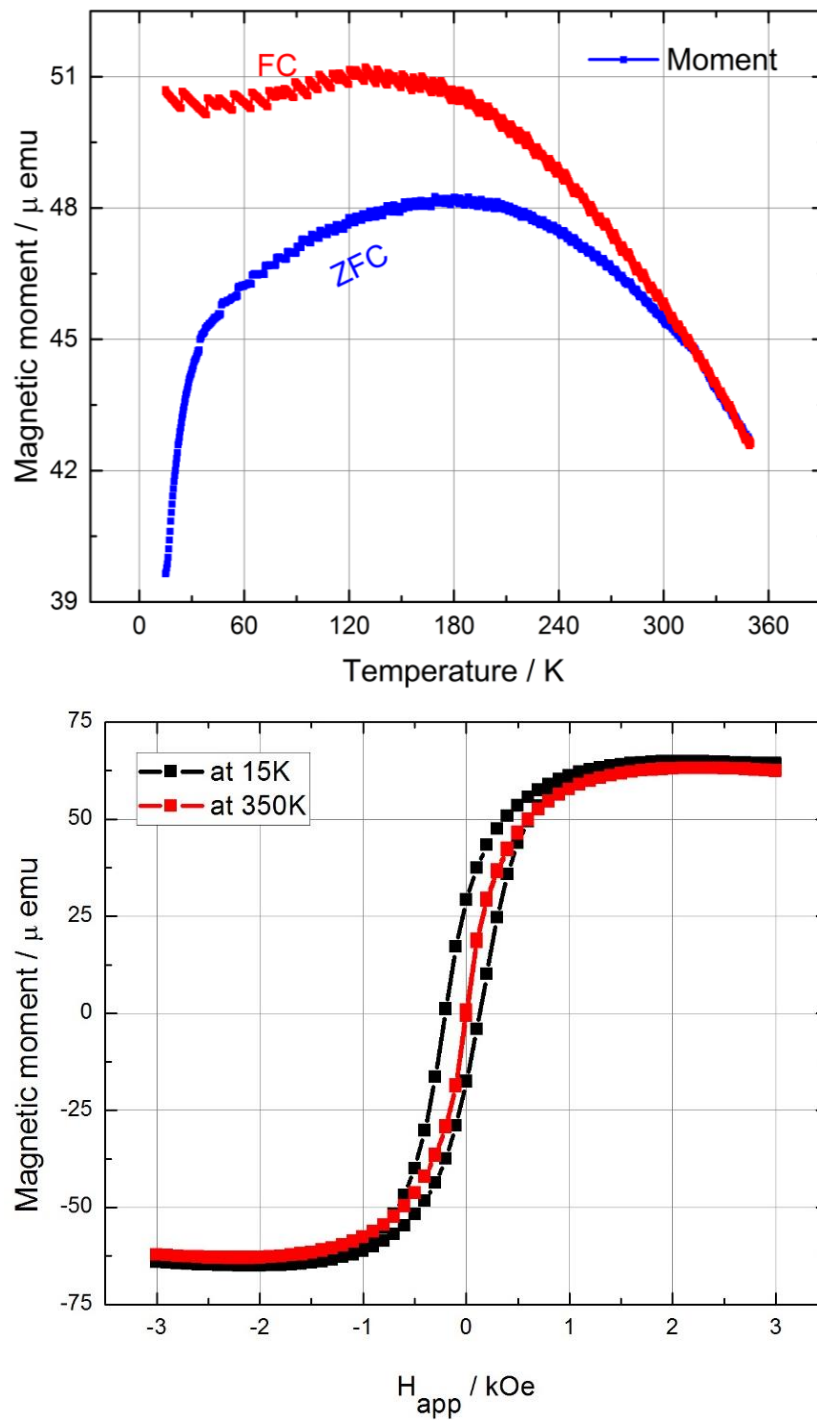


**Figure 4.3** SQUID-VSM measured  $M(H)$  hysteresis loop for quartz substrate, glue and sample holder (background) for in-plane applied magnetic field at 20 K and 300 K.

The curves of ZFC and FC magnetization for SPION were shown in Figure 4.4A. Since magnetic field was not applied while cooling the sample (ZFC), the spins are frozen in random directions, and the result showed the small magnetic moment ( $M \approx 40 \mu \text{ emu}$ ). Furthermore, the magnetic moment was observed to increase with the temperature up to  $172 \pm 20 \text{ K}$ , but magnetic moment gradually decrease after this temperature. The maximum temperature ( $172 \pm 20 \text{ K}$ ) represented the blocking temperature, and the blocking temperature is characteristic features of magnetic nanoparticles. That the behavior was explained by Park *et al.*,[56] as these nanoparticles can be considered as some single domain magnets, the magnetization can fluctuate randomly by thermal fluctuation at high enough temperatures. In contrast, at low temperature the thermal energy becomes smaller, and the magnetic moments become blocked.[56] On contrary, in FC curve the magnetization is almost constant for temperature between 15 K to 120 K and decreases while increasing the

temperature because sample was cooled through the blocking temperature in presence of magnetic field. Therefore the spins will now be frozen in the direction of magnetic field.

The  $M(H)$  hysteresis loop measured at the two extremities of the temperature was shown in Figure 4.4B. As anticipated, at 15 K the measured hysteresis resembles ferromagnetic behavior with coercivity  $H_C = 167 \pm 10$  Oe and saturation magnetization  $M_S = 64.61 \pm 0.30 \mu \text{ emu}$  at saturation magnetic field of  $H_S = 1.59 \pm 0.10$  kOe. In contrast, the hysteresis at 350 K has nearly zero remanence and coercivity with saturation magnetization  $M_S = 62.80 \pm 0.31 \mu \text{ emu}$  at saturation magnetic field of  $H_S = 1.60 \pm 0.10$  kOe. The noticeable decrease in the magnetic moment at 350 K could be interpreted as results of disorder and frustration in the spins of SPIONs due to thermal energy. Moreover, it should be noted that the magnetic response ( $M_S$ ) and scale in graph were not presented in standard units ( $\text{emu}/\text{cm}^3$  or  $\text{emu}/\text{g}$ ) as the sample were prepared by drop coating method, and the amount of sample was measured using ICP-OES. The magnetic response per gram of all samples are equal to  $16.79 \pm 0.33 \text{ emu}/\text{g}$ . However, it is difficult to determine the exact thickness of film or the quantity of SPIONs on substrate because drop coating samples were not smooth on the substrate.



**Figure 4.4 (A)**  $M(T)$  hysteresis curve of SPION at 500 Oe for temperature between 15 K to 350 K and **(B)** SQUID-VSM measured normalized  $M(H)$  hysteresis loop for SPION in-plane applied a magnetic field at 15 K and 350 K.

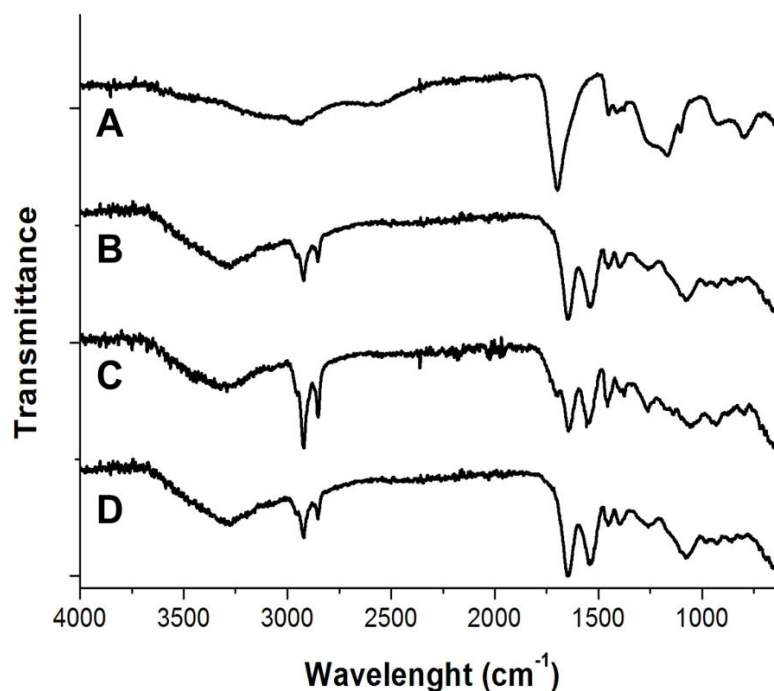
## 4.2 Characterization of BSA/SPIONs-Polymer

### 4.2.1 Characterization of SPIONs-coated with modified poly(acrylic acid) (SPION-mPAA)

#### 4.2.1.1 Characterization of functional group of mPAA and BSA/SPION-mPAA with Fourier transform infrared spectrometer (FTIR)

The poly(acrylic acid) (PAA) was modified as mentioned in the experimental parts (3.2.1). The FTIR spectra were used to identify the change of poly(acrylic acid) (PAA) functional groups comparing before and after modification (Figure 4.5A and B). The PAA spectra exhibit a strong sharp band of C=O stretching at  $1714\text{ cm}^{-1}$ . The band region between  $1130$  and  $1300\text{ cm}^{-1}$  is corresponding to (C-O) stretching and (O-H) bending vibrations. The peak around  $3000\text{ cm}^{-1}$  results from C-H stretching.[57]

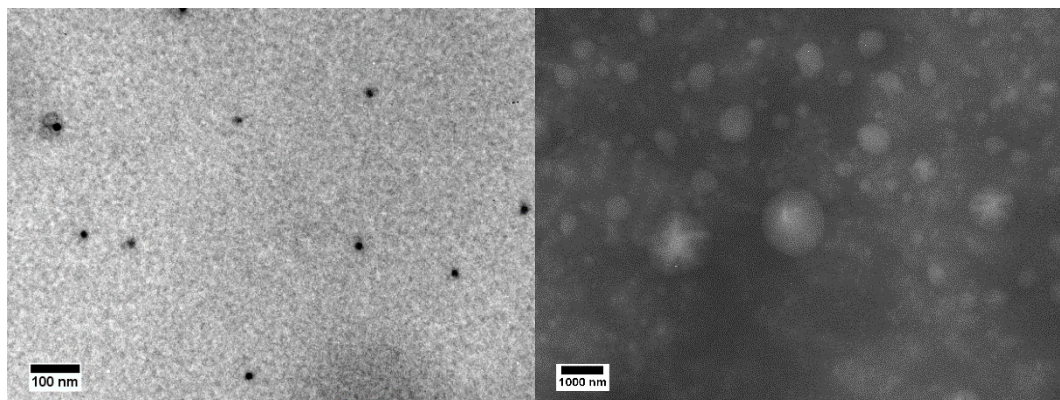
After modification, modified PAA (mPAA) exhibits new peaks between  $3300\text{ cm}^{-1}$  and  $3500\text{ cm}^{-1}$  consistent to characteristic peaks of amine (N-H stretching), and the bands at  $1446\text{ cm}^{-1}$  and  $1600\text{ cm}^{-1}$  are assigned to  $\text{CH}_2$  bending and N-H bending, respectively (Figure 4.5B). The mPAA coated SPIONs (SPION-mPAA) and BSA coated SPION-mPAA were confirmed by the mPAA characteristic peaks (Figure 4.5C and D). Therefore, the spectra could ensure that mPAA is modified on the SPIONs. However, it could not be evidently confirmed that BSA protein were incorporated onto the SPION-mPAA because characteristic peaks of BSA protein (N-H bond) are similar to mPAA peak.[49] The incorporation of BSA onto SPION-mPAA is indicated using SEM-EDX technique (Figure 4.7).



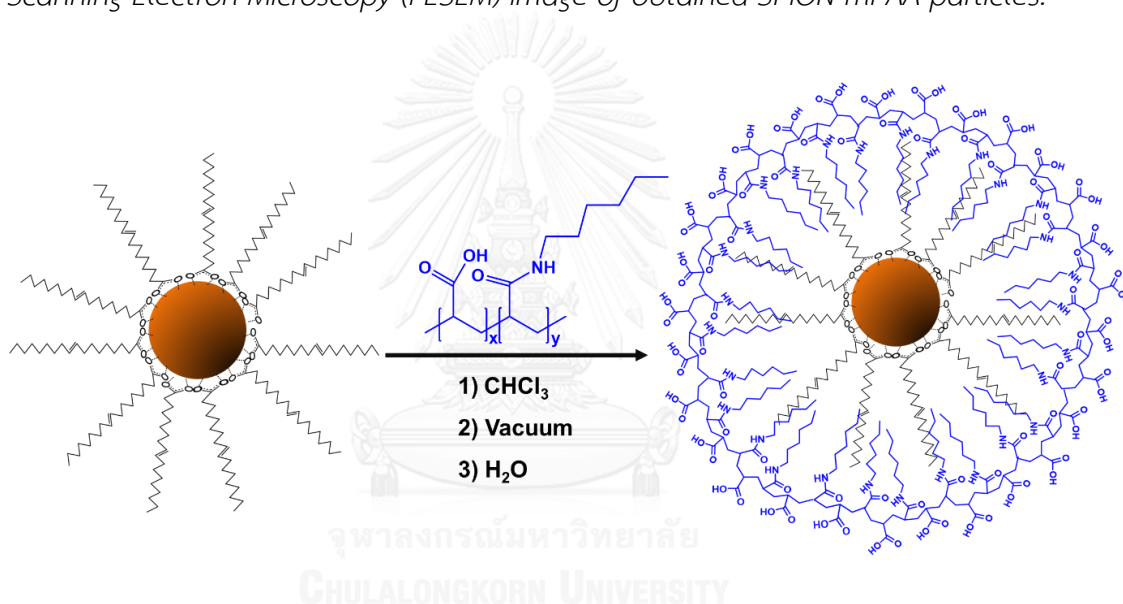
**Figure 4.5** Fourier transform infrared spectroscopy (FT-IR) of (A) poly(acrylic acid) (PAA) (B) modified poly(acrylic acid) (mPAA) (C) superparamagnetic iron oxide nanoparticles (SPION)-mPAA and (D) BSA protein-coated SPION-mPAA (BSA/SPION-mPAA)

#### 4.2.1.2 Characterization of SPION-mPAA morphology and sizes with TEM and FESEM

The TEM and FESEM images of obtained monodispersed SPIONs after coating with mPAA (SPION-mPAA) are demonstrated in Figure 4.6A and B, respectively. The TEM image showed only SPIONs dispersion. It was found that SPIONs dispersed better than one before coating (Figure 4.1A) because mPAA could protect and increase repulsive forces around the iron oxide surface.[22] In addition, the FESEM image of SPION-mPAA illustrates the mPAA polymer surface, as the mPAA formed spherical structures and their sizes are diversified. According to IR spectra, TEM and FESEM images, SPION-mPAA were similar in functional group and morphology to previous report about the quantum dot coated with mPAA from Somers *et al.*[49]. Therefore, we expect that the mPAA is inserted among oleic acid on iron oxide surface, and SPION-mPAA forms micellar of amphiphilic polymer as the scheme in the Figure 4.7.



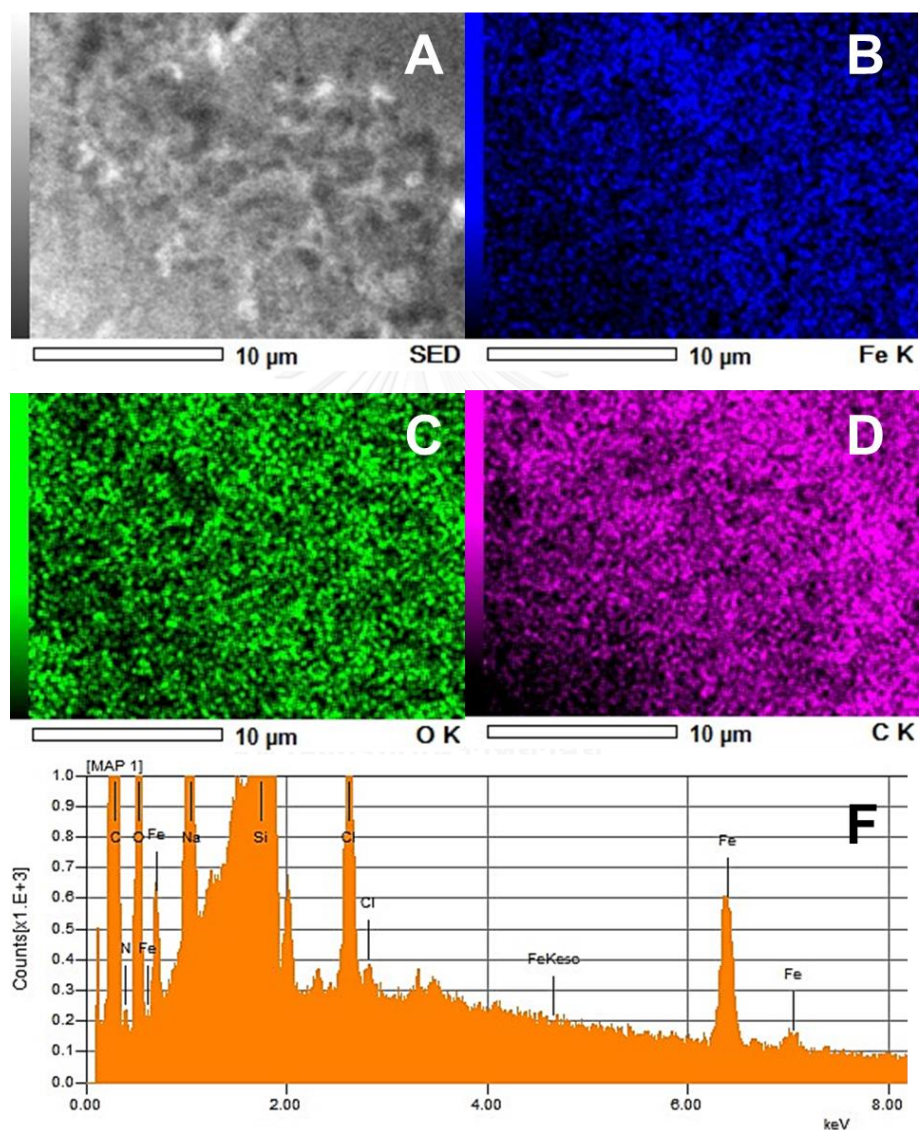
**Figure 4.6** (A) Transmission electron microscopy (TEM) image and (B) Field Emission Scanning Electron Microscopy (FESEM) image of obtained SPION-mPAA particles.



**Figure 4.7** Scheme illustrate the preparation of SPION coated with mPAA (blue) from the SPION coated with oleic acid.

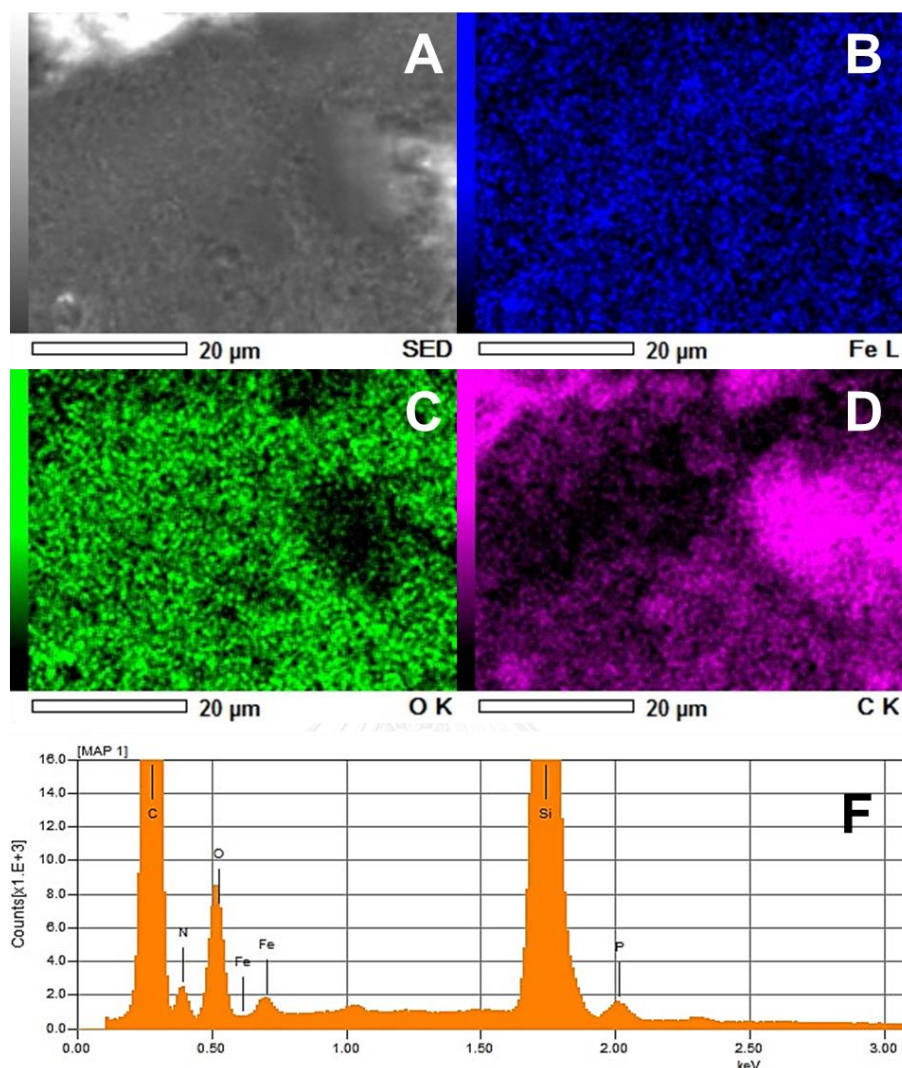
In addition, the BSA protein-coated SPION-mPAA are confirmed using scanning electron microscopy with energy Dispersive x-ray analysis (SEM-EDX). SEM-EDX of SPION-mPAA before coating is shown in Figure 4.8, the EDX mapping illustrated only iron (Fe), oxygen (O) and carbon (C) from iron oxide and mPAA polymer, and it was found that silicon (Si) from substrate (data not show). The nitrogen (N) signal did not show in mapping, but it displayed small peak in EDX spectra as the mPAA has some small quantity of nitrogen in the structure (Figure 4.7). The nitrogen:iron ratio is 1:3. After BSA coating onto SPION-mPAA (Figure 4.9), the mapping is not observed nitrogen

as in the one before coating, but EDX spectra showed more nitrogen percentage comparing to iron (ratio 2:3) because the BSA protein are rich nitrogen in the structure. Therefore, these results could support that the BSA was successfully incorporated in SPION-mPAA.



**Figure 4.8** SEM-EDX of SPION-mPAA (A) SEM image and EDX mapping of various elements: (B) Fe, (C) O and (D) C, and (F) EDX spectra showing all elements in SPION-mPAA particles.





**Figure 4.9** SEM-EDX of BSA/SPION-mPAA (A) SEM image and EDX mapping of various elements (B) Fe, (C) O and (D) C, and (F) EDX spectra showing all elements in BSA/SPION-mPAA particles.

Using a rare earth magnet SPION-mPAA showed weak magnetic responses (Appendix: Figure A1 B) likely because SPIONs with oleic acid as stabilizer were coated with another layer of mPAA as described in Figure 4.7. Each SPION was isolated from others as shown in TEM and FESEM images (Figure 4.6). Therefore, we did not characterize it using other techniques because we foresee that their magnetic response is not enough for further applications.



#### 4.2.2 SPIONs-coated with Poly(D,L-lactide-co-glycolide) (SPION-PLGA)

##### 4.2.2.1 Characterization of SPION-PLGA and BSA/SPION-PLGA morphology, size and charge with TEM, FESEM and Zetasizer analysis

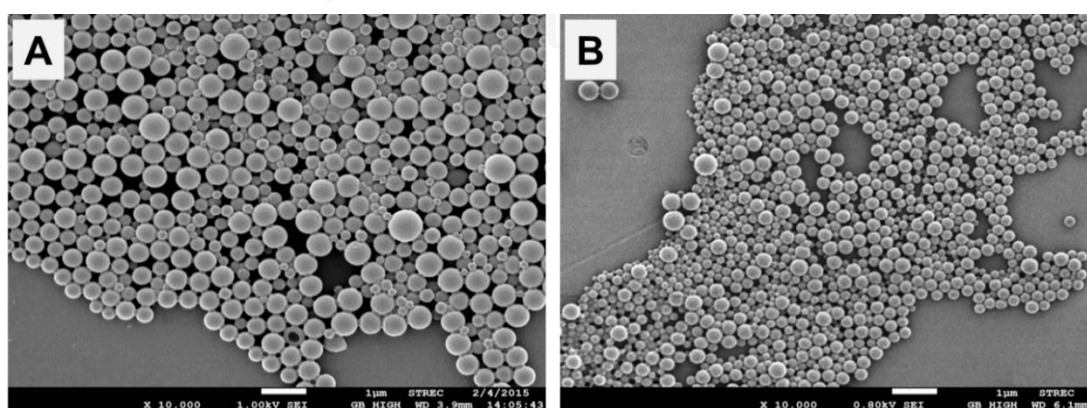
The obtained monodispersed SPIONs composited with the biocompatible PLGA (SPION-PLGA) using emulsion technique and double emulsion technique for encapsulating BSA protein (BSA/SPION-PLGA) were further size separated into two fractions: large and small sizes using centrifugation, with approximate size of 500 nm (called SPION-PLGA-L and BSA/SPION-PLGA-L) and 300 nm (called SPION-PLGA-S and BSA/SPION-PLGA-S). The hydrodynamic sizes of the aqueous suspensions of all the particles are displayed in Table 4.1. Beside the SPION-PLGA and BSA/SPION-PLGA particles, we prepared the PLGA and BSA/PLGA with two different sizes as control samples. The results of hydrodynamic sizes of all large particles showed sizes between 505 and 536 nm, and the small size between 270 and 285 nm, which did not differ significantly for particles from the same fraction. Moreover, all small size samples exhibited narrow size distribution with  $PDI < 0.2$ . [58] On contrary, the larger sizes demonstrated the PDI of more than 0.2, especially the PLGA encapsulating both SPION, and BSA (BSA/SPION-PLGA-L,  $PDI = 0.378 \pm 0.022$ ). The result might be from the process of double emulsion method that successfully included both SPIONs and BSA protein but difficulty in controlling the compositions of the two components, leading to wide distribution of SPIONs and BSA. The wide distribution in mass and density of each particle can lead to the large PDIs of these materials.

The studies of particle surface charge were performed by measuring zeta potentials of colloidal particles in aqueous solution. The zeta potential data in Table 4.1 indicated that all particles exhibited negative charge from -9 to -13 mV at pH 7, which was similar to previous reports. [59] The negative charge on the surface come from the carboxylic acid end groups of PLGA in combination with PVA stabilizer. [59] The negatively-charged colloidal particles are mostly observed for those particles with no aggregations similar to what we found in this study.

**Table 4.1** Characteristics of particles hydrodynamic sizes, polydispersity indices (PDI), and zeta potentials using a Zetasizer

Particles	Hydrodynamic Size (nm) <sup>a</sup>	PDI	Zeta Potential (mV)
PLGA-L	520 ± 57	0.239 ± 0.019	-11.4 ± 0.2
PLGA-S	272 ± 7	0.098 ± 0.027	-10.2 ± 0.1
BSA/PLGA-L	519 ± 43	0.282 ± 0.010	-13.7 ± 0.2
BSA/PLGA-S	270 ± 1	0.115 ± 0.018	-10.0 ± 0.6
SPION-PLGA-L	505 ± 26	0.319 ± 0.023	-11.2 ± 0.2
SPION-PLGA-S	277 ± 18	0.163 ± 0.006	-9.7 ± 0.4
BSA/SPION-PLGA-L	536 ± 11	0.378 ± 0.022	-13.4 ± 0.2
BSA/SPION-PLGA-S	285 ± 20	0.167 ± 0.030	-11.7 ± 0.4

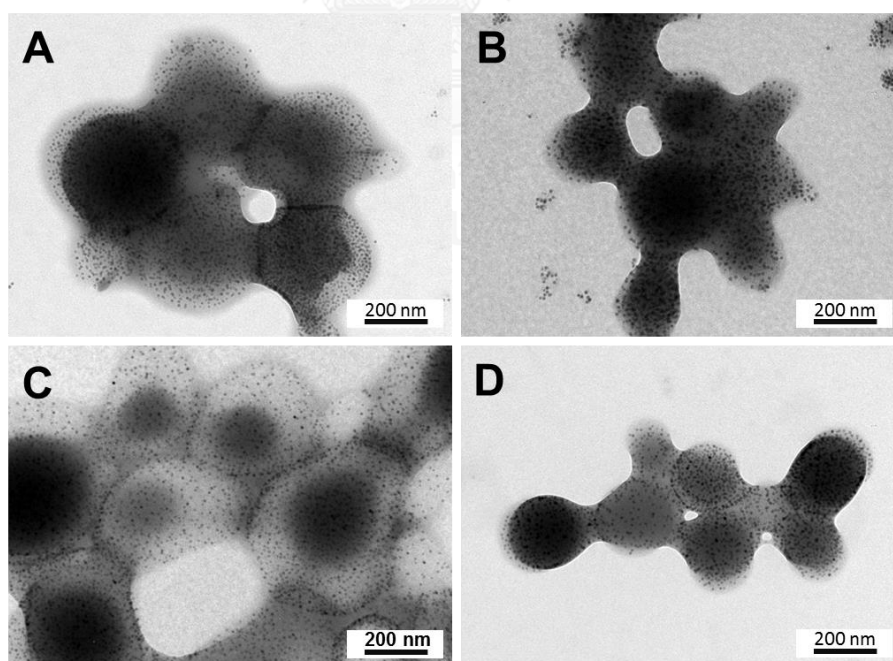
For investigation on particle morphology and confirmation of their sizes using FESEM, two different sizes of PLGA particles were chosen as representatives of all particles (Figure 4.10). FESEM images demonstrated that PLGA particles were spherical with smooth surface with the diameter of  $503.76 \pm 92.45$  nm for large particles (PLGA-L) and  $308.42 \pm 60.10$  nm for small particles (PLGA-S).



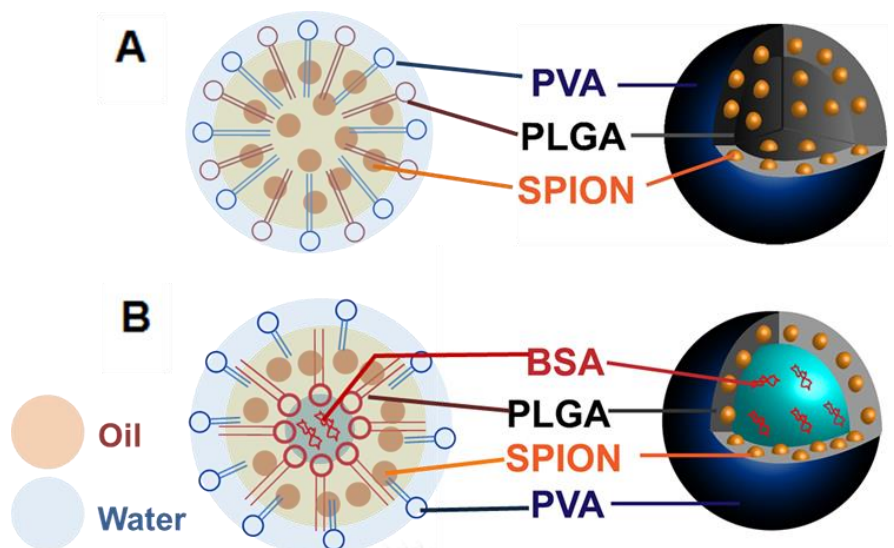
**Figure 4.10** FESEM images showing the morphologies of particles (A) PLGA-L and (B) PLGA-S.

Moreover, relatively uniform distribution of the 10 nm SPIONs in both the SPION-PLGA-L and SPION-PLGA-S could be clearly observed in the TEM images (Figure 4.11 A and B). For TEM images of BSA-loaded particles, BSA/SPION-PLGA-L and BSA/SPION-PLGA-S are (Figure 4.11 C and D) loading of BSA did not induce significant morphological changes to the particles as the size and shape of both the large and the small BSA-loaded particles were similar to their corresponding unloaded particles. However, the BSA/SPION-PLGA-L image showed different contrast in particles suggestions that the particles that the comprised two layers.

From the preparation method and the TEM images, we speculate that the obtained SPION-PLGA particles are oil in water emulsion with the SPION dispersing in oil layer inside PLGA and surfactant (PVA) as shown in Figure 4.12A. Moreover, BSA/SPION-PLGA was observed as a core-shell structure in which the SPION-PLGA forms into the shell, and the core is the aqueous phase containing BSA (structure as in Figure 4.12B). However, for the small size of BSA/SPION-PLGA, a core-shell structure was not noticeable.

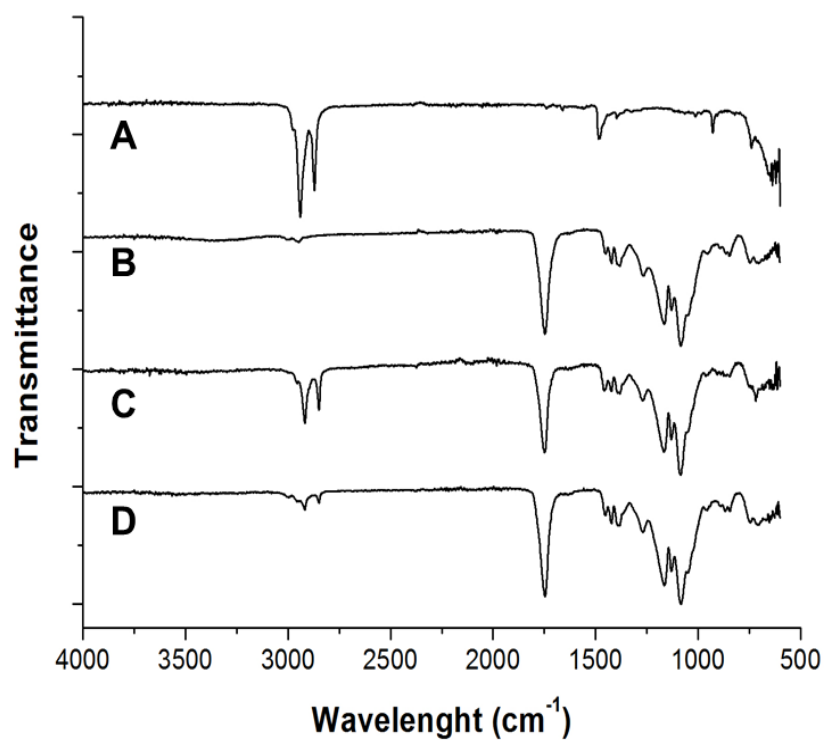


**Figure 4.11** TEM images of SPION encapsulated in PLGA (A) SPION-PLGA-L, (B) SPION-PLGA-S, and SPION with BSA encapsulated in PLGA (C) BSA/SPION-PLGA-L and (D) BSA/SPION-PLGA-S.



**Figure 4.12** Proposed structures of SPIONs encapsulated in PLGA **(A)** SPION-PLGA (oil/water emulsion) and **(B)** BSA/SPION-PLGA (water/oil/water double emulsion).

4.2.2.2 Characterization of functional groups of PLGA and BSA/SPION-PLGA using Fourier transform infrared spectrometer (FTIR)



**Figure 4.13** FTIR spectra of **(A)** SPIONs, **(B)** Poly(D,L-lactide-co-glycolide) PLGA, **(C)** SPION-PLGA and **(D)** BSA-loaded SPION-PLGA (BSA/SPION-PLGA) particles.

The SPIONs, PLGA particles, SPIONs coated with PLGA, and BSA-loaded SPION-PLGA spectra were recorded on FTIR spectrometer (Figure 4.13). The FTIR spectrum of SPIONs (Figure 4.13A) shows the prominent peak at 2950 – 2850  $\text{cm}^{-1}$  corresponding to a C-H stretching of oleic acid [60] on the SPION surface. Figure 4.13B shows the spectrum of PLGA particles with sharp peak at 1765-1750  $\text{cm}^{-1}$  and IR bands at 1300-1090  $\text{cm}^{-1}$  in consistent to C=O stretching and C-C-O stretching, respectively. The peaks at 1190 – 1085  $\text{cm}^{-1}$  and 3100 - 2950  $\text{cm}^{-1}$  are assigned to C-O-C stretching and O-H stretching of the carboxylic acid of the PLGA polymer.[61] The FTIR spectrum of the SPION-PLGA particles (Figure 4.13C) exhibits characteristic peaks of both SPIONs and PLGA particles. Likewise, the BSA/SPION-PLGA (Figure 4.13D) demonstrates the characteristic peaks of both, but two characteristic peaks of BSA (amides I: 1700–1600 and amides II: 1550–1500  $\text{cm}^{-1}$ )[62] were not clearly observed because the peaks are in the same regions as PLGA particles. Moreover, C-H stretching of oleic acid seems to decrease because of the effect of BSA protein.

#### *4.2.2.3 Detection of Iron and BSA protein content in the SPION-PLGA and BSA/SPION-PLGA with inductively-coupled plasma optical emission spectrometer (ICP-OES) and UV-Visible Spectroscopy*

The SPION contents were determined using ICP-OES analysis with the calculation from %Fe content converted to  $\text{Fe}_3\text{O}_4$ . The results found that the particles contain  $21.6 \pm 3.0$  and  $27.1 \pm 2.9$  % w/w of  $\text{Fe}_3\text{O}_4$  in the SPION-PLGA-L and SPION-PLGA-S, respectively (Table 4.2). However, in the presence of BSA in the particles, the SPION percentages reduced to  $15.3 \pm 2.6\%$  and  $15.6 \pm 0.8\%$  in the BSA/SPION-PLGA-L and BSA/SPION-PLGA-S particles, respectively. The decrease in percentage of SPIONs agree with TEM images (Figure 4.11), where the BSA in aqueous phase seems to be at the center or core of particles as obviously seen in BSA/SPION-PLGA-L. Likewise the BSA content in the PLGA particles were approximate 7%, their content reduced to  $5.6 \pm 0.4$  and  $3.1 \pm 0.4$  % for BSA/SPION-PLGA-L and BSA/SPION-PLGA-S, respectively (Table 4.2).

The protein loading content is approximately 3-5 times less than the SPION loading content for both the large and the small composite particles regardless of the

fact that the same weight of BSA and SPIONs were used in the fabrication process. This indicates that SPIONs are more easily retained in the composite particles as compared to the BSA. Bigger size of the phase-separated SPIONs comparing to the water soluble BSA is likely the reason.

**Table 4.2** Investigation of SPION loading and protein loading contents of all prepared particles.

Particles	SPION Contents (%w/w) <sup>a</sup>	BSA Contents (%w/w) <sup>b</sup>
PLGA-L	None	None
PLGA-S	None	None
BSA/PLGA-L	None	6.8 ± 0.1
BSA/PLGA-S	None	7.1 ± 1.5
SPION-PLGA-L	21.6 ± 3.0	None
SPION-PLGA-S	27.1 ± 2.9	None
BSA/SPION-PLGA-L	15.3 ± 2.6	5.6 ± 0.4
BSA/SPION-PLGA-S	15.6 ± 0.8	3.1 ± 0.4

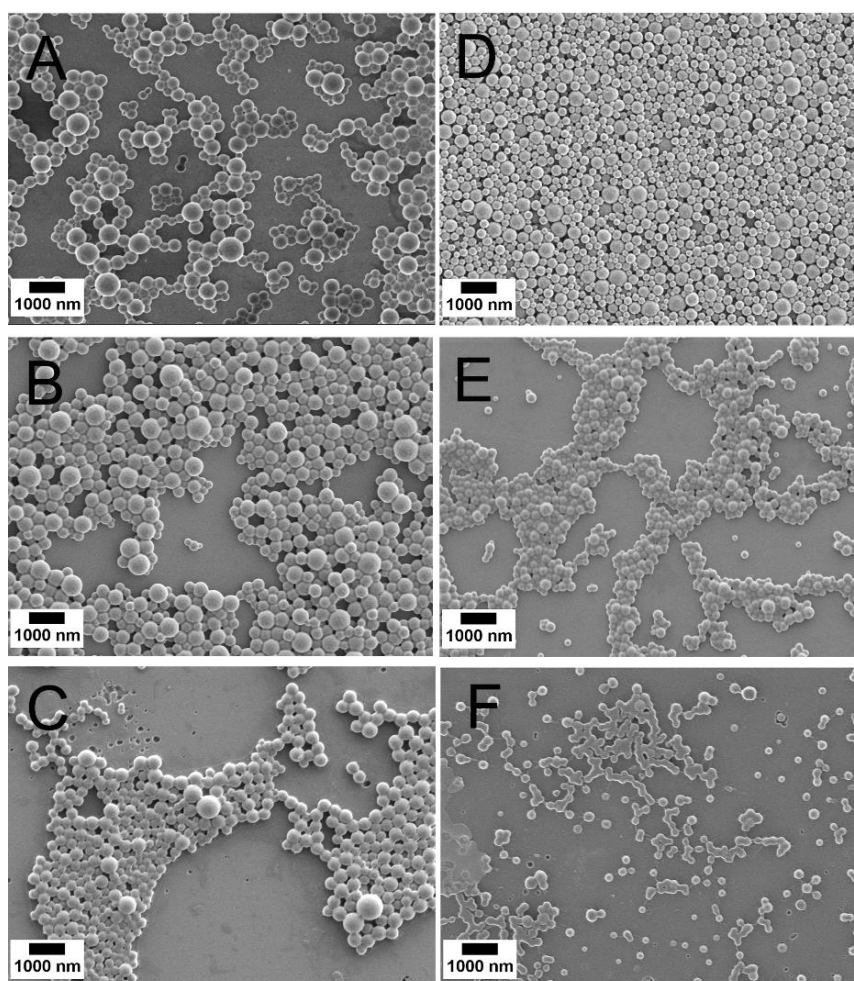
<sup>a</sup> % SPION loading was calculated from the iron content obtained from ICP-OES analysis of the digested particles.

<sup>b</sup> % BSA loading was quantified by UV-Visible spectroscopy from the extracted protein solution.

#### 4.2.2.4 Investigation of PLGA particles stability

In this study, PLGA was selected based on the fact that PLGA is the well accepted biocompatible and biodegradable polymer. Here the biodegradability of the PLGA-L and the PLGA-S particles when kept at 37 °C with 5% CO<sub>2</sub> in PBS buffer of pH 7.4 (similar as cells culture condition) was also confirmed through their morphological change and decrease in size using FESEM (Figure 4.14). The both PLGA particles sizes (PLGA-L and PLGA-S) appear as spherical shape with smooth surface before incubation (Figure 4.10), and they remain the same sizes and surface structures after one day of incubation (Figures 4.14A and D), respectively. However, after two days of incubation

as shown in Figure 4.14B and E, both sizes of particles start to agglomerate and fuse together. Moreover, the fused particles appeared smaller after seven days of incubation (Figure 4.14C and F). This results indicate the degradation of the polymer, and this phenomenon was likely more obvious in PLGA-S. This observation suggests that the PLGA particles are biodegradable and can gradually release the protein or other molecules after incubation at 37 °C mimic as body temperature [63], and PLGA can be kept at 4 °C more than 2 weeks without fusion.



**Figure 4.14** FESEM images of PLGA-L particles (A-C) and PLGA-S (D-F) after being incubated in a 24 well-plate at 37 °C with 5% CO<sub>2</sub> in PBS buffer pH 7.4 for 1 (A, D), 2 (B, E), and 7 (C, F) days.

From these characterizations, we chose the SPION-PLGA to test for cytotoxicity, protein delivery and cell activation due to its stronger magnetic response than SPION-

mPAA (Appendix: Figure A1). As the FESEM and TEM results show that PLGA encapsulate many SPION particles and can gradually release the protein at 37 °C (body temperature), the particles are suitable to use in the application that we are interested.

### 4.3 Cytotoxicity Testing and Cellular Uptake and Protein Delivery

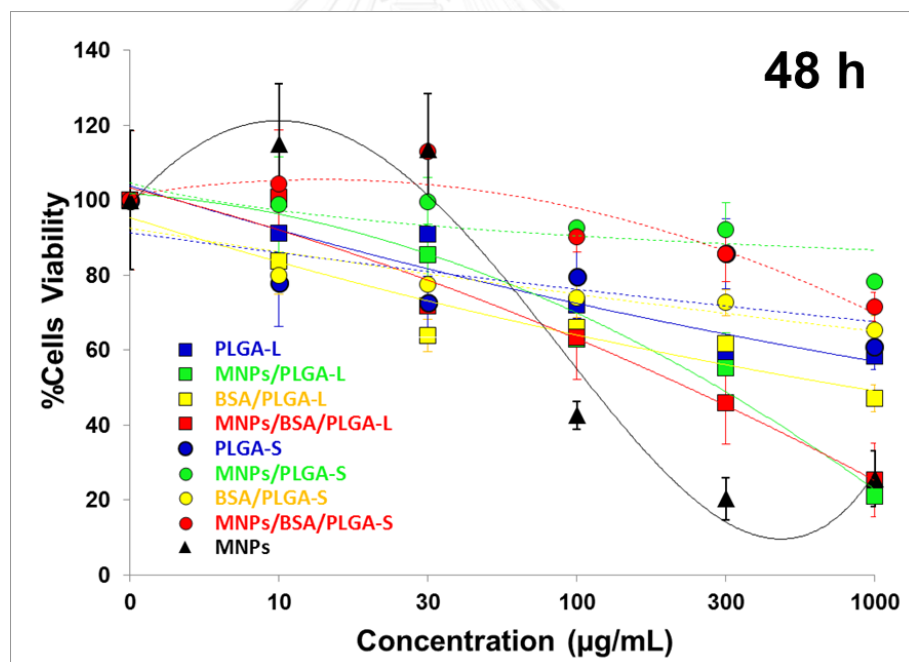
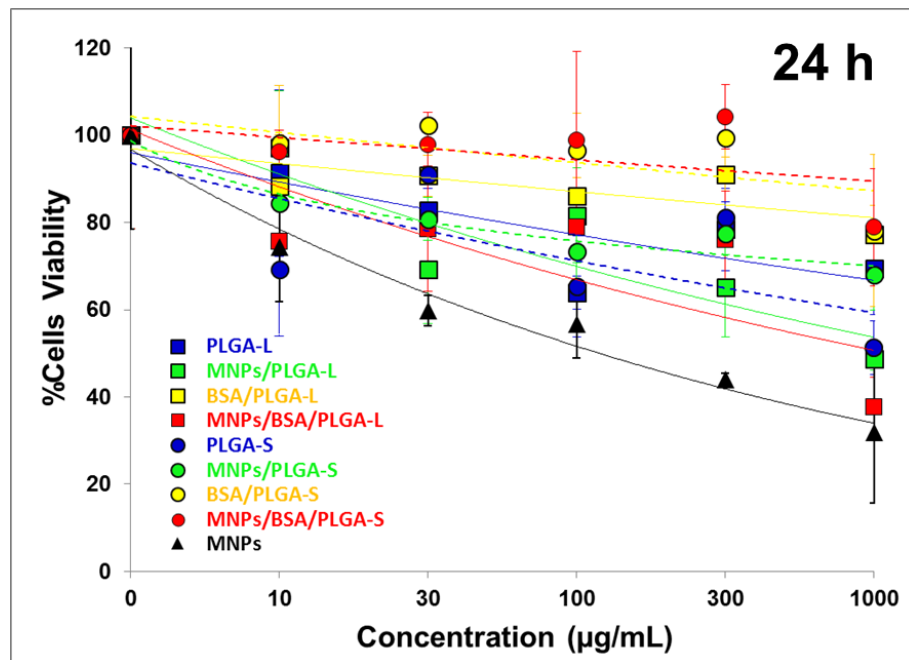
#### 4.3.1 Cytotoxicity testing

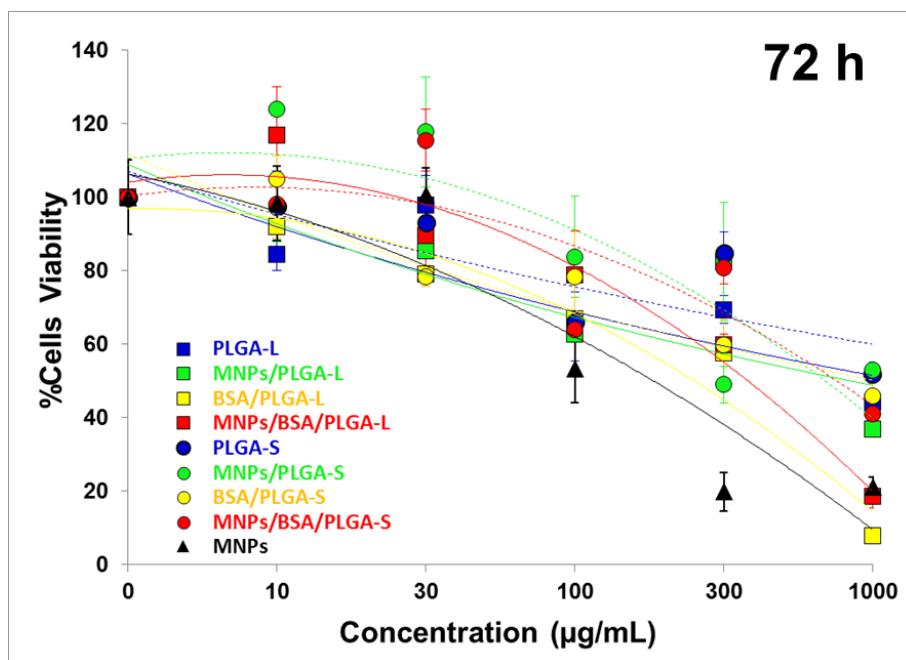
Before antigen presenting cells activation testing, it is important to evaluate the toxicity of the BSA/SPION-PLGA compared with particles without BSA protein or SPION. Here, the *in vitro* cytotoxicity of them with different administered concentration ranging from 10 to 1000 µg/mL on macrophage cell line (Raw264.7 cell).

This experiment was studied via MTT assay and discovered at 24, 48 and 72 hours as shown in Figure 4.15. Many researches have reported that PLGA polymer and magnetic iron oxide nanoparticles are biocompatible to many cells [11, 40]. In this study, all nanoparticles and magnetic nanocomposites at the concentrations of lower than 100 µg/mL exhibited very biocompatible with Raw264.7 cell. However, we chose the concentration of 100 µg/mL for cellular activation even though the cell viability was lower because high SPIONs concentration has been reported to show high activation [64]. Moreover, Raw264.7 (macrophage) cells were reported to be more sensitive than other cell such as epithelium and stem cells [65, 66], so the cell viability reported here were lower than the value reported normally.

Furthermore, particles with SPIONs show increase toxicity with increasing concentration. This can probably be related to the ability of the SPIONs to generate reactive oxygen species and thus produce dose-dependent cytotoxicity.[67] More pronounced toxicity was observed after for 48 h and 72 h incubation (Figure 4.15). Moreover, the large particles (solid line) exhibited more cytotoxicity than small size (dashed line) and obviously observed after 24 h. Therefore, we have concluded that both sizes (300 nm and 500 nm) of SPION-PLGA and BSA/SPION-PLGA particles should be used at the concentrations of 100 µg/mL, and our further experiments conform to this concentration limit.



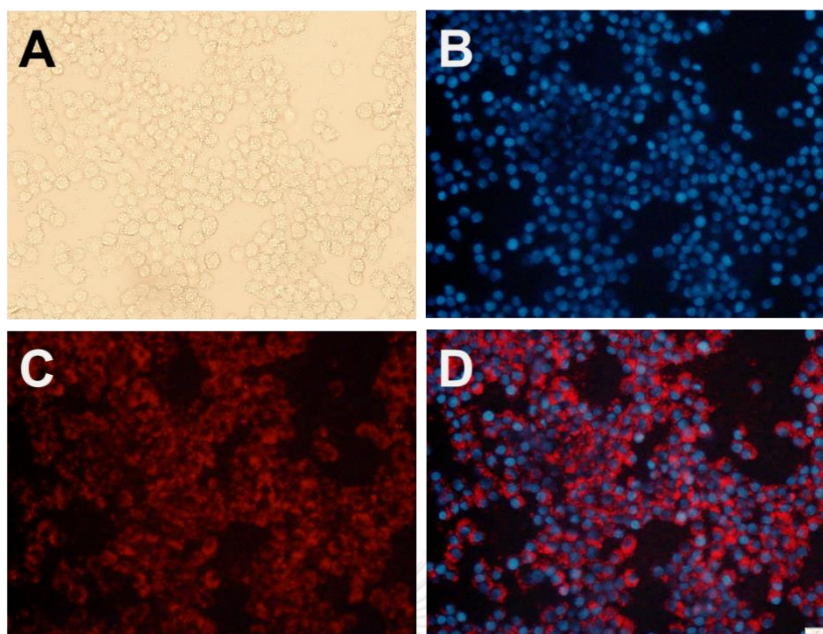




**Figure 4.15** Cytotoxicity of the SPION, PLGA and SPION-PLGA with and without BSA protein in macrophages cell line (Raw 264.7). Cell viability from the MTT assay after incubating the cells with the tested particles at 37 °C with 5% CO<sub>2</sub> for 24 h, 48 h and 72 h. Data are shown as mean  $\pm$  SD, derived from 3 repeats.

#### 4.3.2 Cellular uptake of particles and protein delivery

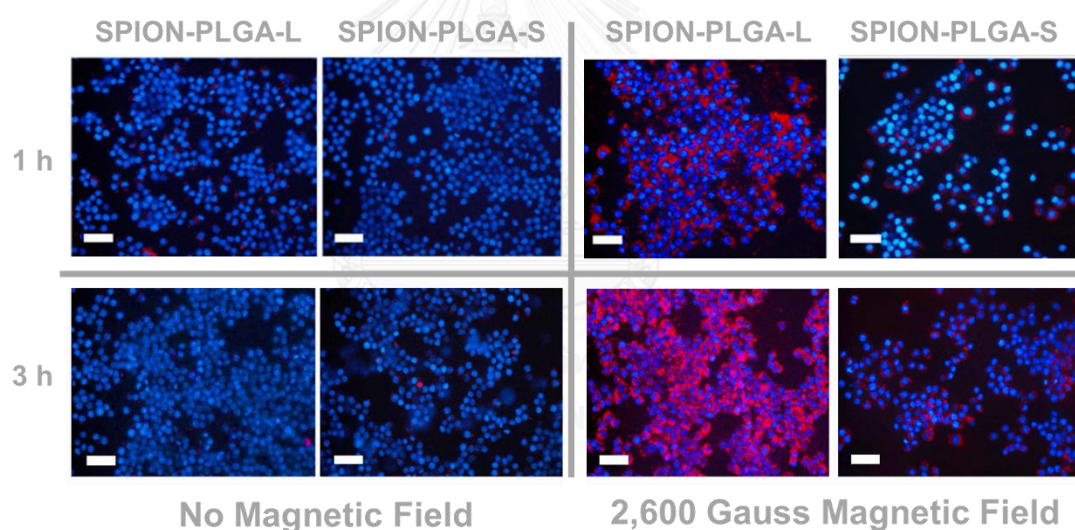
Cellular uptake of the different sizes of PLGA encapsulating SPION (SPION-PLGA-L and SPION-PLGA-S) were evaluated on Raw 264.7 cells under an external magnetic field. Here the TAMRA-labeled SPION-PLGA-L and TAMRA-labeled SPION-PLGA-S were used (100 µg of particles contained 180 ng of TAMRA). The particles were incubated with 250,000 cells. The image examples from fluorescent microscope measurement are shown in Figure 4.16. For investigation of cellular uptake, the blue fluorescence from nuclei stained with DAPI dye was observed at  $\lambda_{\text{ex/em}}_{\text{emit}}$  of 330/385 nm (Figure 4.16B). The red fluorescence of TAMRA dye represented SPION-PLGA particles was detected at  $\lambda_{\text{ex/em}}_{\text{emit}}$  of 520/550 nm (Figure 4.16C). For better observation of the particles uptake into cells, the overlay of cells and particles was performed in this study. Figure 4.16D demonstrated the particles penetrated into the cytoplasm of the cells, they enclosed the nucleus.



**Figure 4.16** Cellular uptake of particles. Fluorescent microscopic images of particles uptake into Raw 264.7 cells under various light wavelength **(A)** normal white light, **(B)** blue fluorescence from nucleus of Raw 264.7 cells stained with DAPI dye, **(C)** red fluorescence from particles encapsulating TAMRA dye and **(D)** overlay of nuclei (blue) and particles (red).

The tested SPION-PLGA-L and SPION-PLGA-S were incubated with the cells for 1 h and 3 h under normal condition (control, no magnetic field) and under an external magnetic field of 2,600 Gauss (Figure 4.17). Under normal condition, almost no TAMRA fluorescence signal could be observed inside the cells that were incubated with both sizes of the particles (Figure 4.17 Rows 1-2, and Columns 1-2), even after 1 h and 3 h incubation, indicating that the particles were not taken up into the cells. In contrast, in the presence of the magnetic field, obvious TAMRA fluorescence could be observed inside the cells that had been incubated with the large particles (SPION-PLGA-L) for 1 h (Figure 4.17 Row 1, Column 3) and more pronounced signals were observed at 3 h incubation (Figure 4.17 Row 2, Column 3), implying significant cellular uptake of the particles. The location of the TAMRA signal was in the cytoplasm outside the nucleus, indicating that the particles were in the cytoplasm area of the cells. Interestingly, in presence of the same magnetic field, the small size particles (SPION-PLGA-S) were not

significantly taken up into the cells for 1 h incubation. However, the results of 3 h incubation exhibits that little fluorescent signals of the TAMRA could be observed inside the cells incubated with TAMRA-labeled SPION-PLGA-S. It should be noted here that the two sizes of particles containing the same loading of SPIONs in term of mass ratios. This means that when comparing the numbers of SPIONs per particle, the larger particles actually contain more SPIONs than the smaller particles. The reason for the discrepancy in cellular uptake between the 300 and the 500 nm TAMRA-labeled SPION-PLGA under a magnetic field may relate to the fact that the larger particles contain higher numbers of the SPIONs, and thus respond better to the magnetic field. From the results, we conclude that an external magnetic field can significantly increase cellular uptake of the SPION-PLGA particles, and the stimulation by the magnetic field is more pronounced for the larger particles, comparing to the smaller ones.

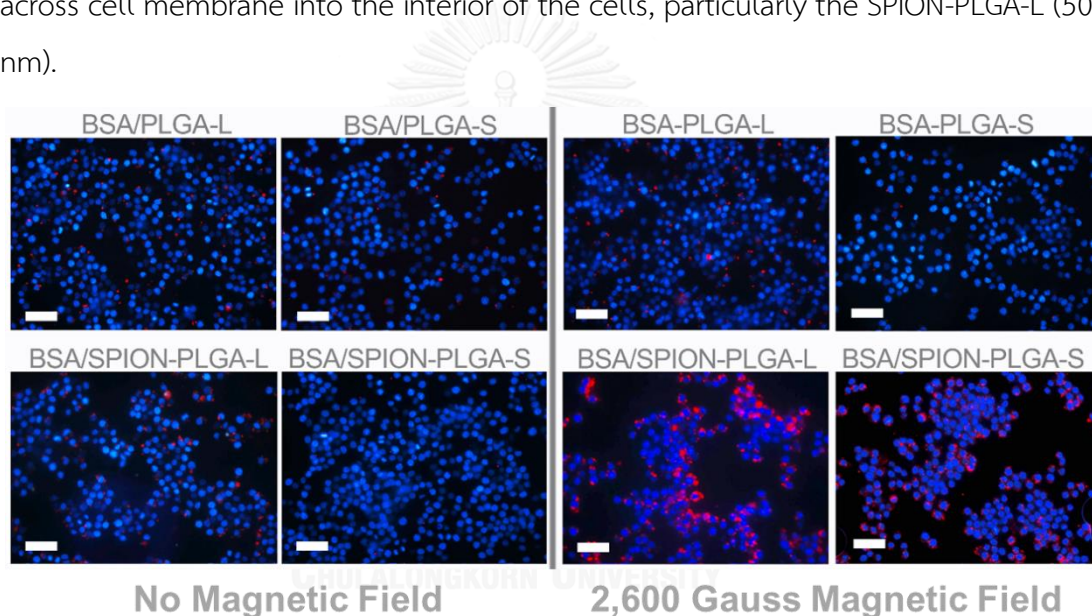


**Figure 4.17** Cellular uptake of particles. Fluorescent microscopic images of RAW264.7 cells after 1 h (Row 1) and 3 h (Row 2) incubation at 37 °C with 5% CO<sub>2</sub>, under no magnetic field and under 2,600 Gauss magnetic field, with BSA-unloaded SPION-PLGA particles: TAMRA-labeled SPION-PLGA-L, TAMRA-labeled SPION-PLGA-S. Scale bars in all figures indicate 40 μm.

For investigation of the potential of particles for BSA protein delivery, the particles encapsulating TAMRA-labeled BSA protein (BSA/SPION-PLGA) were studied in



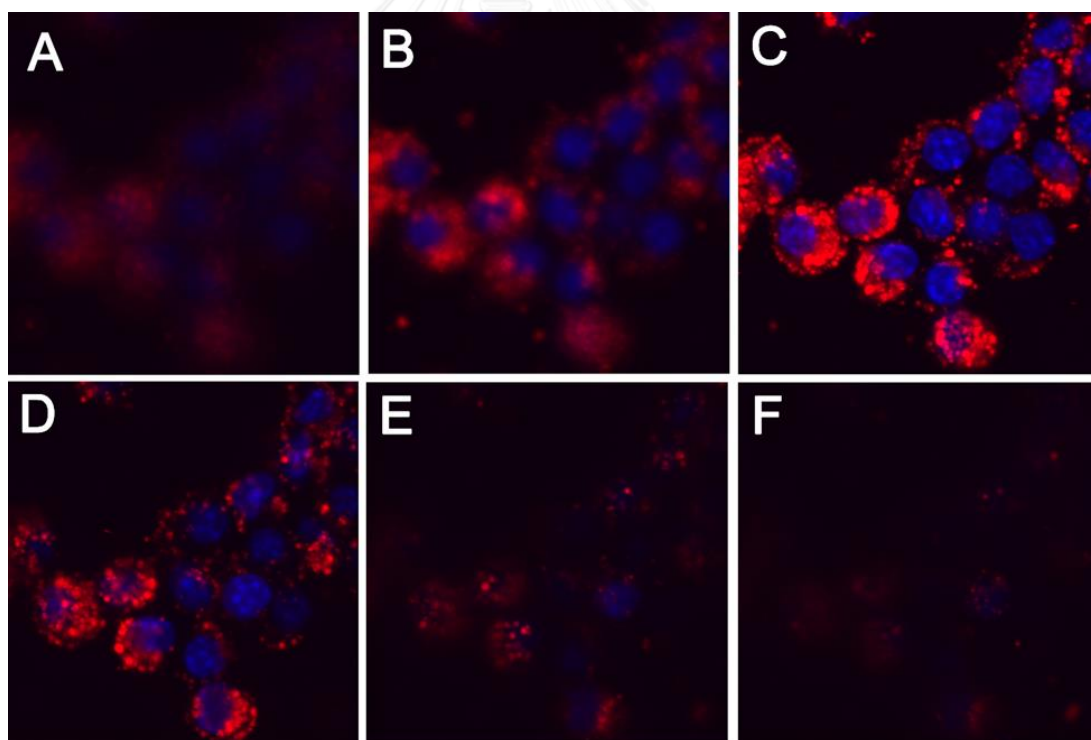
this experiment. The BSA/SPION-PLGA-L and the BSA/SPION-PLGA-S were tested for their ability to be taken up into the RAW264.7 cells under a presence/absence of an external magnetic field, the highest uptake was observed for the large particles with a presence of the magnetic field (Figure 4.18 Rows 1-2, Columns 3-4), similar to the previous uptake experiment (Figure 4.17). Without SPIONs embedding in the particles, no significant uptake could be observed, i.e., both the large and the small BSA/PLGA particles (Figure 4.18 Row 1) produced no significant TAMRA fluorescence inside the cells. Therefore, we conclude that we can load protein into the 300 and 500 nm SPION-PLGA particles and use a magnetic field to help directing these protein-loaded particles across cell membrane into the interior of the cells, particularly the SPION-PLGA-L (500 nm).



**Figure 4.18** Cellular uptake of TAMRA- labeled BSA particles. Fluorescent microscopic images of RAW264.7 cells after 3 h- incubation at 37 °C with 5% CO<sub>2</sub>, under no magnetic field and under 2,600 Gauss magnetic field, BSA-loaded SPION-free particles (**Row 1**), TAMRA-labeled BSA/PLGA-L, TAMRA-labeled BSA/PLGA-S, TAMRA-labeled BSA-loaded SPION-PLGA particles (**Row 2**), TAMRA-labeled BSA/SPION-PLGA-L, TAMRA-labeled BSA/SPION-PLGA-S in absence/presence of magnetic field. Scale bars in all figures indicate 40 μm.

To confirm that the particles were internalized into Raw264.7 cells, the SPION-PLGA-L was chosen to be further investigated using confocal laser scanning microscopy

(CLSM) technique because it showed the most uptake into the cells under an external magnetic field as shown in fluorescent microscopic images (Figure 4.17). The CLSM was performed in Z stacking mode to observe particles (red) and nucleuse cells (blue) at different planes along the Z axis. At the uppermost layer (Figure A), low signals from particles were observed. Then, when images was captured at deeper planes, the red signals of many particles are clearly observed at the same layer as the nucleuses (Figure C and D). These results suggested that the higher concentration of SPION-PLGA-L particles were taken into the cytoplasm around the nucleuses as mentioned in report of Arruebo, et al. [18] that the magnetic nanoparticles can be internalized into dendritic or macrophage cells through endocytosis or phagocytosis. However, some particles may be localized outside cell membrane as small signals were observed at the top and bottom of the cells when nucleuses signals disappeared at the highest and lowest layers of z planes (Figure A and F).



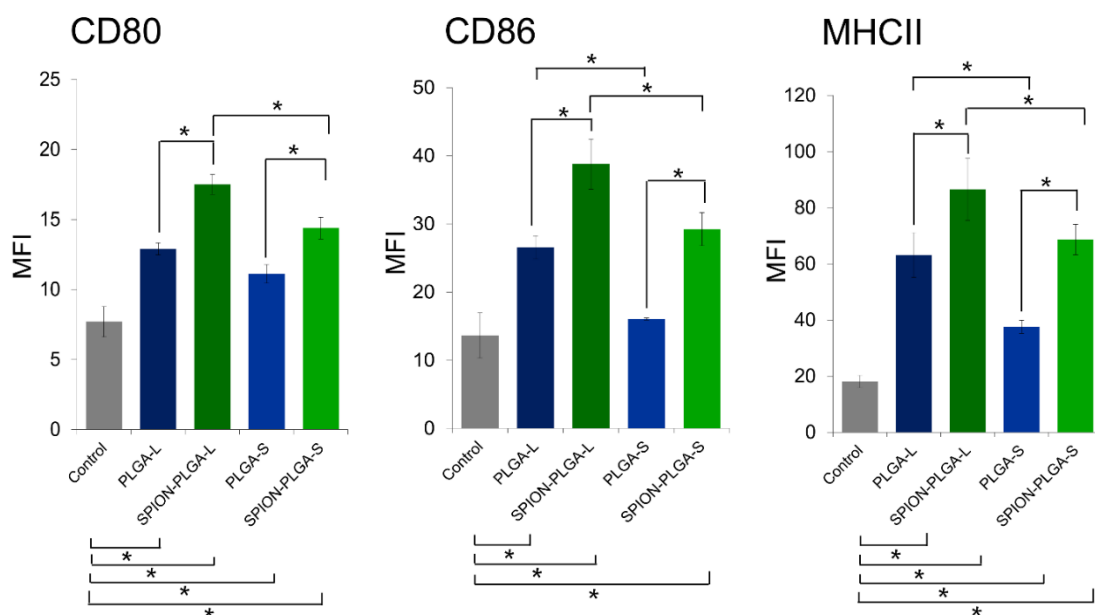
**Figure 4.19** Cellular uptake of particles. Confocal laser scanning microscopic (CLSM) images of RAW264.7 cells (nucleuse cells: blue) with TAMRA-labeled SPION-PLGA-L (TAMRA: red) after 3 h incubation at 37 °C with 5% CO<sub>2</sub>, under 2,600 Gauss magnetic field.

## 4.4 Induction of Dendritic Cell Maturation and Cytokine Production

### 4.4.1 Induction of dendritic cell Maturation with flow cytometry analysis (FACS)

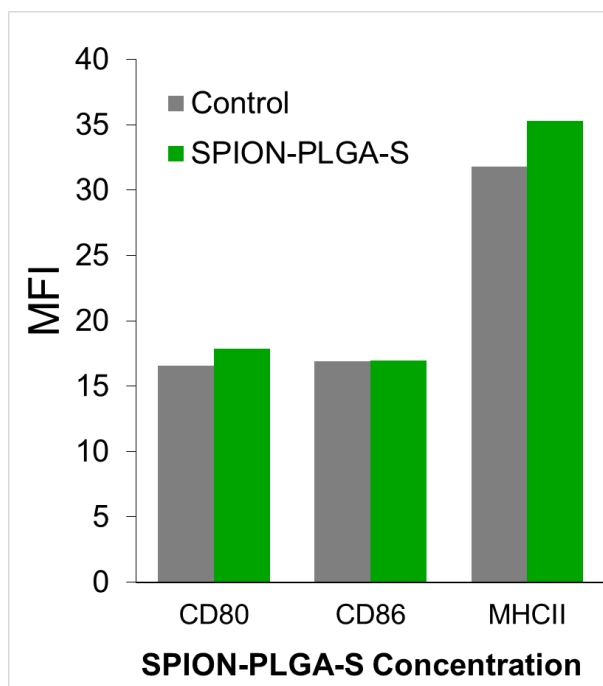
The induction of dendritic cell maturation were performed using murine bone marrow-derived dendritic cells (BM-DCs) of mice. Mature BM-DCs are capable of inducing potent adaptive immune responses that consequently result in an ability to eliminate the recognized invading pathogens.[68] The antigen carrier for vaccination should thus possess the immunogenic properties to induce DC maturation.[69] To investigate the effects of the 300 and 500 nm BSA loaded/unloaded SPION-PLGA compared with SPION-free PLGA particles on BM-DC maturation, BM-DCs were incubated with the particles in a presence or absence of an external magnetic field, and the surface expressions of the maturation markers CD80, CD86 and MHC class II were then determined through the use of specific fluorescence labeled antibodies coupled with a flow cytometry. Under an external magnetic field, the cells treated with all PLGA-based particles showed significantly increased CD80, CD86 and MHC class II levels (Figure 4.19) as compared to the negative control, with the exception of only in cells treated with the PLGA-S where their CD86 level did not significantly differ from the negative control. The results are consistent to the stimulation effect of PLGA reported previously.[70] The small sized particles seemed to own less efficacy to exert DC maturation. Particles containing SPIONs showed significantly higher stimulation effect comparing to the PLGA particles with no SPIONs.

It should be noted here that under no external magnetic field, SPION-containing PLGA (SPION-PLGA-S) particles possess similar degree of maturation induction to the SPION-free PLGA (PLGA-S) particles (Figure 4.20). It is likely that under the presence of an external magnetic field, the SPION-PLGA particles were more efficiently taken up into the BM-DCs as compared to the SPION-free PLGA particles. It has been reported previously that metal-based nanoparticles can activate innate immune cells, including DCs, through the mediation of Toll-like receptor (TLR) signaling.[71] Thus, it is likely that iron oxide nanoparticles may be a key factor for the enhanced immunogenic properties observed for the SPION-PLGA.



**Figure 4.20** Induction of DC maturation. BM-DCs were incubated with each of the PLGA and SPION-PLGA particles (100  $\mu\text{g}/\text{mL}$ ) at 37  $^{\circ}\text{C}$  under 5%  $\text{CO}_2$  in the presence of 2,600 Gauss magnetic field for 3 h, then the magnetic field was removed and incubation was carried out for another 48 h. BM-DC maturation markers were determined by flow cytometric analysis. The DC marker, CD11c was gated and the mean fluorescence intensity (MFI) of CD80, CD86 and MHC class II were evaluated. \*indicates the statistical significant difference between the samples, as determined by one way ANOVA Tukey HSD ( $n=3$ ) at  $p < 0.05$ .

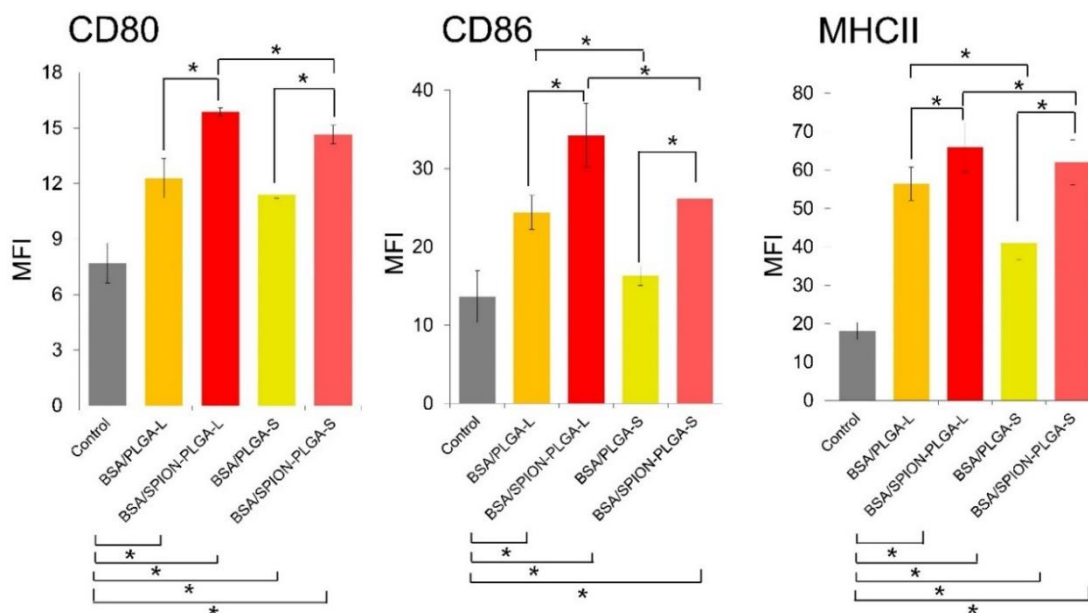




**Figure 4.21** Induction of DC maturation. BM-DCs were incubated with each of the SPION-PLGA-S particles (100  $\mu\text{g}/\text{mL}$ ) at 37  $^{\circ}\text{C}$  under 5%  $\text{CO}_2$  incubation for another 48 h, under absence of magnetic field. BM-DC maturation markers were determined by flow cytometric analysis. The DC marker, CD11c was gated and the mean fluorescence intensity (MFI) of CD80, CD86 and MHC class II were evaluated.

Moreover, both sizes of the PLGA and SPION-PLGA loading BSA protein exhibited DC maturation as shown in Figure 4.21. The BSA/PLGA particles showed similar activation results of the BM-DCs maturation as PLGA particles. However, with the presence of BSA, SPION-PLGA exhibited slightly lower surface expressions of the maturation markers CD80, CD86 and MHC class II than the absence of BSA protein because when BSA loading the SPION will decrease and less uptake into the cells.

Therefore, this experiment could ensure us that the BSA protein seemingly show no significance in stimulation of BM-DCs, but the cells stimulation depending on SPIONs content in the particle. The effect from cellular uptake and ability of SPIONs for cell activation may be the main reason for this observation.



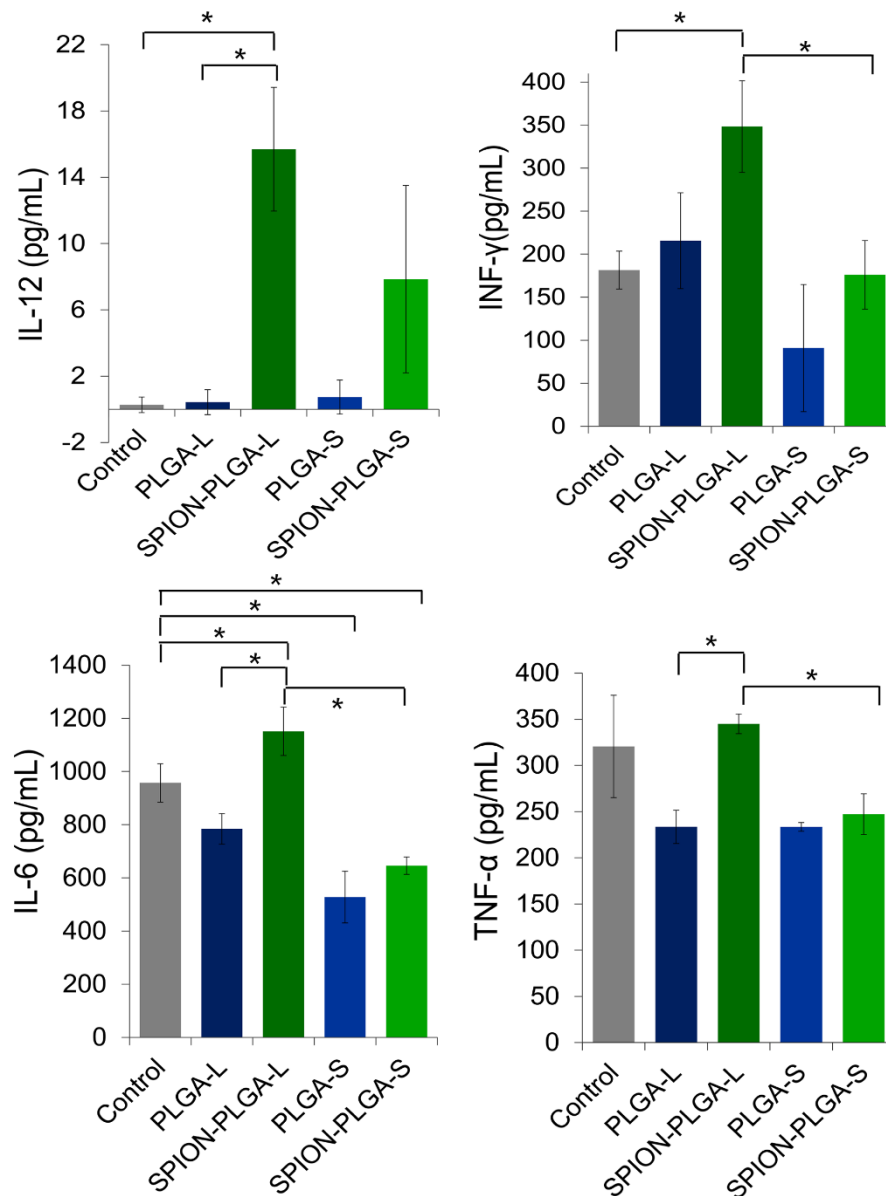
**Figure 4.22** Induction of DC maturation. BM-DCs were incubated with each of the BSA/PLGA and BSA/SPION-PLGA particles (100  $\mu\text{g}/\text{mL}$ ) at 37  $^{\circ}\text{C}$  under 5%  $\text{CO}_2$  in the presence of 2,600 Gauss magnetic field for 3 h, then the magnetic field was removed and incubation was carried out for another 48 h. BM-DC maturation markers were determined by flow cytometric analysis. The DC marker, CD11c was gated and the mean fluorescence intensity (MFI) of CD80, CD86 and MHC class II were evaluated. \* indicates the statistical significant difference between the samples, as determined by one way ANOVA Tukey HSD ( $n=3$ ) at  $p < 0.05$ .

#### 4.4.2 Cytokine Production performing with ELISA assay

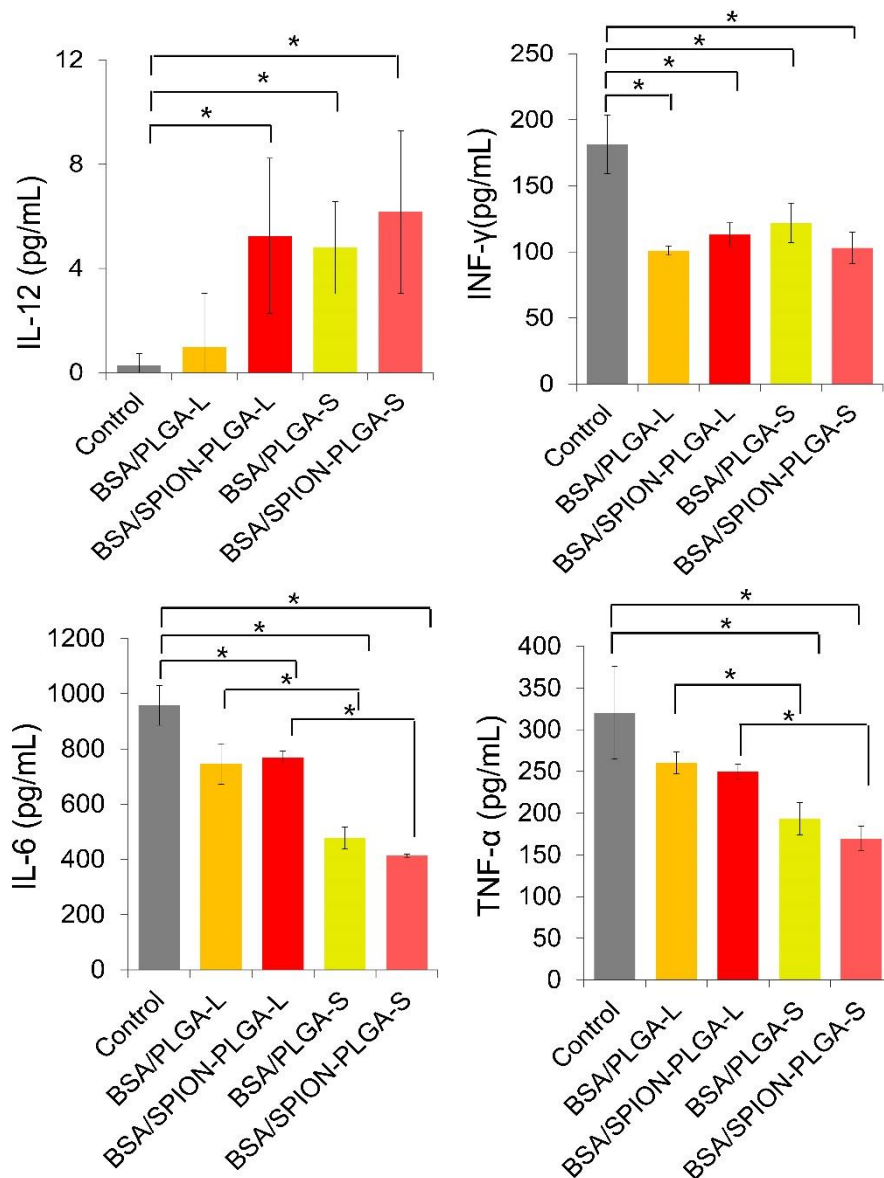
The induction of dendritic cells maturation usually leads to the production of cytokines that subsequently govern the responses of adaptive immunity and the amplification of innate immune functions.[5, 72] Therefore, we next examined the effect of the PLGA and SPION-PLGA particles on the pro-inflammatory cytokine secretion of the BM-DCs. BM-DCs were stimulated with the tested particles in the presence of an external magnetic field, and the production of IL-12, IFN- $\gamma$ , IL-6 and TNF- $\alpha$  were measured by ELISA (Figure 4.22). Although the SPION-free PLGA particles were capable of inducing some BM-DC maturation (Figure 4.18), they poorly mediated the cytokine production, i.e., all the four cytokine levels of the PLGA particle-treated

cells were not significantly different from those of the controls. Interestingly, the SPION-PLGA-L particles (500 nm of size) could notably enhance the levels of IL-12, IFN- $\gamma$  and IL-6, as significantly compared to the control. These effects were limited to only the large particles; the SPION-PLGA-S particles (300 nm of size) did not produce any significantly increased levels of the four cytokines. It is likely that the stimulation effect of the SPION-PLGA-L particles is related to their ability to be effectively taken up into cells under an external magnetic field. Nevertheless, other factors may play a role, e.g., the size of PLGA particles has been shown to be critical for the functional properties of dendritic cells.[73] The size of less than 200 nm are more favorable for triggering the inflammatory and cell-mediated immune responses, while the sizes of larger than 300 nm, as our PLGA-L and PLGA-S particles, are less effective to induce the pro-inflammatory cytokine production.[73] It is possible that the upregulation of the three cytokines (IL-12, IFN- $\gamma$  and IL-6) observed for the SPION-PLGA-L occurs through the TLR signaling pathway since an ability of the SPION particles to mediate TLR signal transduction via MyD88 adaptor and pro-inflammatory cytokine upregulation have been reported.[74] In fact, several metal-based nanoparticles can stimulate pro-inflammatory cytokine production in immune cells in a dose- and size-dependent manners.[71], [75] Furthermore, the BSA/PLGA and BSA/SPION-PLGA results exhibited that enhance only IL-12 cytokines production more than PLGA but still less than SPION-PLGA-L as shown in Figure 4.23. However, BSA-loaded particles significantly inhibited upregulation of the three cytokines (IFN- $\gamma$ , TNF- $\alpha$  and IL-6).

IL-12 and IFN- $\gamma$  are the key cytokines that drive Th1 differentiation[76] and exert cytotoxic T lymphocyte (CTL) effector functions[77], [78] as well as memory CD8 T cell generation.[79], [80] Therefore, an ability of the SPION-PLGA-L particle to upregulate these two cytokines implies that targeting DCs by this antigen carrier could possibly help provoking the protective immunity against specific pathogens such as intracellular bacteria and viruses.



**Figure 4.23** Stimulation of cytokine production. BM-DCs were incubated with each of the tested PLGA and SPION-PLGA particles (100  $\mu\text{g}/\text{mL}$ ) at 37  $^{\circ}\text{C}$  under 5%  $\text{CO}_2$  in the presence of 2,600 Gauss magnetic field for 3 h. Then the magnetic field was removed and incubation was carried out for another 48 h. Cytokine analysis was evaluated through ELISA. \* indicates the statistical significant difference between the samples, as determined by one way ANOVA Tukey HSD (n=3) at  $p < 0.05$ .



**Figure 4.24** Stimulation of cytokine production. BM-DCs were incubated with each of the BSA-loaded particles (100  $\mu\text{g/mL}$ ) at 37  $^{\circ}\text{C}$  under 5%  $\text{CO}_2$  in the presence of 2,600 Gauss magnetic field for 3 h, then the magnetic field was removed and incubation was carried out for another 48 h. Cytokine analysis was evaluated through ELISA. \* indicates the statistical significant difference between the samples, as determined by one way ANOVA Tukey HSD (n=3) at  $p < 0.05$ .

## CHAPTER V

### CONCLUSION

In this study, we show the synthesis of the superparamagnetic iron oxide nanoparticles (SPION) using two different methods. The thermal decomposition using iron-oleate as starting materials, oleic acid as surfactant, and 1-octadecene as solvent exhibit more uniform SPIONs and better dispersion than co-precipitation method. Then, the obtained SPIONs were used to prepare SPION-Polymer and also load the BSA (a model protein antigen) by comparing two biocompatible polymer: mPAA and PLGA. SPION-PLGA particles showed advantages over SPION-mPAA particles in that the SPION-PLGA particles exhibit stronger magnetic response and could control protein release by temperature.

The biocompatible/biodegradable PLGA particles containing SPIONs (SPION-PLGA particles) and the BSA-loaded SPION-PLGA particles (BSA/SPION-PLGA) were investigated for their toxicity, cellular uptake and efficiency in BM-DCs activation. The cytotoxicity and cellular uptake were performed on macrophage cell line (Raw 264.7). From the cytotoxicity studies, PLGA-based particles with the concentration of 100  $\mu\text{g}/\text{mL}$  and below exhibit acceptable low toxicity and could be used in biological experiments. Moreover, under an external magnetic field, we have demonstrated a significantly better cellular uptake of the relatively non-toxic SPION-PLGA and the BSA/SPION-PLGA particles into Raw 264.7 cells, as compared to the uptake of the particles under no external magnetic field. The large particles (500 nm) SPION-PLGA particles perform better in cellular uptake and BSA protein delivery than the small SPION-PLGA (300 nm) particles.

In addition, the effects of SPION-PLGA and BSA/SPION-PLGA on BM-DC activation were tested. From the experiment, it is clearly shown that the combined SPIONs with PLGA and an external magnetic field can significantly enhance BM-DCs maturation by upregulating surface molecule MHC II, CD80 and CD86 expression. Nevertheless, the BM-DCs maturation significantly decrease from SPION-PLGA in the presence of BSA protein in particles because of less SPIONs content in particles leading to lower cellular

uptake. We also verify that our SPION-PLGA particles can significantly produce upregulation of the IL-12, IFN- $\gamma$  and IL-6 in the BM-DC cells under an external magnetic field.

With the abilities of our SPION-PLGA particles when combined with an external magnetic field to significantly induce immune response, we anticipate more investigations on this novel platform for vaccine applications, including a possible replacement of the needle antigen injection with the magnetic field-guided antigen delivery. More improvement and development are needed to increase the BM-DCs activation with cytokines production efficiency and develop effective systems for *in vivo* applications.



## REFERENCES

- [1] Yue, H. and Ma, G. Polymeric micro/nanoparticles: Particle design and potential vaccine delivery applications. Vaccine 33(44) (2015): 5927-36.
- [2] Zhao, L., et al. Nanoparticle vaccines. Vaccine 32(3) (2014): 327-37.
- [3] Smith, D.M., Simon, J.K., and Baker, J.R., Jr. Applications of nanotechnology for immunology. Nat Rev Immunol 13(8) (2013): 592-605.
- [4] Zhang, M., Hong, Y., Chen, W., and Wang, C. Polymers for DNA Vaccine Delivery. ACS Biomaterials Science & Engineering 3(2) (2016): 108-125.
- [5] Steinman, R.M. Decisions about dendritic cells: past, present, and future. Annu Rev Immunol 30 (2012): 1-22.
- [6] Liu, Y., Chen, X., Wang, L., Yang, T., Yuan, Q., and Ma, G. Surface charge of PLA microparticles in regulation of antigen loading, macrophage phagocytosis and activation, and immune effects in vitro. Particuology 17 (2014): 74-80.
- [7] Sun, C., Lee, J.S., and Zhang, M. Magnetic nanoparticles in MR imaging and drug delivery. Adv Drug Deliv Rev 60(11) (2008): 1252-65.
- [8] Baumjohann, D., Hess, A., Budinsky, L., Brune, K., Schuler, G., and Lutz, M.B. In vivo magnetic resonance imaging of dendritic cell migration into the draining lymph nodes of mice. Eur J Immunol 36(9) (2006): 2544-55.
- [9] Tavare, R., et al. Monitoring of in vivo function of superparamagnetic iron oxide labelled murine dendritic cells during anti-tumour vaccination. PLoS One 6(5) (2011): e19662.
- [10] DeMuth, P.C., Min, Y., Irvine, D.J., and Hammond, P.T. Implantable silk composite microneedles for programmable vaccine release kinetics and enhanced immunogenicity in transcutaneous immunization. Adv Healthc Mater 3(1) (2014): 47-58.
- [11] Waeckerle-Men, Y. and Groettrup, M. PLGA microspheres for improved antigen delivery to dendritic cells as cellular vaccines. Adv Drug Deliv Rev 57(3) (2005): 475-82.



- [12] Schmid, G. Nanoscale Materials as Intermediate between Atomic and Bulk Matter. Nanoparticles, ed. 1. Germany: WILEY-VCH Verlag GmbH, 2004.
- [13] Jain, P.K., Huang, X., El-Sayed, I.H., and El-Sayed, M.A. Review of Some Interesting Surface Plasmon Resonance-enhanced Properties of Noble Metal Nanoparticles and Their Applications to Biosystems. Plasmonics 2(3) (2007): 107-118.
- [14] Petros, R.A. and DeSimone, J.M. Strategies in the design of nanoparticles for therapeutic applications. Nat Rev Drug Discov 9(8) (2010): 615-627.
- [15] Mahmoudi, M., Sant, S., Wang, B., Laurent, S., and Sen, T. Superparamagnetic iron oxide nanoparticles (SPIONs): Development, surface modification and applications in chemotherapy. Advanced Drug Delivery Reviews 63(1-2) (2011): 24-46.
- [16] Lu, A.H., Salabas, E.L., and Schuth, F. Magnetic nanoparticles: synthesis, protection, functionalization, and application. Angew Chem Int Ed Engl 46(8) (2007): 1222-44.
- [17] Wu, W., Wu, Z., Yu, T., Jiang, C., and Kim, W.S. Recent progress on magnetic iron oxide nanoparticles: synthesis, surface functional strategies and biomedical applications. Sci Technol Adv Mater 16(2) (2015): 023501.
- [18] Arruebo, M., Fernández-Pacheco, R., Ibarra, M.R., and Santamaría, J. Magnetic nanoparticles for drug delivery. Nano Today 2(3) (2007): 22-32.
- [19] Alexandre, M. and Dubois, P. Polymer-layered silicate nanocomposites: preparation, properties and uses of a new class of materials. Materials Science and Engineering: R: Reports 28(1-2) (2000): 1-63.
- [20] Veisoh, O., Gunn, J.W., and Zhang, M. Design and fabrication of magnetic nanoparticles for targeted drug delivery and imaging. Adv Drug Deliv Rev 62(3) (2010): 284-304.
- [21] Alimohammadi, S., Salehi, R., Amini, N., and Davaran, S. Synthesis and Physicochemical Characterization of Biodegradable PLGA-based Magnetic Nanoparticles Containing Amoxicilin. Bulletin of the Korean Chemical Society 33(10) (2012): 3225-3232.

- [22] Wu, W., He, Q., and Jiang, C. Magnetic iron oxide nanoparticles: synthesis and surface functionalization strategies. Nanoscale Res Lett 3(11) (2008): 397-415.
- [23] Redl, F.X., et al. Magnetic, Electronic, and Structural Characterization of Nonstoichiometric Iron Oxides at the Nanoscale. Journal of the American Chemical Society 126(44) (2004): 14583-14599.
- [24] Farrell, D., Majetich, S.A., and Wilcoxon, J.P. Preparation and Characterization of Monodisperse Fe Nanoparticles. The Journal of Physical Chemistry B 107(40) (2003): 11022-11030.
- [25] Park, J., et al. Ultra-large-scale syntheses of monodisperse nanocrystals. Nat Mater 3(12) (2004): 891-5.
- [26] Frey, N.A., Peng, S., Cheng, K., and Sun, S. Magnetic nanoparticles: synthesis, functionalization, and applications in bioimaging and magnetic energy storage. Chem Soc Rev 38(9) (2009): 2532-42.
- [27] Kango, S., Kalia, S., Celli, A., Njuguna, J., Habibi, Y., and Kumar, R. Surface modification of inorganic nanoparticles for development of organic-inorganic nanocomposites—A review. Progress in Polymer Science 38(8) (2013): 1232-1261.
- [28] Cayre, O.J., Chagneux, N., and Biggs, S. Stimulus responsive core-shell nanoparticles: synthesis and applications of polymer based aqueous systems. Soft Matter 7(6) (2011): 2211-2234.
- [29] Parkin, J. and Cohen, B. An overview of the immune system. The Lancet 357(9270) (2001): 1777-1789.
- [30] Dranoff, G. Cytokines in cancer pathogenesis and cancer therapy. Nat Rev Cancer 4(1) (2004): 11-22.
- [31] Gause, K.T., Wheatley, A.K., Cui, J., Yan, Y., Kent, S.J., and Caruso, F. Immunological Principles Guiding the Rational Design of Particles for Vaccine Delivery. ACS Nano 11(1) (2017): 54-68.
- [32] Zhang, W., et al. Comparison of PLA Microparticles and Alum as Adjuvants for H5N1 Influenza Split Vaccine: Adjuvanticity Evaluation and Preliminary Action Mode Analysis. Pharmaceutical Research 31(4) (2014): 1015-1031.

- [33] Kaur, G. and Dufour, J.M. Cell lines Valuable tools or useless artifacts. Spermatogenesis 2(1) (2012): 1-5.
- [34] Lonza. Primary Cells vs. Cell Lines [Online]. 2017. Available from: <http://www.lonza.com/products-services/bio-research/primary-cells/primary-cells-vs-cell-lines.aspx>
- [35] Terry, L.R., et al. Cell Viability Assays. Assay Guidance Manual (2013): 1-31.
- [36] Jahan-Tigh, R.R., Ryan, C., Obermoser, G., and Schwarzenberger, K. Flow Cytometry. Journal of Investigative Dermatology 132(10): 1-6.
- [37] Csernok, E. and Moosig, F. Current and emerging techniques for ANCA detection in vasculitis. Nat Rev Rheumatol 10(8) (2014): 494-501.
- [38] Li, T., et al. Folate-Functionalized Magnetic-Mesoporous Silica Nanoparticles for Drug/Gene Codelivery To Potentiate the Antitumor Efficacy. ACS Appl Mater Interfaces 8(22) (2016): 13748-58.
- [39] Shen, B., Ma, Y., Yu, S., and Ji, C. Smart Multifunctional Magnetic Nanoparticle-Based Drug Delivery System for Cancer Thermo-Chemotherapy and Intracellular Imaging. ACS Appl Mater Interfaces 8(37) (2016): 24502-8.
- [40] Cui, Y., Zhang, M., Zeng, F., Jin, H., Xu, Q., and Huang, Y. Dual-Targeting Magnetic PLGA Nanoparticles for Codelivery of Paclitaxel and Curcumin for Brain Tumor Therapy. ACS Applied Materials & Interfaces 8(47) (2016): 32159-32169.
- [41] Kanchan, V. and Panda, A.K. Interactions of antigen-loaded polylactide particles with macrophages and their correlation with the immune response. Biomaterials 28(35) (2007): 5344-5357.
- [42] Manolova, V., Flace, A., Bauer, M., Schwarz, K., Saudan, P., and Bachmann, M.F. Nanoparticles target distinct dendritic cell populations according to their size. Eur J Immunol 38(5) (2008): 1404-13.
- [43] Yue, H., et al. Particle size affects the cellular response in macrophages. European Journal of Pharmaceutical Sciences 41(5) (2010): 650-657.
- [44] Yue, Z.-G., et al. Surface Charge Affects Cellular Uptake and Intracellular Trafficking of Chitosan-Based Nanoparticles. Biomacromolecules 12(7) (2011): 2440-2446.

- [45] Chen, X., et al. Enhanced Humoral and Cell-Mediated Immune Responses Generated by Cationic Polymer-Coated PLA Microspheres with Adsorbed HBsAg. Molecular Pharmaceutics 11(6) (2014): 1772-1784.
- [46] Liu, Y., et al. Surface hydrophobicity of microparticles modulates adjuvant activity. Journal of Materials Chemistry B 1(32) (2013): 3888.
- [47] Barua, S., Yoob, J.-W., Poornima, K., Wakankarc, A., Gokarn, Y.R., and Mitragotri, S. Particle shape enhances specificity of antibody-displaying nanoparticles. Proceedings of the National Academy of Sciences of the United States of America 110(9) (2013): 3270–3275.
- [48] Majewski, A.P., Schallon, A., Jérôme, V., Freitag, R., Müller, A.H.E., and Schmalz, H. Dual-Responsive Magnetic Core–Shell Nanoparticles for Nonviral Gene Delivery and Cell Separation. Biomacromolecules 13(3) (2012): 857-866.
- [49] Somers, R.C., Snee, P.T., Bawendi, M.G., and Nocera, D.G. Energy transfer of CdSe/ZnS nanocrystals encapsulated with rhodamine-dye functionalized poly(acrylic acid). Journal of Photochemistry and Photobiology A: Chemistry 248 (2012): 24-29.
- [50] Putnam, F.W. 2 - Alpha, Beta, Gamma, Omega—The Structure of the Plasma Proteins. in The Plasma Proteins (Second Edition), pp. 45-166: Academic Press, 1984.
- [51] Yoon, S.B., et al. Anti-inflammatory effects of Scutellaria baicalensis water extract on LPS-activated RAW 264.7 macrophages. J Ethnopharmacol 125(2) (2009): 286-90.
- [52] Inaba, K., Swiggard, W.J., Steinman, R.M., Romani, N., Schuler, G., and Brinster, C. Isolation of dendritic cells. Current protocols in immunology. Vol. Chapter 3, 2009.
- [53] Inaba, K., Swiggard, W.J., Steinman, R.M., Romani, N., Schuler, G., and Brinster, C. Isolation of dendritic cells. Curr Protoc Immunol Chapter 3 (2009): Unit 3 7.
- [54] BioLegend, I. Sandwich ELISA Protocol [Online]. 2017. Available from: [http://www.biolegend.com/media\\_assets/support\\_protocol/BioLegend\\_Sandwich\\_ELISA\\_protocol.pdf](http://www.biolegend.com/media_assets/support_protocol/BioLegend_Sandwich_ELISA_protocol.pdf)

- [55] Kim, D., Lee, N., Park, M., Kim, B.H., An, K., and Hyeon, T. Synthesis of Uniform Ferrimagnetic Magnetite Nanocubes. Journal of the American Chemical Society 131(2) (2009): 454-455.
- [56] Park, T.-J., Papaefthymiou, G.C., Viascas, A.J., Moodenbaugh, A.R., and Wong, S.S. Size-Dependent Magnetic Properties of Single-Crystalline Multiferroic BiFeO<sub>3</sub> Nanoparticles. Nano Letters 7(3) (2007): 766-772.
- [57] Schilli, C.M., et al. A New Double-Responsive Block Copolymer Synthesized via RAFT Polymerization: Poly(N-isopropylacrylamide)-block-poly(acrylic acid). Macromolecules 37(21) (2004): 7861-7866.
- [58] Cun, D., Foged, C., Yang, M., Frokjaer, S., and Nielsen, H.M. Preparation and characterization of poly(DL-lactide-co-glycolide) nanoparticles for siRNA delivery. Int J Pharm 390(1) (2010): 70-5.
- [59] Gaumet, M., Gurny, R., and Delie, F. Fluorescent biodegradable PLGA particles with narrow size distributions: preparation by means of selective centrifugation. Int J Pharm 342(1-2) (2007): 222-30.
- [60] Bloemen, M., Brullot, W., Luong, T.T., Geukens, N., Gils, A., and Verbiest, T. Improved functionalization of oleic acid-coated iron oxide nanoparticles for biomedical applications. J Nanopart Res 14(9) (2012): 1100.
- [61] Alimohammadi, S., Salehi, R., Amini, N., and Davaran, S. Synthesis and Physicochemical Characterization of Biodegradable PLGA-based Magnetic Nanoparticles Containing Amoxicilin. Bull. Korean Chem. Soc. 33(10) (2012): 3225-3232.
- [62] Maruyama, T., et al. FT-IR analysis of BSA fouled on ultrafiltration and microfiltration membranes. Journal of Membrane Science 192(1-2) (2001): 201-207.
- [63] Kim, J.H., Taluja, A., Knutson, K., and Han Bae, Y. Stability of bovine serum albumin complexed with PEG-poly(L-histidine) diblock copolymer in PLGA microspheres. J. Control Release 109(1-3) (2005): 86-100.
- [64] Park, E.J., et al. Magnetic iron oxide nanoparticles induce autophagy preceding apoptosis through mitochondrial damage and ER stress in RAW264.7 cells. Toxicol In Vitro 28(8) (2014): 1402-12.

- [65] Vu-Quang, H., et al. Chitosan-coated poly(lactic-co-glycolic acid) perfluorooctyl bromide nanoparticles for cell labeling in  $(^{19}\text{F})$  magnetic resonance imaging. Carbohydr Polym 136 (2016): 936-44.
- [66] Injumba, W., Ritprajak, P., and Insin, N. Size-dependent cytotoxicity and inflammatory responses of PEGylated silica-iron oxide nanocomposite size series. Journal of Magnetism and Magnetic Materials 427 (2017): 60-66.
- [67] Hsieh, H.-C., Chen, C.-M., Hsieh, W.-Y., Chen, C.-Y., Liu, C.-C., and Lin, F.-H. ROS-induced toxicity: exposure of 3T3, RAW264.7, and MCF7 cells to superparamagnetic iron oxide nanoparticles results in cell death by mitochondria-dependent apoptosis. Journal of Nanoparticle Research 17(2) (2015).
- [68] Schuler, G., Schuler-Thurner, B., and Steinman, R.M. The use of dendritic cells in cancer immunotherapy. Curr Opin Immunol 15(2) (2003): 138-47.
- [69] Klippstein, R. and Pozo, D. Nanotechnology-based manipulation of dendritic cells for enhanced immunotherapy strategies. Nanomedicine 6(4) (2010): 523-9.
- [70] Hamdy, S., Haddadi, A., Hung, R.W., and Lavasanifar, A. Targeting dendritic cells with nano-particulate PLGA cancer vaccine formulations. Adv Drug Deliv Rev 63(10-11) (2011): 943-55. มหาวิทยาลัย
- [71] Luo, Y.H., Chang, L.W., and Lin, P. Metal-Based Nanoparticles and the Immune System: Activation, Inflammation, and Potential Applications. Biomed Res Int 2015 (2015): 143720.
- [72] Ueno, H., Schmitt, N., Palucka, A.K., and Banchereau, J. Dendritic cells and humoral immunity in humans. Immunology and cell biology 88(4) (2010): 376-80.
- [73] Cruz, L.J., Tacke, P.J., Rueda, F., Domingo, J.C., Albericio, F., and Figdor, C.G. Targeting nanoparticles to dendritic cells for immunotherapy. Methods Enzymol 509 (2012): 143-63.
- [74] Huang, Y., et al. An optimized magnetite microparticle-based phosphopeptide enrichment strategy for identifying multiple phosphorylation sites in an immunoprecipitated protein. Anal Biochem 408(1) (2011): 19-31.

- [75] Elsabahy, M. and Wooley, K.L. Cytokines as biomarkers of nanoparticle immunotoxicity. Chem Soc Rev 42(12) (2013): 5552-76.
- [76] DuPage, M. and Bluestone, J.A. Harnessing the plasticity of CD4(+) T cells to treat immune-mediated disease. Nat Rev Immunol 16(3) (2016): 149-63.
- [77] Henry, C.J., Ornelles, D.A., Mitchell, L.M., Brzoza-Lewis, K.L., and Hiltbold, E.M. IL-12 produced by dendritic cells augments CD8+ T cell activation through the production of the chemokines CCL1 and CCL17. J Immunol 181(12) (2008): 8576-84.
- [78] Whitmire, J.K., Tan, J.T., and Whitton, J.L. Interferon-gamma acts directly on CD8+ T cells to increase their abundance during virus infection. J Exp Med 201(7) (2005): 1053-9.
- [79] Pearce, E.L. and Shen, H. Generation of CD8 T cell memory is regulated by IL-12. J Immunol 179(4) (2007): 2074-81.
- [80] Sercan, O., Stoycheva, D., Hammerling, G.J., Arnold, B., and Schuler, T. IFN-gamma receptor signaling regulates memory CD8+ T cell differentiation. J Immunol 184(6) (2010): 2855-62.
- [81] McGowan, K.L. Specimen Collection, Transport, and Processing: Mycology. in Manual of Clinical Microbiology, Eleventh Edition: American Society of Microbiology, 2015.



APPENDIX

จุฬาลงกรณ์มหาวิทยาลัย  
CHULALONGKORN UNIVERSITY



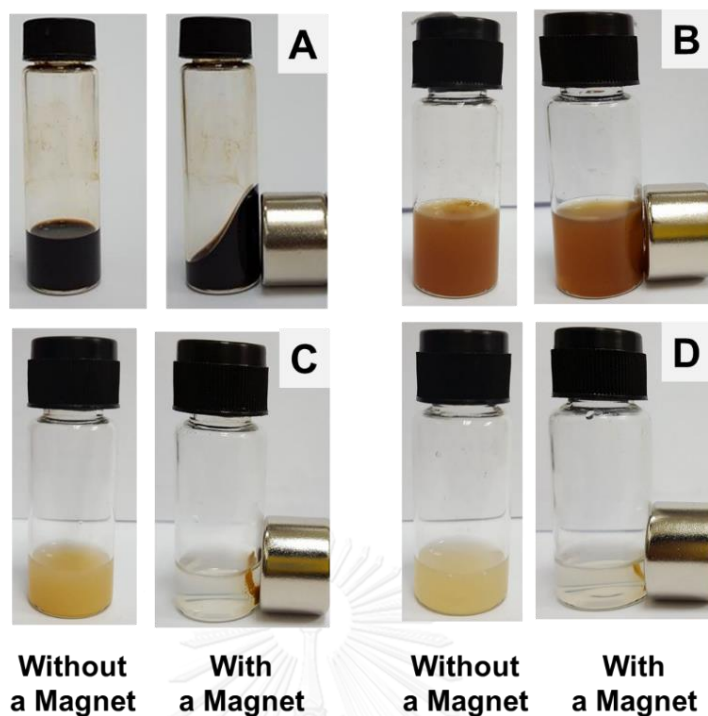


Figure A1 SPIONs and SPIONs-polymer particles including (A) SPIONs, (B) SPION-mPAA, (C) SPION-PLGA-L and (D) SPION-PLGA-S without and with a magnet for 1 h.

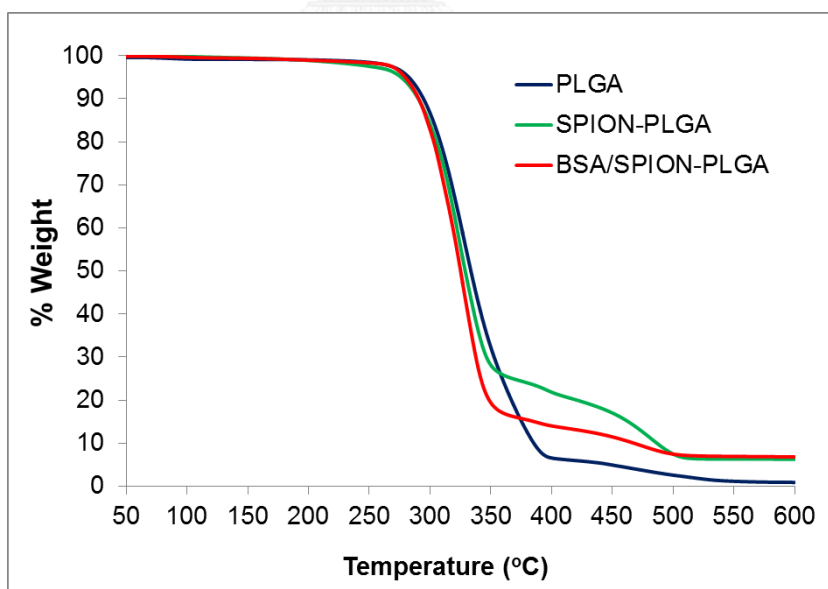
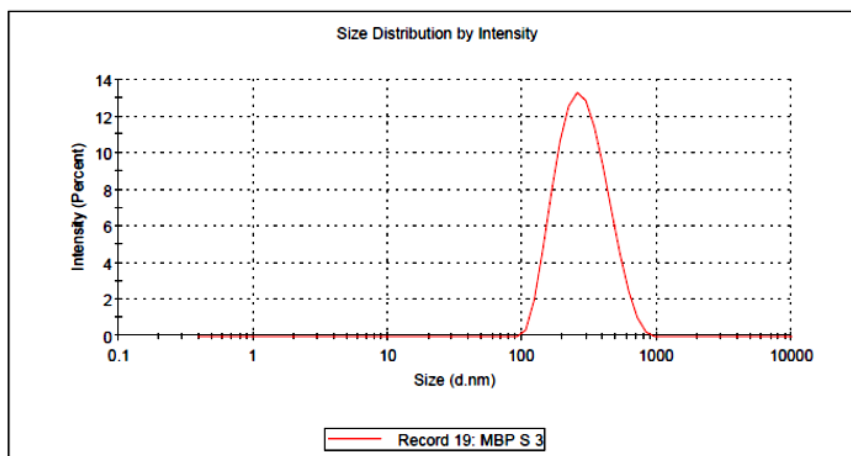


Figure A2 TGA curves for measuring weight loss of PLGA (Blue), SPION-PLGA (Green), and BSA/SPION-PLGA particles (Red)

**A**

	Size (d.n...	% Intensity:	St Dev (d.n...
<b>Z-Average (d.nm):</b> 259.0	<b>Peak 1:</b> 297.4	100.0	125.7
<b>Pdl:</b> 0.168	<b>Peak 2:</b> 0.000	0.0	0.000
<b>Intercept:</b> 0.939	<b>Peak 3:</b> 0.000	0.0	0.000

Result quality **Good**



**B**

	Mean (mV)	Area (%)	St Dev (mV)
<b>Zeta Potential (mV):</b> -11.9	<b>Peak 1:</b> -11.8	99.3	5.49
<b>Zeta Deviation (mV):</b> 5.65	<b>Peak 2:</b> -32.6	0.7	1.88
<b>Conductivity (mS/cm):</b> 0.254	<b>Peak 3:</b> 0.00	0.0	0.00

Result quality **Good**

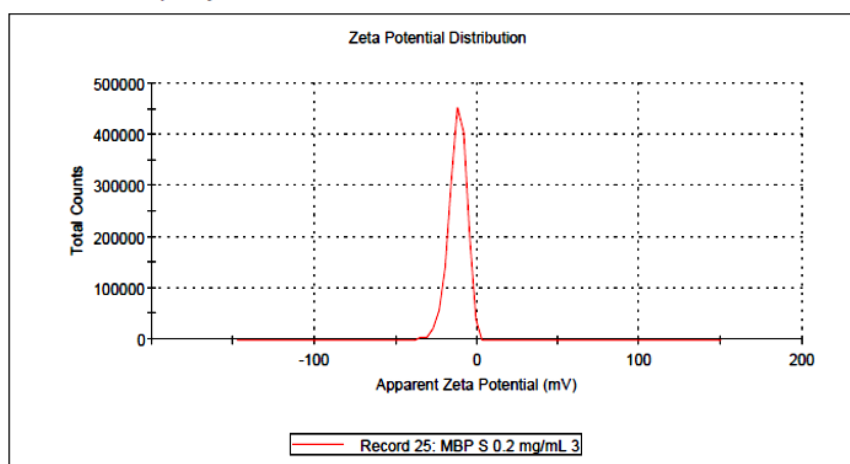
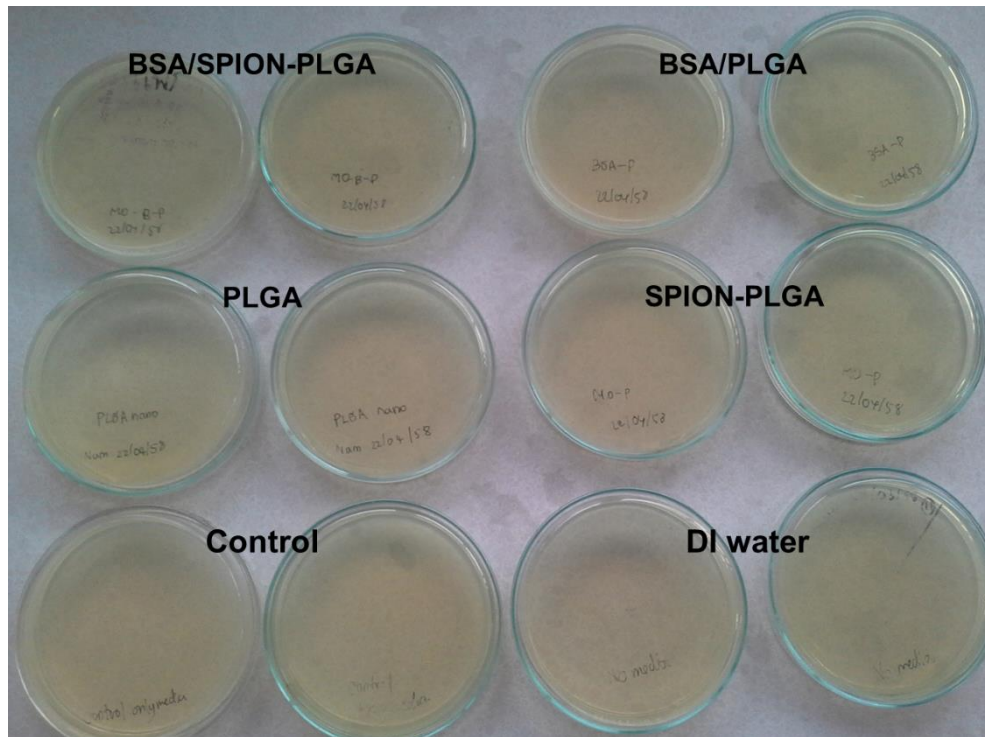
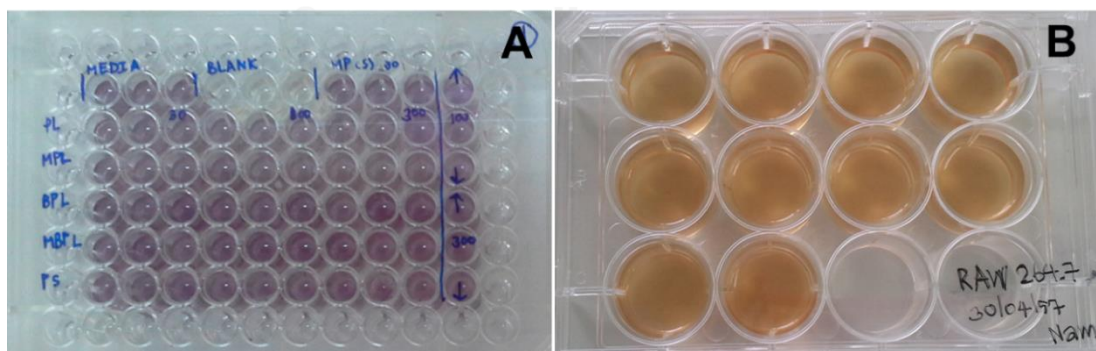


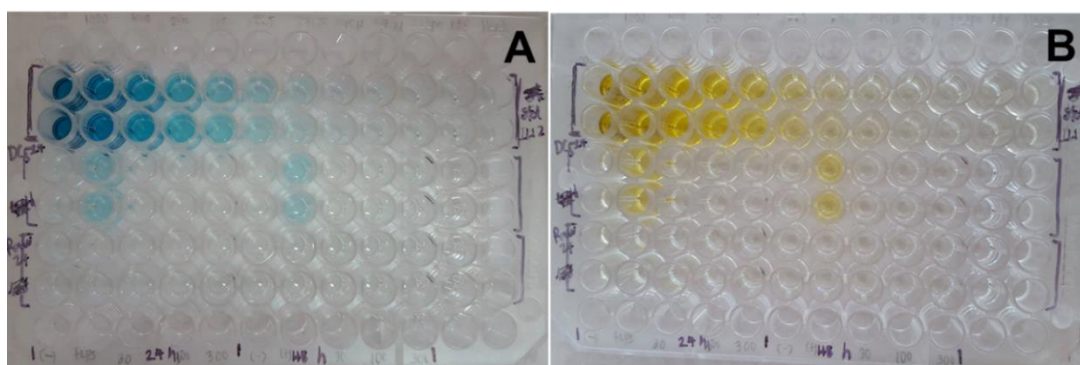
Figure A3 Examples of Zeta sizer analysis of (A) particles size curve and polydispersity indices (PDI), and (B) zeta potential curve



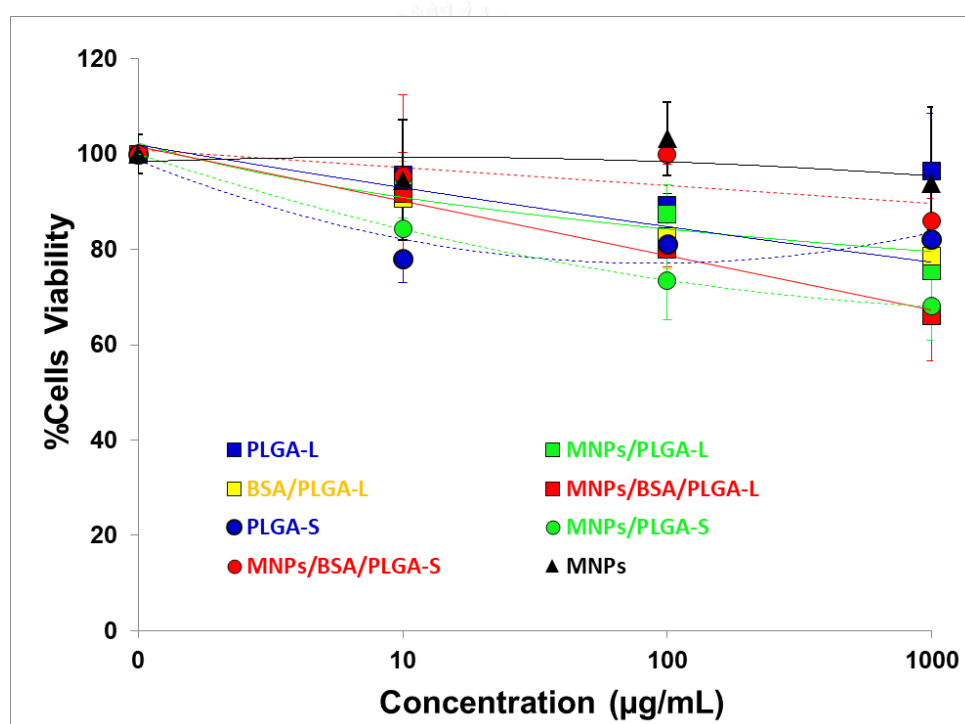
**Figure A4** Particle contamination testing, particles and DI water spreading onto brain heart infusion (BHI) agar after 2 day incubation at 37 °C with 5% CO<sub>2</sub>. (BHI agar is recommended as a universal medium for testing aerobic bacteria and primary recovery of fungi contaminations[81])



**Figure A5** Cytotoxicity study after cellular uptake of particles onto Raw264.7 in 96-well plate and 12-well plate



**Figure A6** ELISA testing of supernatant dendritic cells in 96-well plate (A) after adding TMB substrate and (B) after stop reaction using  $H_2SO_4$

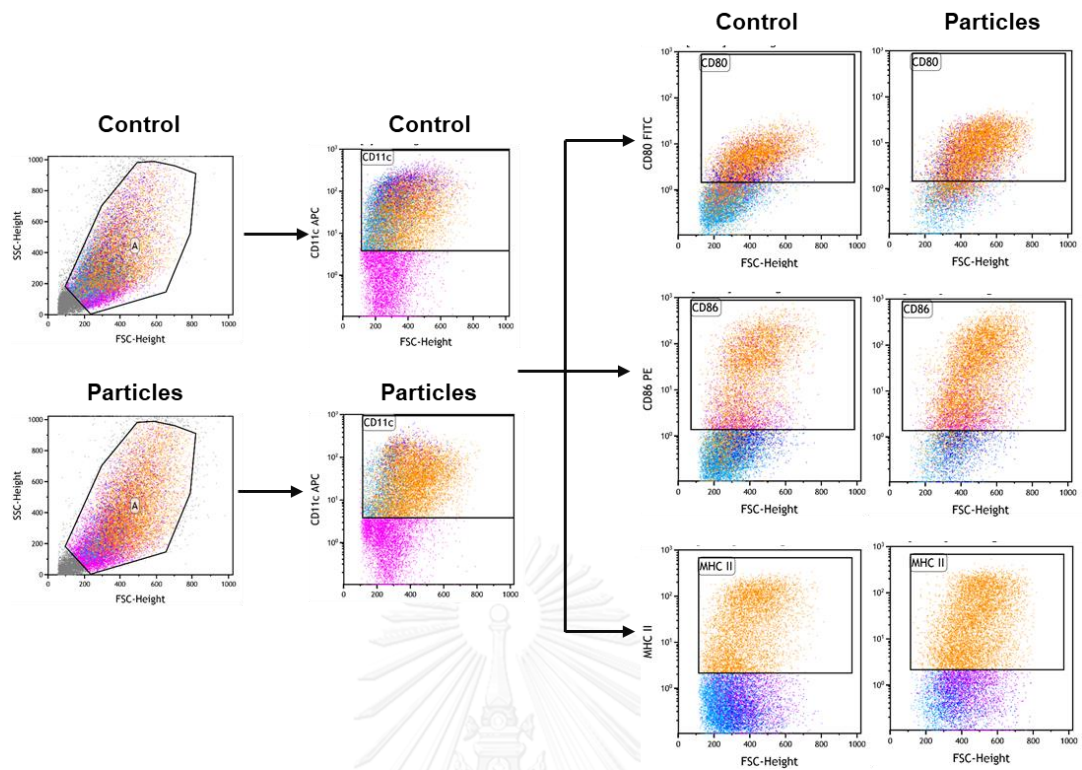


**Figure A7** Cytotoxicity of the SPION, PLGA and SPION-PLGA with and without BSA protein in dendritic cell line (Jaw II). Cell viability from the MTT assay after incubating the cells with the tested particles at 37 °C with 5%  $CO_2$  for 24 h. Data are shown as mean  $\pm$  SD, derived from 3 repeats.

The Raw264.7 cell viability after incubated with particles were used to calculate Inhibitory dose concentration ( $IC_{50}$ ) of particles using linear curves equation between particle concentration and cell viability. From the calculation, all small particles showed  $IC_{50}$  of more than 1 mg/mL for 24 and 48 hours but they showed increases in toxicity at 72 hours. Large nanocomposites and SPIONs showed more toxicity than the small sizes, as the large particles exhibited  $IC_{50}$  of more than 400  $\mu\text{g/mL}$  (Table A1). However, the particle concentration of 100  $\mu\text{g/mL}$ , which were used in cell activation experiment, exhibited low toxicity of less than 60% cell viability (Figure 4.15).

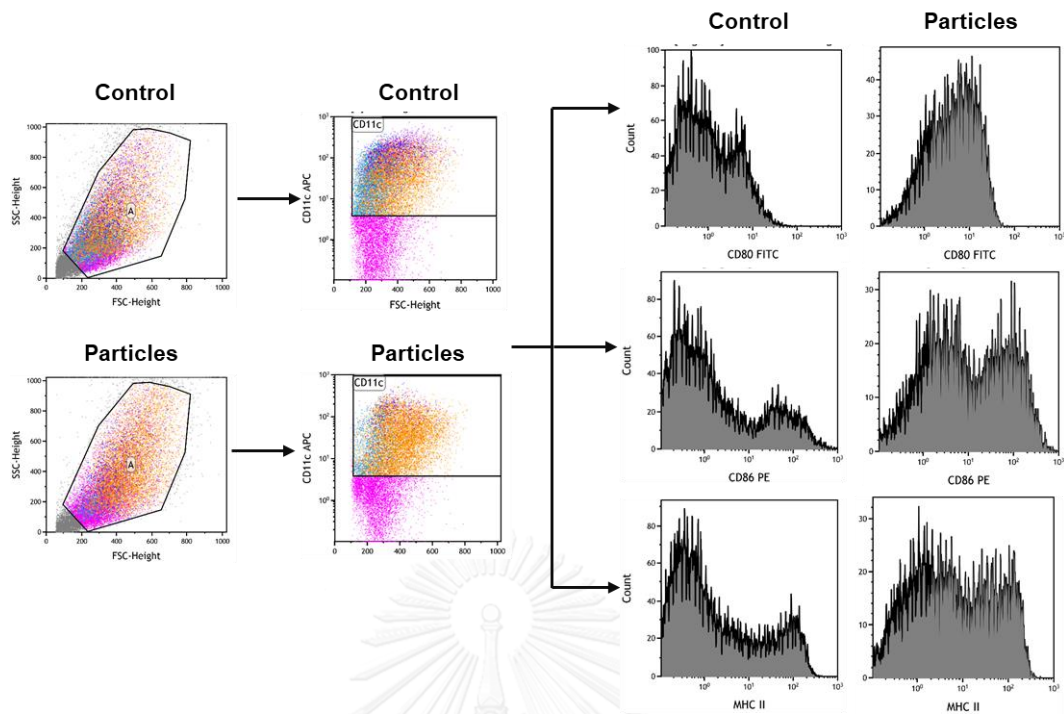
**Table A1** Inhibitory dose concentration ( $IC_{50}$ ) of SPIONs, PLGA particles and nanocomposites (mg/mL) on Raw264.7 cells at various time incubations.

Particles	24 h	48 h	72 h
PLGA-L	1.89	1.06	0.81
PLGA-S	1.00	1.59	1.03
BSA/PLGA-L	2.80	0.83	0.45
BSA/PLGA-S	2.37	1.65	0.81
SPION-PLGA-L	0.89	0.53	0.76
SPION-PLGA-S	1.86	2.33	0.56
BSA/SPION-PLGA-L	0.76	0.52	0.56
BSA/SPION-PLGA-S	2.68	1.58	0.86
SPIONs	0.48	0.48	0.43



**Figure A8** Examples of flow cytometry analysis data from control (dendritic cells were unstimulated) and particles (activated with particles): forward scattering (FSC) against side scattering (SSC), and cell population of surface maturation marker CD11c, CD80, CD86 and MHC II.





**Figure A9** Examples of flow cytometry analysis data from control (dendritic cells were unstimulated) and particles (activated with particles): forward scattering (FSC) against side scattering (SSC), and cell surface expression of CD11c, CD80, CD86 and MHC II. Filled histograms represent isotype matched control antibody staining. Numbers indicate MFI of stained cells.

## VITA

Miss Chalathan Saengruengrit was born on December 22, 1988 in Bangkok Thailand. She graduated in Bachelor Degree of Science in Chemistry from Burapha University in 2011. Then, she received her Master's Degree of Science in Chemistry from Burapha University in 2013. In the same year, she continued her Ph.D in Chemistry at Chulalongkorn University. She became a member of Material Chemistry and Catalysis Research Unit under the supervision of Dr. Numpon Insin. Moreover, she had received the scholarship by Science Achievement Scholarship of Thailand.

On 21 - 23 January 2015, she participated Pure and Applied Chemistry International Conference 2015 (PACCON2015) in the title of "Synthesis of Magnetic Nanoparticles Coated with Biocompatible Polymers for Drug Delivery Application". Moreover, she attended the 11th International Conference on the Scientific and Clinical Applications of Magnetic Carriers on May 31 - June 4, 2016 in the title of "Synthesis of Magnetic Nanocomposites for Application in Protein Delivery to Immune Cell" by poster presentation.

Email: nam\_scim@hotmail.com